

AN ABSTRACT OF THE DISSERTATION OF

Hayley Peter-Contesse for the degree of Doctor of Philosophy in Soil Science presented on June 13, 2023.

Title: Spatiotemporal Patterns in Soil Carbon Distribution, Persistence, and CO₂ Respiration in a Pacific Northwest Montane Forest

Abstract approved: _____

Kate Lajtha

Given their considerable ability to store and stabilize carbon (C), soils are a critical resource to maintain in the face of the accelerated effects of climate change on natural systems. Pacific Northwest montane forests are hotspots of above- and belowground C storage globally, yet the combined effects of extended seasonal drought, longer and more extreme fire seasons, and warming temperatures are already disrupting C cycling in these systems and stimulating release of soil C to the atmosphere. Accelerated release of CO₂ may intensify C-temperature feedbacks, fueling further global changes. The processes that influence organic matter accumulation and C stabilization and destabilization in forest soils are still not fully understood, and can be especially hard to tease apart in areas with complex interactions among spatial and temporal drivers of soil C. Quantifying landscape-scale (km) and finer grain (m) resolution estimates of soil C, soil C cycling rates, and drivers of soil C stabilization and destabilization can help inform ecosystem models that feed into land management decisions. The H.J. Andrews Experimental Forest (HJA) is a 6400-ha Long Term Ecological Research (LTER) site in Oregon's western Cascade Mountains with complex terrain, varied vegetation assemblages, steep slopes, and a substantial gradient in elevation. HJA hosts the Detrital Input and Removal Treatment (DIRT) experiment, which has manipulated organic matter input rates of needle litter, woody debris, and root-derived C for over two decades. The first chapter of this dissertation examines the effects of sustained additions or removals of detritus on soil respiration to address questions about the longevity of the soil organic matter priming effect. While adding a more labile C source in the form of needle

litter resulted in slightly increased release of soil CO₂ beyond the amount expected from litter additions, there were compensatory gains in soil C relative to control treatments. I provide evidence that soil organic matter priming is a short-term phenomenon and that there are more likely seasonal changes in moisture availability that are driving changes in plant and microbe soil C allocation. Surprising diurnal trends in soil respiration illustrate the tightly regulated relationship between tree stomatal conductance, midday vapor pressure deficit, and root-derived soil respiration. Additionally, root and rhizosphere respiration contributed the most to total respiration, while above- and belowground decomposition of organic matter contributed less. The second chapter of this dissertation expands in scope to a spatial analysis of soil carbon distributions across mid- and high- elevations of HJA. This research addresses questions about the interplay between topographic and vegetative drivers of persistent and labile soil C pools in complex terrain. Ratios of C to nitrogen (N) tended to be greater in valley versus ridge sites and were much greater in forest versus meadow sites, which may be an artifact of the N-limitations in lower elevations where nutrients are cycling more quickly – in contrast to higher elevations where decomposition is slowed and vegetative growth is less resource-limited. In chapter three, I further expanded the study area to the entirety of HJA and investigated the large- and small-scale drivers of total soil C and of soil C fractions, in addition to soil N. I found that, unsurprisingly, soil depth was the most significant predictor of soil C, but that important environmental controls included elevation (as a proxy for temperature and moisture regimes) and proximity to the nearest stream. I was surprised to find that aboveground biomass and landscape position were less important to prediction of soil C relative to climate thresholds. Using a combination of my field data and machine learning techniques, I produced maps of soil C, N, and mineral-associated and particulate organic matter C distributions across HJA. I compared my mapped soil C products with publicly available soil datasets and found wide variation in predicted soil C across different datasets that can be explained in part by their coarse resolution and interpolation across too few field samples. The insights gained from the studies in this dissertation point to the importance of matching the spatial and temporal scale of sampling to the scale of ecological processes, a critical step in producing higher resolution estimates of soil C across complex landscapes.

©Copyright by Hayley Peter-Contesse
June 13, 2023
All Rights Reserved

Spatiotemporal Patterns in Soil Carbon Distribution, Persistence, and CO₂ Respiration in a
Pacific Northwest Montane Forest

by
Hayley Peter-Contesse

A DISSERTATION

submitted to

Oregon State University

in partial fulfillment of
the requirements for the
degree of

Doctor of Philosophy

Presented June 13, 2023
Commencement June 2023

Doctor of Philosophy dissertation of Hayley Peter-Contesse presented on June 13, 2023

APPROVED:

Major Professor, representing Soil Science

Head of the Department of Crop and Soil Science

Dean of the Graduate School

I understand that my dissertation will become part of the permanent collection of Oregon State University libraries. My signature below authorizes release of my dissertation to any reader upon request.

Hayley Peter-Contesse, Author

ACKNOWLEDGEMENTS

I owe the utmost gratitude to my major advisor, Dr. Kate Lajtha, for helping guide me through this process with gentle or firm nudges as needed to keep me on the right track. Thank you for always making time for your grad students, whether day or night. I attribute much of my growth as a scientist to your leadership, whether it was leading by example, making opportunities available for me to prove myself and grow, connecting me with other scientists, or the hours spent in lab meetings patiently teaching us how to critically analyze others' research. I truly would not be where I am today without your guidance. Thank you for putting your trust in me and for clearing the path for me to take advantage of opportunities to grow my confidence and to become a better scientist.

I owe many thanks to my current and former lab mates who collaborated with me in the lab and field, and on all aspects of planning and executing research projects. Derek Pierson, Amy Mayedo, Regina O'Kelley, and Ester Helbling: each and every one of you helped me learn and provided support when needed.

To the cohort of graduate students who have joined me in this journey, I offer my thanks. The soils, forestry, and other OSU grad students offer a collaborative community that fosters growth and support over individual competition. I'd like to particularly thank my former officemates Trang Nguyen, Kelsey Kerwin, and Ashley Waggoner for all the fun mixed with an appropriate amount of hard work and talking science.

To the many scientists who have lent me equipment or offered up their lab space, I thank you. Claire Phillips, Jen Moore, Jeff Hatten, Kevin Bladon, and Matt Konkler, my research was made orders of magnitude better by your generous contributions and support. Thanks to the CSS Department and all those who spend their time passing knowledge to the next generation of students. Thanks also to my graduate committee members Julia Jones, Dave Bell, Jen Moore, and Alyssa Shiel for giving up many hours of your lives to meet with me and help guide my research and writing.

Many undergraduate students have helped in the field and lab, and they were integral to my research success. Ngoc Nguyen, Judy Fleming, Shea Fleetwood, Emmy Formiga, Abigail

Evered, Martin Hankins, and Jamie Bowden, thank you for your cheerful willingness to spend long hours getting covered in soil in the summer heat while attempting to avoid poison oak and angry yellow jackets, followed by long hours in the lab performing maddeningly mundane tasks, all in the name of science.

Thanks to all of my friends and family who have been unfailingly supportive throughout these years. My Southtown Corvallis neighbors and dear friends have helped me more than they know with their potlucks, opening of their homes, and formation of a truly special community. My parents and family have enthusiastically encouraged me to pursue a career in science and have always provided support when I needed it.

And finally, I owe more gratitude than I can say to my husband, Aron Boettcher, who's been with me this whole time. You have always put aside everything else to support me when I needed it, whether in the woods when I couldn't field a crew during COVID, at the computer talking through machine learning techniques and data visualization, or anywhere else we happen to find ourselves endlessly discussing science (which, it turns out, is just about everywhere!). I look forward to our continued exploration in science together.

CONTRIBUTION OF AUTHORS

Dr. Lajtha contributed to study design for Chapters 1-3. Aron Boettcher assisted with field data collection for Chapters 1 and 2 and contributed to study design and data analysis for Chapters 1-3.

TABLE OF CONTENTS

	<u>Page</u>
General Introduction.....	1
Chapter 1: Revisiting contributions to soil CO ₂ efflux to determine the longevity of priming effects in a temperate coniferous forest	
Introduction	3
Methods	6
Results	11
Discussion	17
Chapter 2: Vegetation and topography as competing drivers of soil C distribution and persistence in HJ Andrews' mid and high elevations	
Introduction	29
Methods	33
Results	39
Discussion	55
Chapter 3: Multi-scale spatial patterns in soil carbon distribution across complex mountain terrain	
Introduction	59
Methods	60
Results	65
Discussion	86
Bibliography	104

LIST OF FIGURES

<u>Figure</u>	<u>Page</u>
1.1 Seasonal and cumulative annual soil CO ₂ efflux.....	12
1.2 Partitioned contributions of functionally heterotrophic and functionally autotrophic sources to total soil respiration.....	14
1.3 Litter decay modeling results for measured and predicted soil organic carbon and soil respiration by treatment.	16
1.4 Seasonal and diurnal trends in environmental covariates and soil respiration	21
1.5 Concurrent CO ₂ efflux measurements at 10-minute intervals from CTL and NR plots in June 2018.....	23
2.1 Distribution of sampling site locations with HJA Administrative Boundary Layer.....	35
2.2 Mean SOC concentration by depth in ridge and valley sites \pm SE of the mean.....	40
2.3 Mean SOC stocks of the fine earth fraction in forested ridge and valley sites \pm 1 SE of the mean by soil depth increment.....	41
2.4 Mean C:N ratio in ridge and valley sites by soil depth.....	42
2.5 Mean SOC concentration by depth and cover type \pm 1 SE of the mean...	44
2.6 Mean SOC stock in the fine earth fraction by cover type \pm 1 SE of the mean per soil depth increment.....	45
2.7 Mean C:N for forest and meadow sites by depth \pm 1 SE of the mean.....	46
2.8 The proportion of mean MAOM-C to bulk soil C by depth in ridge and valley sites \pm 1 SE of the mean.....	47
2.9 The proportion of mean MAOM-C to bulk soil C by depth in forest and meadow sites \pm 1 SE of the mean.....	48
2.10 Mean C concentration of the MAOM soil fraction as a proportion of bulk soil mass in ridge and valley sites, \pm 1 SE of the mean.....	49

LIST OF FIGURES (Continued)

<u>Figure</u>	<u>Page</u>
2.11 Mean C concentration of the MAOM soil fraction as a proportion of bulk soil mass in forest and meadow sites, ± 1 SE of the mean.....	50
2.12 Mean C concentration of the POM soil fraction as a proportion of bulk soil mass ± 1 SE of the mean in ridge and valley sites.....	52
2.13 Mean C concentration of the POM soil fraction as a proportion of bulk soil mass ± 1 SE of the mean in forest and meadow sites.....	53
2.14 Ratio of mean POM-C to MAOM-C ± 1 SE of the mean in ridge and valley sites.....	54
2.15 Ratio of mean POM-C to MAOM-C ± 1 SE of the mean in forest and meadow sites.....	55
3.1 Variable importance plot for RF prediction of soil C % with an inset plot of the regression of the predicted model versus the measured data and the goodness of fit of the cross-validated bootstrapped model.....	67
3.2 Variable importance plot for RF prediction of soil C stock to 1 m depth, excluding depth as a predictor variable, with an inset plot of the regression of the predicted model versus the measured data and the goodness of fit of the cross-validated bootstrapped model.....	68
3.3 Variable importance plot for RF prediction of soil N with an inset plot of the regression of the predicted model versus the measured data and the goodness of fit of the cross-validated bootstrapped model.....	70
3.4 Variable importance plot for RF prediction of soil C:N with an inset plot of the regression of the predicted model versus the measured data and the goodness of fit of the cross-validated bootstrapped model.....	71
3.5 Spatial distribution of predicted soil C concentration across HJA in the 0-10 cm soil depth increment at a 10 m x 10 m pixel size.....	72
3.6 Elevation map of HJA in meters.	73
3.7 Lookout Mountain region enlarged to show patterns in soil C concentration at finer spatial scale.....	73

LIST OF FIGURES (Continued)

<u>Figure</u>		<u>Page</u>
3.8	Map of predicted soil C concentration across HJA in the 75-100 cm depth increment at 10 m x 10 m spatial resolution.....	74
3.9	Map of predicted soil N concentration in the 0-10 cm depth increment across HJA.....	75
3.10	Map of predicted C:N in 0-10 cm depth across HJA.....	76
3.11	Map of predicted soil C stock to 1 m depth across HJA.....	77
3.12	Map of predicted POM-C concentrations across HJA in the 0-10 cm soil depth increment.....	78
3.13	Map of predicted POM-C concentration in the 75-100 cm soil depth across HJA.....	78
3.14	Map of predicted MAOM-C concentration in the 0-10 cm depth increment across HJA.....	79
3.15	Map of predicted MAOM-C concentration in the 75-100 cm depth across HJA.....	79
3.16	RF model prediction comparison between my RF-predicted SOM and measured SOC (converted to SOM; ‘HPC’) and between my RF-predicted values and Griffiths’ measured SOM.....	80
3.17	Range in distribution of estimated SOC in the top 1 m of soil for HJA.	82
3.18	Regression of my RF-predicted soil C stock (‘hpc’) and the Polaris estimated C stock.....	83
3.19	Regression of my RF-predicted soil C stock (‘hpc’) and the Soil Grids estimated C stock.....	83
3.20	Regression of my RF-predicted soil C stock (‘hpc’) and the SSURGO estimated C stock.....	84

LIST OF FIGURES (Continued)

<u>Figure</u>	<u>Page</u>
3.21 Correlation matrix for comparisons among publicly available datasets and my site-level (“Site”), transect-level (“Transect”), and RF-predicted (“hpc”) data, as well as another dataset generated by Robert Griffiths (“Griffiths”) from soil sampling 0-10 cm along HJA roads in the late 1990s.....	85
3.22 Relationship between SOC stock and distance to nearest stream across HJA.....	87
3.23 Relationship between SOC stock and mean daily maximum temperature across HJA.....	88
3.24 Relationship between SOC stock and percent slope across HJA.....	89
3.25 Relationship between elevation and soil N across HJA.	91
3.26 Relationship between mean daily maximum temperature and soil N across HJA.....	91
3.27 Map of predicted N stock to 1 m soil depth across HJA, classified and visualized by natural breaks in the data.....	92
3.28 Relationship between aboveground biomass (AGB) and C:N across HJA.....	93
3.29 Map of C:N across HJA in the 0-10 cm depth increment, visualized by significant peaks in the C:N data.....	93
3.30 Correlation matrix for RF-modeled SOC and SOC from publicly available datasets.....	94
3.31 Relationship between mean distance to nearest stream and C:N across HJA.....	94
3.32 Relationship between MAOM-C concentration and SSURGO clay content in the 0-10 cm soil depth increment.....	98
3.33 Map of SSURGO estimated clay percentage across HJA to 1 m depth (bottom) paired with MAOM-C concentration (top) for visual comparison.....	99

LIST OF FIGURES (Continued)

<u>Figure</u>		<u>Page</u>
3.34	Map of soil bulk density at 0-10 cm depth increments across HJA.....	100
3.35	Relationship between bulk density and MAOM-C concentration in the 0-10 cm soil depth increment (left) and 75-100 cm depth increment (right).....	100
3.36	Mapped rocks, cliffs, talus, steep tag alder patches, wetlands, and dry meadows across HJA.....	101

LIST OF TABLES

<u>Table</u>		<u>Page</u>
1.1	Description of detrital manipulation treatments.....	8
2.1	Soil bulk density (Db) by depth in vegetation and topographic position classes.	36
3.1	Sources of data and associated spatial resolution.....	62

INTRODUCTION

Carbon dynamics in forests are directly related to projected global climate change scenarios as global temperatures trend upwards and seasonal moisture regimes change, influencing nutrient cycling rates in natural ecosystems. Despite over a century of documented soil C measurements, major uncertainties still exist in the spatial distribution of terrestrial carbon (C) sources and sinks and, in particular, the interplay between factors that influence soil C distribution and persistence. Global soils contain more than three quarters of all terrestrial C (Jackson et al. 2017), so any changes to soil C or its inputs will influence global climate dynamics, whether through increased losses of soil C as CO₂ to the atmosphere, increased C assimilation through changing vegetation regimes, or imbalances between soil C stabilization and destabilization. Temperate and boreal forests serve as a net sink of atmospheric CO₂; as plants assimilate C into their biomass, much of that C makes its way into soil reservoirs over time via biogeochemical pathways including decomposition processes and root exudates. The pathways by which soil C is stabilized tend to be microbially mediated and root derived, while the pathways by which soil C is destabilized may be decoupled from those stabilization processes in space and time. Stabilized soil C is not entirely resistant to decomposition but tends to have longer residence times due to strong mineral associations. Stable soil C, or mineral-associated organic matter (MAOM), and the more ephemeral particulate organic matter, POM, differ not only in mean soil residence time, but also in their respective biogeochemical pathways of formation and will thus display differing responses to environmental conditions. These pathways of formation and biogeochemical drivers remain poorly understood, leading to large uncertainties in soil C response to global change.

Identifying small-scale and large-scale drivers of not only bulk soil C distributions, but also distributions of POM and MAOM, across landscapes is an important part of assessing global C stocks and their vulnerability to climate change. The interplay between climate, vegetation, parent material, landscape position, and organisms as drivers of soil C distributions is complex in mountainous landscapes such as those of the H.J. Andrews Experimental Forest (HJA) in western Oregon, USA. Decomposition processes that can destabilize soil C and result in soil respiration (CO₂ efflux from soils) are also varied in response to aboveground and belowground

organic matter sources. Long term experiments like the Detrital Input and Removal Treatment (DIRT) experiment in HJA can help elucidate those drivers by isolating the sources of aboveground and belowground organic matter inputs and measuring soil functional responses across decades.

Advances in geospatial data products and computing capabilities over the past decade allow us to measure and model features of landscapes at increasingly finer grain resolution (e.g., 1 m² lidar). There is enormous potential for these data products to be used to improve digital soil mapping, which in its current form is coarse resolution and highly interpolated from small numbers of field samples (e.g., NRCS SSURGO). Using machine learning (ML) methods to model and predict soil C distributions is a promising approach that is increasingly utilized but still in the early stages of development. By calibrating models to large numbers of fine-grain soil samples (1 m), relationships can be built among both fine-scale and landscape-scale drivers of soil C, and spatial patterns may be elucidated in the context of competing environmental covariates.

CHAPTER 1: Revisiting contributions to soil CO₂ efflux to determine the longevity of priming effects in a temperate coniferous forest

Introduction

Global soils serve as a storage reserve for over two-thirds of terrestrial carbon and even small perturbations to controls on soil carbon flux can cause net CO₂ release to the atmosphere (Crowther et al., 2016). Loss of soil CO₂ to the atmosphere enhances the greenhouse effect, resulting in increased global surface temperatures. Consequently, the overall carbon (C) balance and the rate of C exchange between soils and the atmosphere influence global climate. Examining the mechanisms that control the balance between soil C stabilization and soil C mineralization will help inform predictions of current and future soil C losses in the face of global change.

While major uncertainties exist in estimates of the magnitude and spatial distribution of terrestrial C mineralization sources and C sinks, there is consensus that temperate and boreal forests represent considerable above- and belowground C stores (Hyvönen et al., 2007). Disruptions to forest soil C cycling will alter the capacity and functioning of these significant terrestrial C reservoirs. Annual global soil respiration (R_s) from mineralization of soil C is estimated at 87.5 Pg C (1999–2016 mean; Lei et al., 2021) -- a C flux second only to that of the world's oceans (Janzen, 2015). The intertwined forces of global change and land use change threaten to transform net C sinks into net C sources through the positive climate feedbacks of increasing surface temperatures and accelerated release of soil C as CO₂ (Crowther et al., 2016; Adamczyk et al., 2019). The continued capacity for soils to both mediate temperature and to function as a global C sink will weaken if the accelerated release of CO₂ to the atmosphere surpasses the rate of plant and microbially-derived C inputs to soils and disrupts C retention through soil organo-mineral interactions. Further, increased potential for soils to transform from net C sinks to net C sources is associated with positive soil organic matter priming caused by elevated microbial metabolism in response to altered C inputs and sources (Sulzman et al., 2005; Fontaine et al., 2007; Crow et al., 2009a; Bernard et al., 2022; Castañeda-Gómez et al., 2022).

Forest C dynamics are an integral part of projected global climate change scenarios as global temperatures increase and changes in seasonal moisture availability influence nutrient cycling rates, including soil respiratory losses, in natural ecosystems. While some biomes may experience increased NPP in response to an accelerated nutrient cycling rate associated with climate warming, this increased aboveground productivity does not directly translate to increased belowground C sequestration (Lajtha et al., 2018; Pierson et al., 2021b). Instead, accelerated rates of vegetative growth and senescence have been widely shown to positively prime soil organic matter (SOM) across ecosystems, causing mineralization and release of soil C in excess of that added by increased NPP (Sulzman et al., 2005; Kuzyakov, 2010; Bernard et al., 2022). Diverse ecosystem responses to accelerated organic matter inputs can be explained in part by the varied avenues for soil C stabilization and destabilization, especially through interactions between microbial metabolism and plant roots in the rhizosphere.

As the largest component of ecosystem respiration, soil CO₂ efflux represents a significant loss of not only recent photosynthates, but potentially also loss of previously stabilized soil organic C (SOC). While changes in the belowground SOC store generally contribute little to overall soil R_s, ecosystem processes may act to destabilize additional stored SOC by inducing SOM priming. SOM priming represents the multiplicative effects caused by additions of labile organic inputs that then cause the release of additional CO₂ due to stimulation of microbial activity that destabilizes previously stored C (Lajtha et al., 2018). This is just one example of the nonlinearities that exist along the stabilization/destabilization continuum as organic matter decomposes, transforms, and cycles between soil, aquatic ecosystems, and atmosphere.

Soil CO₂ efflux results from plant root and rhizosphere activity, including bacterial and fungal metabolism, plus the activity of soil fauna (Hanson et al., 2000; Sulzman et al., 2005). The rate of soil CO₂ evolution therefore depends on the relative contributions of the above processes plus the ecological and physiological conditions that influence those processes (e.g., tree metabolism, plant-available water, soil pore network structure and oxygen availability, etc.). Soil mineralogy,

like that present in the allophane-rich Andisols and Inceptisols in Oregon's Cascade Mountains, influences the potential for the electrostatic interactions and organo-mineral complexation that help retain C-containing compounds and will in part dictate the native C status of the soil. The balance between these SOC stabilization and destabilization processes will dictate total soil CO₂ efflux rates across varied temporal and spatial scales.

Numerous studies since the early 2000s have attempted to disentangle the heterotrophic and autotrophic components of soil respiration because those components have been shown to respond differently to changes in environmental drivers (Hanson et al., 2000; Olsson et al., 2005; Schindlbacher et al., 2009). While it remains unlikely that these respiration sources can be truly separated using current methods, a common approach is to distinguish between organisms that receive their photosynthates from the plant canopy as functional autotrophs and those that metabolize dead/dying organic matter as functional heterotrophs (Högberg et al., 2004; Sulzman et al., 2005). Soil respiration can then be separated into three categories; root and rhizosphere derived CO₂, CO₂ evolved from decomposition of aboveground litter, and CO₂ evolved from decomposition of belowground (mostly root) litter. A valuable approach to predicting SOC losses under global change conditions is to measure and model soil respiration under native and accelerated aboveground input conditions, in addition to restricted input conditions, which can help disentangle the heterotrophic and autotrophic components of soil respiration and provide insight into how the drivers of decomposition are influenced by both biotic and abiotic factors.

My goals were to investigate the temporal bounds on the SOM priming effect by revisiting a western Cascade Mountains temperate forest site that had exhibited significant priming effects in response to manipulated litter additions two decades earlier (HJA DIRT site; Sulzman et al., 2005). The H.J. Andrews Experimental Forest LTER (HJA) hosts the Detrital Input and Removal Treatment (DIRT) experiment, which was established in 1996 and has been maintained as detrital addition, exclusion, and control treatments ever since. The positive priming of added litter, found previously by Sulzman, cannot last indefinitely, or soils would be free of SOM, yet

few studies follow priming over time scales long enough to see the relative balance between priming by litter and SOM stabilization of litter inputs over time. Thus, my primary objective was to study the longevity of SOM priming in order to answer the question: is priming a short- or long-lived phenomenon? Specifically, I asked the questions: (1) with added detritus (woody and needle litter) inputs, does the rate of CO₂ efflux from soils remain elevated or stabilize with time relative to the input C rate?; and (2) with reduced detritus inputs, does the soil CO₂ efflux rate remain constant or slow over time? I also investigated the seasonal and diurnal variation in autotrophic and heterotrophic soil CO₂ efflux to explore whether these relationships changed after two decades of repeated annual detritus manipulation.

Hypotheses

I hypothesized that: (1) the loss of live roots, as one might expect from a catastrophic natural disturbance like wildfire, will cause cessation of SOM priming because root exudation will cease. This will cause continued decline in soil respiration rates over time because microbial communities no longer have the ready source of metabolites from root exudates and fine roots that allow them to “prime” a potentially more persistent pool of SOC, even with additional needle litter inputs; (2) SOM priming is a short-lived phenomenon; after a decade or more of repeated needle litter additions, a new equilibrium state has been established such that the SOC stabilization rate has effectively caught up with priming. Whereas an initial phase of priming was established with the addition of a labile C source (needle litter) that allowed the microbial community to overcome an activation energy threshold and metabolize a previously more persistent SOC pool, the microbial community quickly adapted to the new accelerated litter input rate and is able to metabolize the newly added litter without inducing additional priming.

This study presents findings from in situ CO₂ efflux measurements following two decades of detrital manipulations in a temperate PNW forest and compares relative efflux contributions to those reported by Sulzman et al. (2005) at DIRT experiment inception.

Methods

Site Description

The H.J. Andrews Experimental Forest LTER is the 6,400-ha drainage basin of Lookout Creek in the foothills of Oregon's Western Cascade Mountains. Closed canopy, coniferous forests with assemblages of Douglas-fir (*Pseudotsuga menziesii*), western hemlock (*Tsuga heterophylla*), and western redcedar (*Thuja plicata*) dominate the lower elevations where the Detrital Input and Removal Treatment (DIRT) study site is located (44°15' N, 12°10' W). This region's climate is maritime Mediterranean, with wet mild winters and dry cool summers (Waring & Franklin, 1979; Zald et al., 2016). Mean monthly temperature at a low elevation meteorological station (Primary Meteorological Station: PRIMET) near the study site ranges from -1-2 °C in January to a high of 18-20 °C in August (mean air temperature of sensors at 150 cm and 250 cm height above ground from 2016 through 2018). Precipitation, averaging 2,300 mm yr⁻¹, falls primarily from November to March as a mix of rain and snow, with snowpack rarely lasting more than a couple of weeks (Zald et al., 2016).

Soils at the HJA DIRT experiment site are classified (USDA Soil Survey Staff, 1999) as a mix of coarse loamy mixed mesic Typic Hapludands, Andic Dystrudepts, and Vitrandic Dystrudepts (Dixon, 2003). The relatively flat (slopes <5% steepness), south-facing study site lies at an elevation ranging from 531 to 556 m on colluvial and alluvial fan deposits with a generally thick (4–8 cm) organic soil horizon and abundant coarse woody debris (Dixon, 2003; Pierson et al., 2021b). Additional DIRT soil chemical and physical properties are described in Sulzman et al. (2005), Lajtha et al. (2005), and Pierson et al. (2021b).

DIRT Experimental Design

DIRT is an ongoing, long-term (25+ year) experiment which assesses the role of plant detrital inputs to soil and their influence on short- and long-term nutrient cycling (Lajtha et al., 2005). The DIRT concept is replicated across ecosystems in the United States and worldwide (Nadelhoffer et al., 2004). The HJA DIRT site consists of replicated plots (3 replicate plots per treatment and control) with treatments that include elevated woody or needle litter inputs, restricted aboveground inputs, restricted belowground (i.e., root-derived) inputs, and plots with

restricted above- and belowground inputs, alongside control plots with undisturbed old-growth (>500-year-old) forest conditions (Table 1.1). Plot sizes for all control plots and treatments except the No Root (NR) and No Input (NI) plots are $\sim 150 \text{ m}^2$, while the NR and NI plots range from 55 to 75 m^2 .

Table 1.1

Description of detrital manipulation treatments.

Treatment	Abbreviation	Description
Control	CTL	Natural above- and belowground detrital inputs
Double litter	DL	Aboveground needle litter inputs doubled annually
Double wood	DW	Wood chips applied every other year at a doubled input rate
No litter	NL	1-mm mesh screen on soil surface prevents aboveground needle litter inputs, which are removed annually
No roots	NR	Trees girdled at experiment inception; live roots excluded via tarp-lined trenches around plots
No input	NI	Aboveground inputs excluded as in <i>No litter</i> plots; belowground inputs prevented as in <i>No roots</i> plots

In-situ soil respiration measurements

Plot-level soil CO₂ efflux

From November 2017 to November 2018, soil CO₂ efflux was measured roughly weekly in May-July and once per month during the remainder of the year using a portable infrared gas analyzer (LI-8100A; LI-COR Inc., Lincoln, NE) attached to a closed dynamic respiration chamber (LI-8100-102) placed over a 10-cm diameter polyvinyl chloride (PVC) collar. Each PVC collar measures 5 cm in height and is inserted 2 cm into the mineral soil. Three PVC collars

were installed permanently in each plot (n=54) and collar volumes measured frequently, with updated volumes of collars + chamber headspace used for soil CO₂ flux calculations at each collar location. The portable infrared gas analyzer (IRGA) measures buildup of CO₂ in the collar + chamber headspace over 90 s and the IRGA purges gas after each measurement. Plot-level gas flux measurements were typically taken between 0900 h and 1300 h to minimize temporal effects on CO₂ efflux.

Diurnal continuous soil CO₂ efflux

To examine temporal trends in CO₂ efflux across 24+ hour periods, continuous IRGA measurements were taken at a single location in a CTL plot at a ten-minute sampling interval for between 24 and 144 hours once per month in June-September 2018. An additional set of continuous gas flux measurements was made with two LI-COR IRGAs to investigate the contribution of plant roots to total CO₂ efflux in June and July 2019. These sets of measurements were made concurrently at a single location in a CTL plot and a single location in a NR plot over a 120-hour period, set to a ten-minute sampling interval.

Statistical analysis and annual summation

Loess, local polynomial regression fitting, was used to interpolate plot-level mean daily CO₂ efflux, which was then summarized by treatment between sampling dates for the time period spanning the end of 2017 through the end of 2018. Measured CO₂ efflux was first averaged by treatment for replicate plots, then loess CO₂ efflux models were fitted to each treatment. Estimated mean daily flux rates were extracted from loess regressions and summed to create annual treatment-specific values. The statistical significance of treatment was tested using two-sample t-tests at $p < 0.1$ and $p < 0.05$ significance levels for each treatment's mean daily CO₂ efflux estimate and standard errors were calculated by treatment and tested against CTL standard error.

Partitioning soil respiration components

I used two separate methods to investigate the question of SOM priming. The first was to partition the respiration components by source, using differences between annual respiration rates in addition and removal treatments compared with CTL. Annual litterfall was estimated

from the mean mass of litter removed from NL and NI plots between 2016 and 2018 ($293 \pm 29 \text{ g m}^{-2} \text{ y}^{-1}$) and the mean C concentration of needle litter ($459 \pm 3 \text{ mg C g}^{-1}$, reported in Pierson et al. 2021b). Following the methods of Sulzman et al. (2005), I calculated the carbon dioxide attributed to each source as follows:

Aboveground litter: Equivalent to long-term annual litterfall, $134 \text{ g C m}^{-2} \text{ y}^{-1}$

Rhizosphere respiration, R_r: No Roots mean annual R_s subtracted from Control mean annual R_s (CTL-NR)

Belowground litter: Aboveground litter C and mean rhizosphere respiration subtracted from total annual R_s (Total R_s - aboveground litter C - R_r)

Partitioning R_s components relies on a number of assumptions about SOC stores and the dynamics of litter decomposition. I assumed that SOC stores remain relatively constant over the short term and that annual aboveground litter inputs are equal to total respiration from decomposition of current litter and litter deposited previously across the years of experimental manipulation. I also assumed that severed roots surrounding trenched NR and NI plots were not contributing to respiration and that any root regrowth into those plots is minimal. Though I have not directly assessed this since the time of plot installation, I am confident that the combination of a 1-m deep trench around each plot, thick plastic lining, and soil backfilling remain effective against root intrusion. Sulzman et al. (2005) further corroborates this assumption, citing observations from DIRT plots in Pennsylvania - which were re-trenched 10 years after plot installation - indicate minimal root regrowth in that time.

Priming calculations and litter decay modeling

My second method to examine the question of SOM priming was to use litter decay models to assess the proportion of respiration that could be attributed to decomposition of the needle and woody litter added annually. Following the methods of Sulzman et al. (2005), I calculated the expected contributions to soil CO₂ efflux using the CO₂ efflux attributed to decomposition of aboveground litter each year over the twenty years since plot installation. I then calculated the difference between this expected R_s rate and the measured R_s rate for CTL, DL, and DW

treatments. For NL treatments, I subtracted the amount of litter C that was predicted to have been added under native conditions annually ($134 \text{ g C m}^{-2} \text{ y}^{-1}$). I used the SOC stocks reported in Pierson et al. (2021b) and litter decay models (described below) to predict the amount of additional SOC that could be expected annually given our double litter (double needle litter and double woody litter: DL and DW, respectively) treatments, and compared those estimates with measured values normalized to CTL values. I similarly used litter decay modeling to predict the amount of litter C that is predicted to have been excluded from NL treatments over two decades of sustained exclusions, and compared those with measured SOC values, again normalized to CTL. The same process was used to compare the amount of added or restricted C to soil CO_2 efflux expected due to each DW or DL addition, or NL removal treatment.

I calculated the CO_2 efflux expected from the amount of litter added to DL plots for each treatment year using a first-order decay model with a decay constant for needle litter in Douglas-fir-western redcedar assemblages at HJA. The same method was used for DW treatments, but a decay constant for Douglas-fir small branches (Fogel & Cromack, 1977) was substituted in the decay function. I ran each model over twenty years, iteratively adding or subtracting litter annually depending on the type of treatment (addition or removal).

Results

Seasonal and annual cumulative soil CO_2 efflux by treatment

Seasonal differences in mean soil CO_2 efflux resulted from both addition and exclusion treatments relative to CTL (Fig. 1.1a). Mean annual cumulative soil CO_2 efflux was greatest in DW and DL treatments (1511 ± 129 and $1414 \pm 132 \text{ g C m}^{-2} \text{ y}^{-1}$, respectively), followed by CTL ($1242 \pm 165 \text{ g C m}^{-2} \text{ y}^{-1}$), though on an annual basis, these treatment differences were not significantly different than the CTL efflux (Fig. 1.1b). In the exclusion treatments, NL, NR, and NI exhibited significantly less annual CO_2 efflux than CTL (827 ± 72 , 653 ± 76 , and $616 \pm 51 \text{ g C m}^{-2} \text{ y}^{-1}$, respectively). Statistical significance was tested at the daily level and summarized for visual display due to the distinct seasonality of differences between treatment levels (Fig. 1.1c).

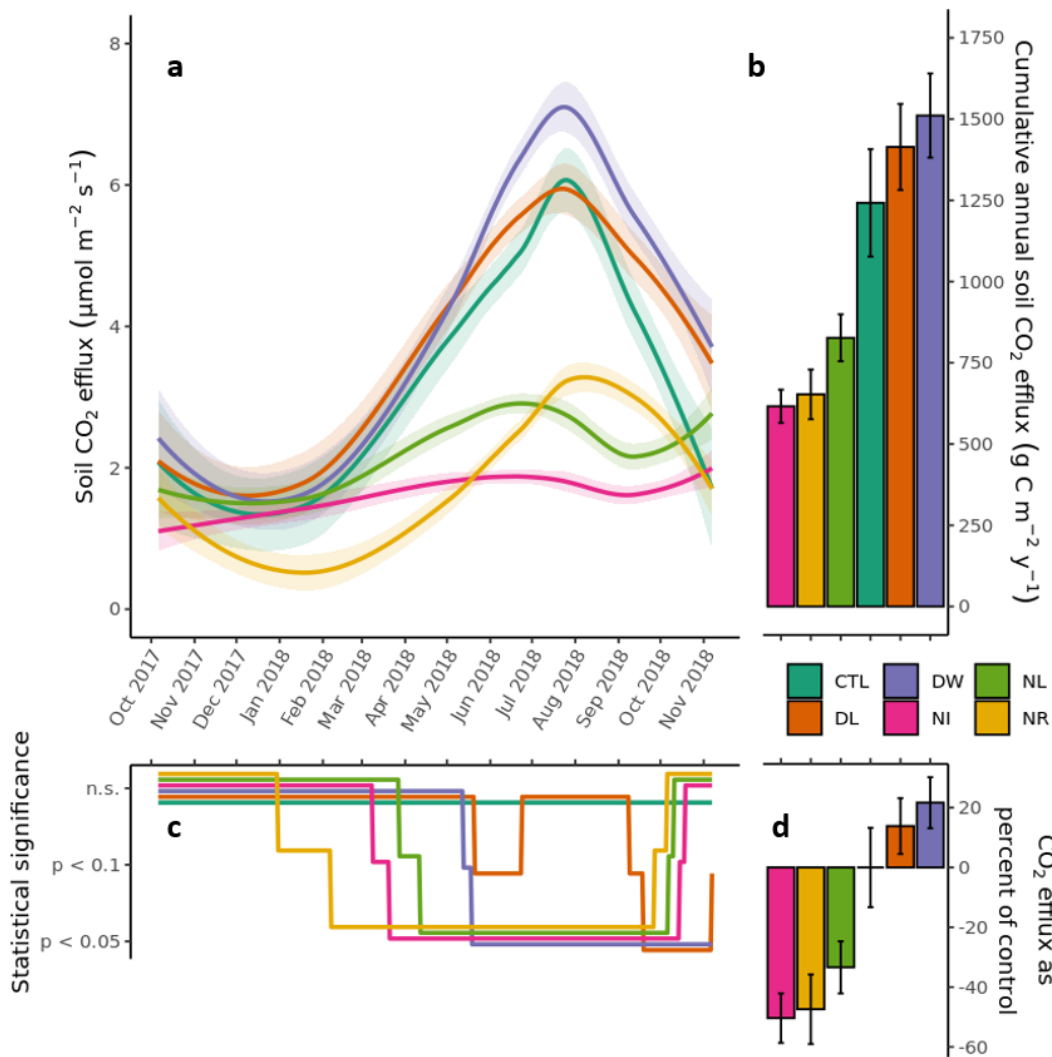


Figure 1.1 Seasonal and cumulative annual soil CO₂ efflux. CTL = Control, DL = Double Litter, DW = Double Wood, NI = No Inputs, NL = No Litter, NR = No Roots. **a** Soil CO₂ loss interpolated efflux shows significantly different seasonal patterns by treatment type (shaded area is one standard error of the mean), with addition treatments (DL and DW) following similar trajectory to CTL, while exclusion treatments (NI, NL, NR) display much lower efflux, particularly during the spring and summer seasons, than do the CTL or addition treatments (DW and DL). **b** Mean annual cumulative soil CO₂ efflux was greatest in DW and DL treatments followed by CTL, though these treatment differences were not significantly different than CTL efflux ($\alpha = 0.05$). In the exclusion treatments, NL, NR, and NI exhibited significantly less annual CO₂ efflux than CTL **c** Statistical significance of daily mean CO₂ efflux is aligned with timesteps in the ‘a’ panel plot of seasonal efflux. Individual t-tests compared mean daily soil CO₂ efflux of each treatment to control at $p < 0.1$ and $p < 0.05$ significance levels. Significance lines were jittered to avoid overlap such that the three statistical significance levels are N.S. (not significant), $p < 0.1$, and $p < 0.05$. **d** Each treatment’s cumulative soil CO₂ efflux is represented as percent of CTL with associated SE.

October through the end of December (2017) mean CO₂ efflux rates were not statistically significantly different between any treatments and CTL (paired t-tests, $p < 0.05$). In January through March, the NR treatment was significantly less ($p < 0.1$) than CTL and in April and May, NI and NL were also significantly less than CTL efflux ($p < 0.1$). Starting in mid-May and lasting through November 2018, DW efflux was significantly greater than CTL ($p < 0.05$). The DL treatment showed shorter periods of statistically significant difference from CTL, including the end of May through the end of June and then again in October through November 2018 ($p < 0.1$). During each of these periods, the DL treatment CO₂ efflux rate was greater than CTL, while between those months, DL efflux was about the same or even slightly less than CTL. The treatment that excluded both aboveground and belowground inputs, NI, showed the fewest seasonal changes in CO₂ efflux, and was significantly lower than the CTL efflux from mid-March through mid-October ($p < 0.05$). The NL treatment showed a similar trajectory to the NI treatment, but had a slightly shorter period of significant difference from CTL (April through early October; $p < 0.05$). The NR treatment showed a different seasonal trajectory, with a sustained low efflux until mid-late summer, when efflux surpassed the other exclusion plot (NI and NL) efflux rates from July until October 2018.

Contributions to total efflux by source

Major avenues for SOC inputs include aboveground forest detritus, belowground root exudates, microbial and fungal activity in the rhizosphere, and root sloughing. Here I differentiate among the Rs that results from aboveground litter decomposition, belowground litter decomposition, and the combination of root and rhizosphere activity.

The contribution of plot-level litter C, introduced by aboveground litterfall, was $134 \text{ g C m}^{-2} \text{ y}^{-1}$ based on the average amount of needle litter mass collected from exclusion plot screens in the study year 2017-2018 (Pierson et al., 2021b). This litterfall estimate is slightly less than Sulzman's reported long-term annual mean of $149.6 \text{ g C m}^{-2} \text{ y}^{-1}$ (average of 1976–1985 data for six locations within each of two old growth stands of the same species composition at the same

elevation as the DIRT plots) or Sulzman's plot-level litterfall of $153.1 \text{ g C m}^{-2} \text{ y}^{-1}$ measured from 2002 to 2003 (Sulzman et al., 2005).

Under the assumption that the equivalent amount of newly added aboveground litter each year is mineralized to CO_2 (i.e, C gains and losses are near steady-state in the short term), I attribute 10.8% of the total 2017-2018 efflux to the decomposition of aboveground litter (Fig. 1.2), a decline of close to 9% from the 2002-2003 value. My estimate of the functionally heterotrophic decomposition of belowground litter in 2017-2018 was about 16% less than the 2002-2003 estimate (41.8% vs. 58%). In contrast, my 2017-2018 functionally autotrophic root and rhizosphere contribution was much greater than the 2002-2003 estimate – 47.4% in 2017-2018 versus 23% in 2002-2003. Taken together, these values represent 77% in 2002-2003 and 53% in 2017-2018 attributed to functionally heterotrophic Rs sources with the remainder attributed to functionally autotrophic sources.

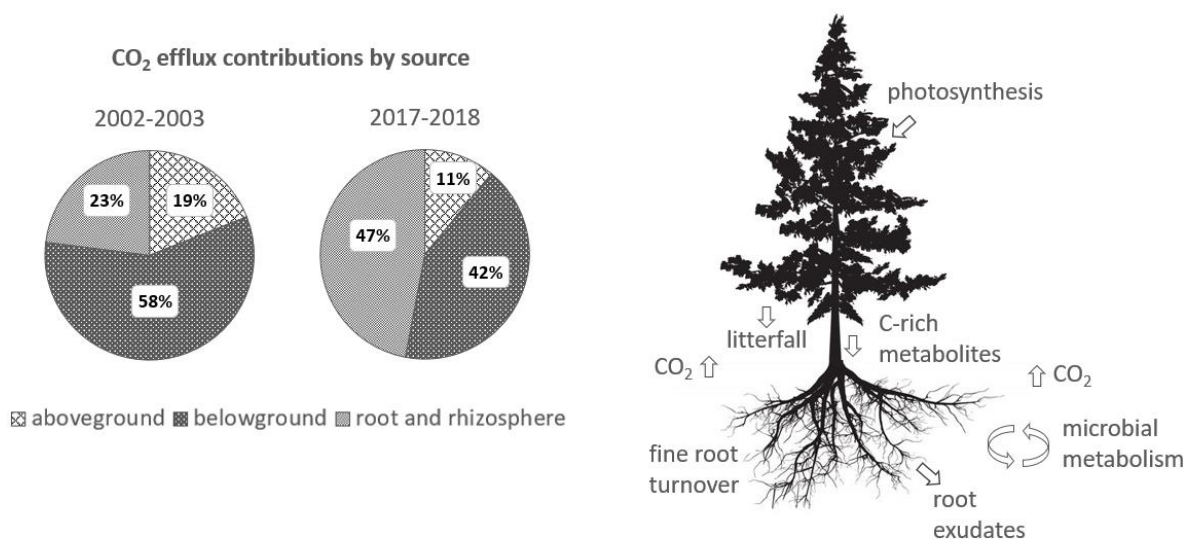


Figure 1.2 Partitioned contributions of functionally heterotrophic (litter decomposition from aboveground and belowground sources) and functionally autotrophic (root and rhizosphere) sources to total soil respiration in 2002-2003 (data from Sulzman et al., 2005) and 2017-2018. Pathways for C transfers among pools and avenues for CO_2 respiration are shown on the schematic diagram on the right side.

Comparisons between expected and observed respiration and SOC

I calculated differences between measured and expected soil CO₂ efflux and changes in SOC after two decades of litter additions or removals for DW, DL, and NL treatments. SOC values that resulted from litter decay modeling were considered to be the amount of C added by decomposition of the annual litter additions or equivalent C removed on a per mass basis, according to treatment type. In the DL treatment, the measured Rs was 1418 g C m⁻² y⁻¹, while the predicted Rs was 1393 g C m⁻² y⁻¹, which, when subtracted from the CTL Rs, represents 18.4% more than expected Rs due to the addition treatment over two decades (Fig. 1.3). The DW treatment showed a much greater increase in Rs than predicted, representing 131.9% more Rs than expected, while NL Rs was much lower than expected (832 g C m⁻² y⁻¹ measured and 991 g C m⁻² y⁻¹ predicted), representing 59.5% more CO₂ loss than expected. At the same time, SOC gains due to the addition treatments were greater than predicted, with 133.9% more SOC than predicted in the DW and 122.7% more in the DL treatment. In the exclusion treatment, I found 15.6% more SOC in the NL treatment than expected based on the amount of litter C excluded over two decades (Fig. 1.3).

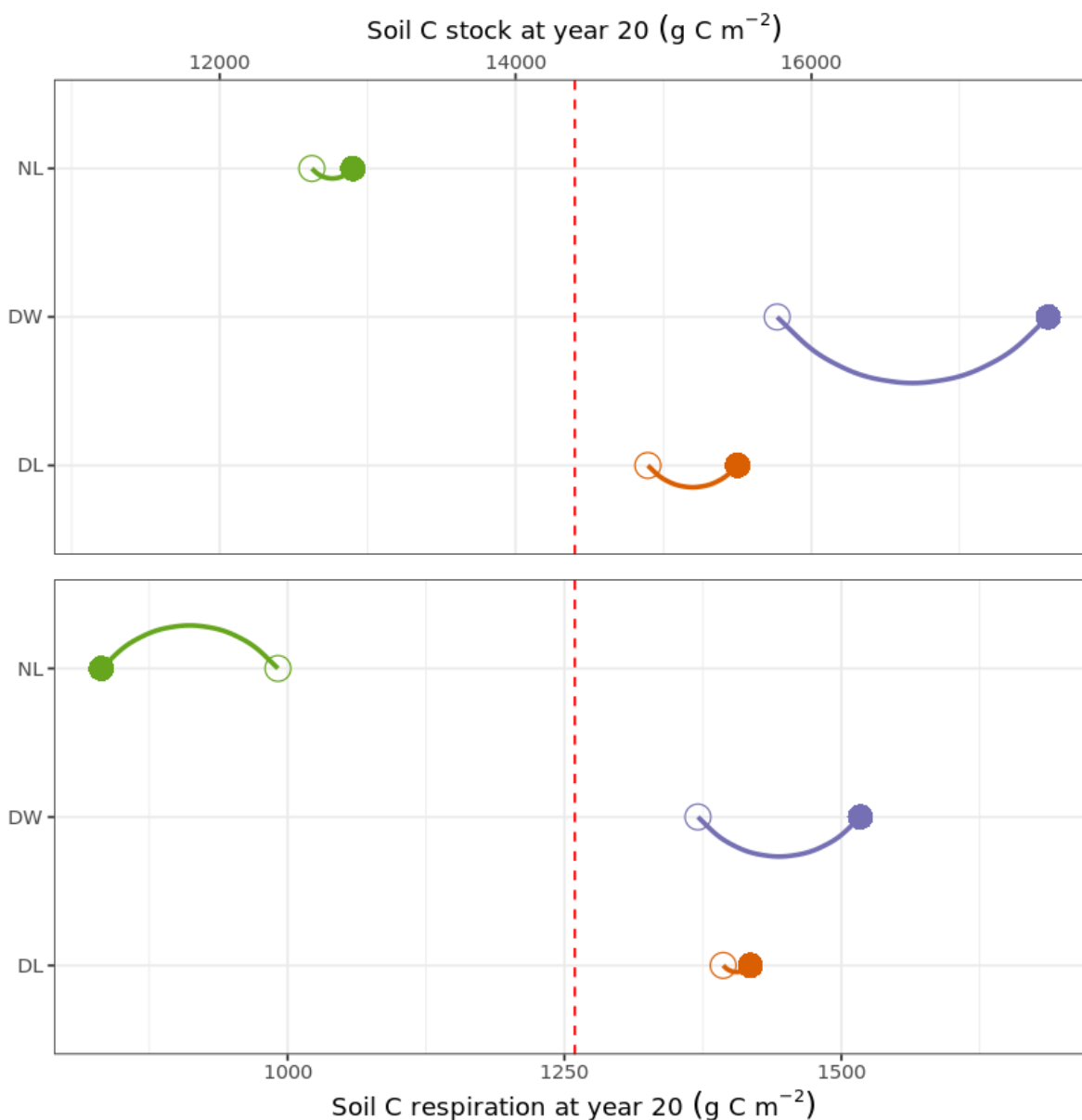


Figure 1.3 Litter decay modeling results for measured and predicted SOC and Rs by treatment. Open circles represent predicted SOC (top) or Rs (bottom) values based on litter decay modeling for additions or removals of needle litter or woody detritus. Filled circles represent measured values of SOC or Rs. Green represents NL, orange represents double litter, and purple represents double wood. The red dashed line represents CTL SOC stock or respired C, respectively. These predictions account for g of C added or removed from a given treatment over the 20 years of sustained detrital manipulations. The DW and DL (addition) treatments showed both greater Rs and greater SOC stock than the predicted value, while the NL (removal) treatment showed greater SOC stock but less Rs than the predicted value.

Discussion

Effects of two decades of root exclusion on Rs

My first hypothesis - that the loss of live roots would cause cessation of SOM priming - was supported. Treatments which excluded belowground, root-derived C inputs (NR) exhibited highly suppressed Rs rates relative to CTL regardless of season (Fig. 1.1a). While living trees provide a consistent supply of metabolites to the rhizosphere through root exudates, trees that were girdled at experiment inception and that have been dead for close to 20 years likely have highly suppressed rhizosphere microbial activity, as evidenced by lower rates of soil CO₂ evolution. Similarly, treatments which excluded aboveground and/or belowground litter C inputs (NI and NL) exhibited low Rs rates across seasons relative to CTL. The lack of a fresh supply of C has likely led to a decrease in overall decomposers, as well as decreases in soil microbial community abundance and activity under each exclusion treatment.

Changes in proportions of Rs contributions over time

Two decades after initial experimental treatments were applied, the contribution of root and rhizosphere Rs to total Rs is much greater, while the proportions of aboveground and belowground decomposition of litter are contributing less to total Rs. This suggests that some of the effects of global change on forest C cycling are already being realized in this late successional forest ecosystem, potentially driving faster C cycling rates through C fixation and decomposition, stimulating additional root growth and microbial and fungal C processing. Additional evidence resulting from litter decay modeling, discussed below, supports this assertion.

At another DIRT site, Bowden et al. (1993) reported a root and rhizosphere contribution of 33% in the mixed deciduous hardwood of Harvard Forest, though pine forests often show greater rhizosphere respiration – between 47 and 62%. Studies in highly productive coniferous forests that resemble our study site have reported a wide range in rhizosphere contributions to total Rs, but these estimates often represent a greater contribution to total Rs than in other systems,

perhaps due to the presence of extensive mycorrhizal fungal networks in these ecosystems (Phillips et al., 2012). Sulzman's 2002-2003 estimate (23%; Fig. 1.2) of the contribution of root and rhizosphere respiration to the total CO₂ efflux was lower than the majority of published values in similar coniferous forests, while my 2017-2018 estimate (47%) falls within the (albeit wide) range of published estimates. A statistical model based on 31 field studies predicts rhizosphere contributions of 30–50% for our site (Bond-Lamberty et al., 2004, reported in Sulzman et al., 2005), which is in agreement with my estimate.

In a more recent meta-analysis of studies from a global soil respiration database, Bond-Lamberty et al. (2018) demonstrated that the heterotrophic component of Rs is increasing. They report that the ratio of heterotrophic Rs to total Rs increased significantly between 1990 and 2014, from 0.54 to 0.63, acknowledging that while the heterotrophic Rs response to ongoing changes in temperature, precipitation and organic matter input to soils remains uncertain, an increasing ratio of heterotrophic Rs to total Rs could be due to rising SOC losses and thus a climate feedback, and/or increasing GPP rates enhancing detritus inputs and thus counterbalancing C losses from SOC. Evidence from our experiment points to both phenomena happening, but we additionally posit that past experiments may have significantly underestimated the functionally autotrophic (root and rhizosphere) component of Rs.

Is priming still happening after two decades of sustained litter additions?

My second hypothesis was that SOM priming is a short-lived phenomenon and that a new equilibrium state would be reached after two decades of sustained needle litter additions. Evidence from in-situ Rs measurements strongly suggests that priming is not currently happening and that it is indeed a short-lived phenomenon, but that the rate of C cycling in this highly productive temperate coniferous forest has increased such that any additional C added via needle litter inputs is quickly utilized in microbial metabolism. Although there were slight increases in Rs beyond the C amount added in DL treatments, there were compensatory gains in SOC relative to the CTL treatments (Fig. 1.3).

It remains possible that our estimate ($134 \text{ g C m}^{-2} \text{ y}^{-1}$) of aboveground litterfall may be somewhat underestimated due to the restricted area of the plots. Sulzman et al. (2005) estimated greater ($153.1 \text{ g C m}^{-2} \text{ y}^{-1}$) aboveground litter contributions from this site and reported a long term mean annual litterfall estimate of 149.6 g C m^{-2} from a nearby site. If our litterfall estimates are indeed underestimates, our measured proportion of DL Rs to the amount of added litter C would be even less, indicating the potential for additional soil C storage. A demonstrated potential for these forests to continue accumulating SOC with added detritus inputs, particularly woody inputs, is corroborated by Pierson et al.'s (2021b) suggestion that mineral surfaces have not reached a saturation point and instead have continued potential to bind additional C compounds.

I explored multiple avenues when investigating the question of soil organic matter priming, and none provided evidence that priming was still happening after two decades of sustained litter additions. Given that my DL mean annual Rs was only slightly greater than the C attributed to the added litter over two decades, and that the SOC stock was slightly increasing at the same time (Fig. 1.3), changes in Rs rates can be explained by the effects of detritus addition treatments on soil moisture availability rather than any increased microbial metabolism of mineral-associated SOC. This suggests that priming is a short-term phenomenon and that perhaps there is a point at which the microbial community adjusts to the relative abundance of litter C rather than attempting to metabolize older/more complex (previously mineral-associated) SOC sources.

Seasonal and diurnal trends in Rs

Diverse biotic and abiotic factors influence the seasonality of the Rs response (e.g. soil temperature, soil water availability, plant phenology, root activity, and C availability and form as litter and root substrates; Lloyd and Taylor, 1994; Davidson et al., 1998; Subke et al., 2006; Savage et al., 2013; Han and Jin, 2018; Mäki et al., 2022). Because these factors can interact at different temporal and spatial scales, disentangling specific drivers of Rs responses can prove difficult. At a seasonal scale, there may be a more predictable temperature-driven response for heterotrophic Rs (i.e., Q_{10} value, the coefficient for the exponential relationship between soil respiration and temperature, multiplied by ten), while plant water status, as a function of soil

moisture, may primarily drive autotrophic R_s . Plant water status varies not only seasonally, but also on a diurnal timescale in response to relative humidity, solar radiation, and soil moisture. Stomatal conductance is a tightly regulated response to water stress (i.e., trees closing stomata to retain moisture), and because water flux and C flux are functionally interconnected, stomatal opening or closure will influence root and rhizosphere R_s over a diurnal period. Indeed, midday depression in both broadleaf and conifer tree species' transpiration and photosynthesis -- resulting from reduced stomatal conductance and associated with timing of the largest daily vapor pressure deficit -- is well-documented (Gao et al., 2002; Johnson et al., 2009).

When I measured CTL R_s continuously (at a 10-minute sampling interval) in June and July 2018, I found differing diurnal trends that may be explained by the seasonal availability of soil moisture and timing of daily photosynthetically active radiation (PAR) extrema (Fig. 1.4). Across ecosystem types, diurnal trends in R_s are well-documented -- where nighttime low air temperatures and lack of solar radiation drive low R_s rates and R_s increases exponentially throughout the day as air temperatures increase and plant and microbial activities increase. However, I was surprised to find a significant midday (~14:00 H) dip in R_s that happened consistently across multiple days in summer months (Fig. 1.4c). This dip manifested as a rapid drop in R_s , often to a nighttime-equivalent low, followed by a rapid R_s increase to a peak often equivalent to, or greater than, the earlier afternoon peak before R_s dropped quickly again into the nighttime. The second peak after the afternoon low typically occurred around 20:00 H, suggesting that there may be a slight lag time between plant assimilation of photosynthates and R_s . There is seemingly a high degree of temporal correlation between the timing of plants closing stomata to prevent desiccation in high temperature, high vapor pressure deficit conditions, and a sudden drop in R_s . The July R_s sampling occurred near peak seasonal PAR and near the seasonal low for soil moisture, while the June sampling took place before peak PAR and while there was still plant-available soil moisture (Fig. 1.4a-c).

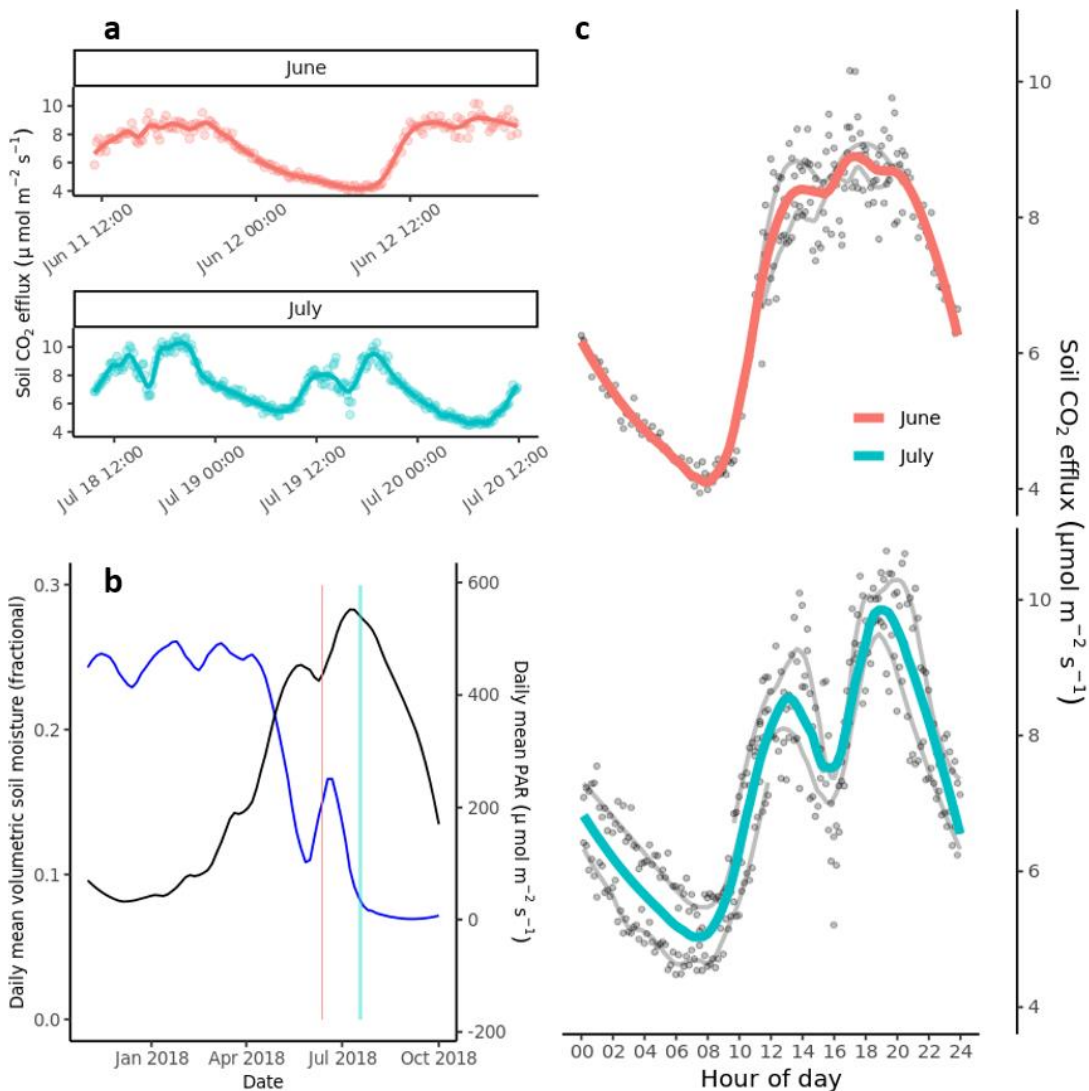


Figure 1.4 Seasonal and diurnal trends in environmental covariates and Rs **a** CTL plot CO₂ efflux across multiple days in June and July plotted as points overlaid with a loess function, demonstrating a clear midday dip in Rs in July that is not present in June. **b** Photosynthetically Active Radiation (PAR) and volumetric soil moisture measured at a nearby meteorological station (HJ Andrews PRIMET) plotted as daily means across one year, showing seasonal changes that may drive Rs responses. Timing of diurnal Rs measurements are indicated by the colored vertical bars and indicate that the July Rs sampling occurred near peak seasonal PAR and near the seasonal low for soil moisture, while the June sampling took place before peak PAR and while there was still plant-available soil moisture. **c** Multiple days of 10-minute sampling interval CO₂ efflux overlaid by hour of the day for each of June and July. Gray lines represent a loess function for each sampling day, while colored lines represent loess functions applied to each monthly set of data. Across multiple days, the July data demonstrate a highly consistent daily midday dip in CO₂ efflux, while the June data show typical midday variance but no pronounced dip.

To examine whether this diurnal trend could be related to plant metabolic activity, I measured diurnal respiration in both a NR plot and CTL plot at the same time (Fig. 1.5). I hypothesized that the lack of live trees and live roots would lead to not only an overall reduction in R_s , but also the lack of a midday drop in R_s . Over multiple sampling events of consecutive days of R_s in CTL and NR treatments, I found convincing evidence that the midday R_s dip is very likely related to plant metabolic activity/current plant water status, as a midday dip was not present in any of the NR diurnal data (one representative diurnal sampling event shown in Fig. 1.5).

Other studies have reported a similar midday depression in R_s , though to the author's knowledge, none have shown such a large magnitude of suppressed midday R_s as the current study, and most report a greater lag time between canopy photosynthesis and root respiration (on the order of days rather than hours). In a study of spatial and temporal variation in R_s in a seasonally dry tropical forest in Thailand, the authors describe a midday depression in R_s during the dry season but not the wet season (Adachi et al., 2009). They report a midday depression of, at most, 42% between 0600 and 1400h. In a temperate coniferous forest in central Japan, Makita et al. (2018) report July and August midday declines in R_s even as air temperature increases, which they attribute to times of high temperature stress and a consequent decline in C supply to the root system.

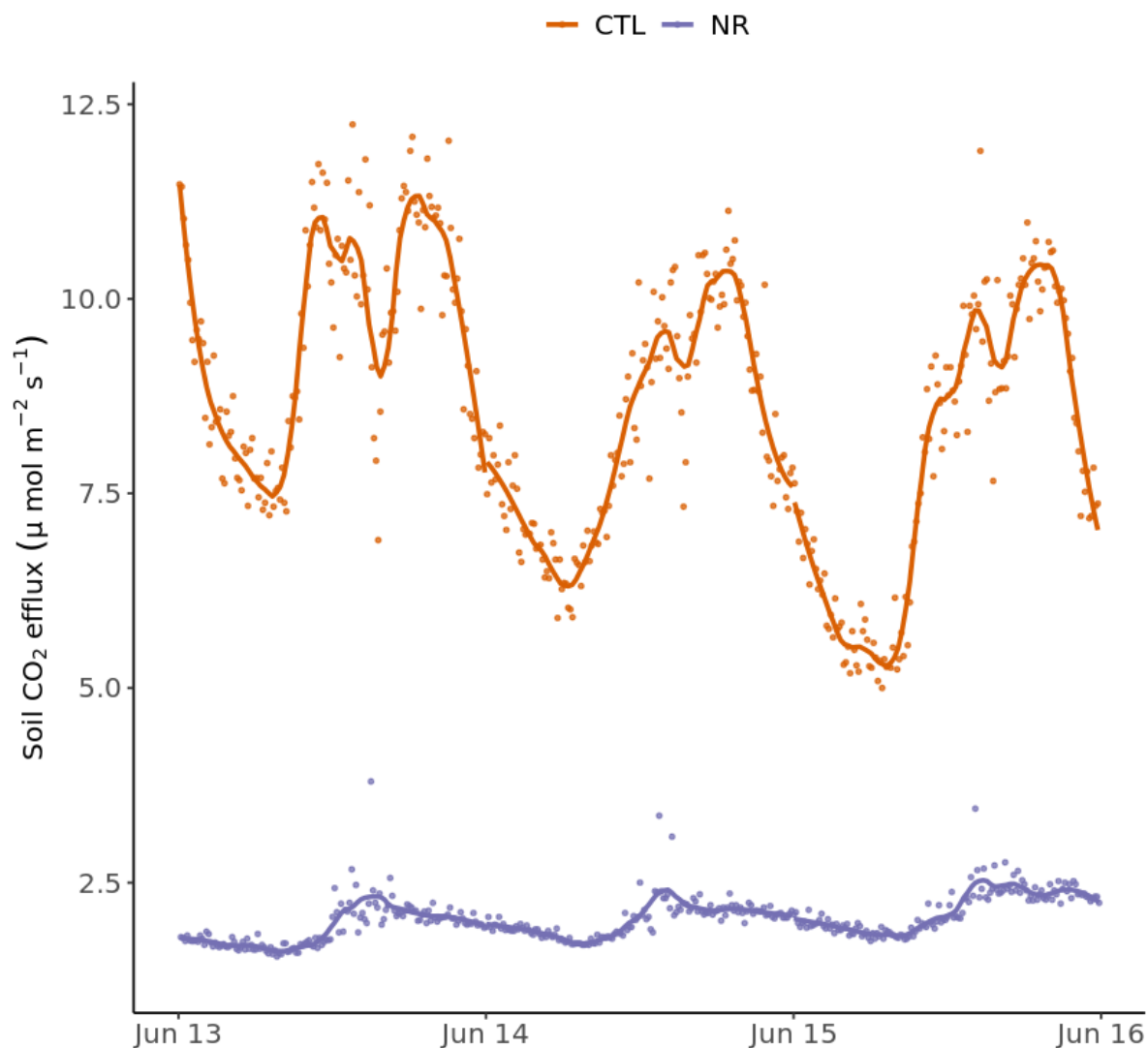


Figure 1.5 Concurrent CO₂ efflux measurements at 10-minute intervals from CTL and NR plots in June 2018. A significantly different diurnal curve over successive 24-hour periods is evident between the two treatments. While NR flux was always less than CTL, both initial peak effluxes aligned in the midafternoon, but Rs patterns then diverged. In the CTL plot, an initial midafternoon peak was followed by an immediate decrease and subsequent peak that was either adjacent to, or greater than, the initial peak. Over each diurnal period, the NR plot demonstrated a morning low climbing to an afternoon peak, then a subsequent steady decline overnight to the next morning's low.

A pulse-labeling experiment on photoassimilates and respiration in grassland soils demonstrated that, under sunny conditions, labeled C compounds were transported and respired belowground within two hours (Bahn et al., 2009). Similar studies in low-lying vegetation have shown comparably fast transfer of C from aboveground to roots (Johnson et al., 2002; Carbone & Trumbore, 2007). However, studies of tree (*Populus* and *Pinus* spp.) C transfer to roots and subsequent soil respiration have shown transfer rates on the order of two to ten days (Horwath et al., 1994; Andrews et al., 1999; Mikan et al., 2000; Ekblad & Högberg, 2001). A three-year study in western Oregon's coniferous forests showed a strong link between VPD 5-10 days earlier than ¹³C-labeled CO₂ respiration, but suggested that lag times varied in response to environmental variables (Bowling et al., 2002). They found a strong correlation between precipitation during the month preceding sampling, leaf predawn water potential and soil water content. In a more recent long-term study of continuous R_s measurements in a Missouri forest, Liu et al. (2020) found that GPP regulated R_s with monthly mean time lags that varied between four to twelve hours, and that variation could be explained by past trajectories of moisture and temperature. Given the diversity of influences on plant photosynthesis and respiration, it remains likely that multiple time lags, rather than a single lag, are possible between photoassimilation and root respiration in a given forest. The rapid R_s response I found, that correlated with times of high plant water stress, is likely one of many lag responses to canopy conditions and a suite of environmental variables.

Constraints imposed by changes in soil moisture availability

Multiple distinct lines of evidence point to soil moisture availability as the most limiting factor for total soil R_s in this system at both diurnal and seasonal scales. At a seasonal level, soil moisture availability seems to be principally modulated by SOC content, while trees modulate soil moisture at a diurnal scale through transpiration and plant water flux. Added needle litter and woody detritus build up the organic soil horizon, acting as a buffering layer between the mineral soil and atmosphere. This additional organic matter helps retain more soil moisture, effectively extending the growing season for vegetation. This is evidenced by the August through November elevated soil CO₂ efflux in the DL and DW treatments compared with the CTL efflux (Fig. 1.1).

May through July efflux is also elevated in the addition treatments relative to the CTL, suggesting that the buffering effect occurs both before and after the seasonal peak respiration.

Additional support is provided by Pierson et al. (2021b), who found measurable decreases in bulk density in DW treatments after two decades of sustained woody detritus inputs (mean soil bulk density in the DW treatment was $0.5 \pm 0.08 \text{ g cm}^{-3}$, compared to $0.6 \pm 0.08 \text{ g cm}^{-3}$ in the CTL). The mineral soil profile from 0-100 cm in the DW treatment demonstrated increases in mean SOC compared with the CTL mineral soil profile, with mean SOC increases of 24% and 54% measured in 0–10 and 10–20 cm depths, respectively. The mass of surface litter (organic soil horizon) increased by 61% from the DW treatment relative to the CTL ($p < 0.04$), while surface litter accumulation from the DL treatment was relatively minimal, with a non-significant mean difference of +15% ($p < 0.92$; Pierson et al., 2021b). These changes in DW treatment soils relative to CTL and DL soils lend additional support to the premise that this treatment is both gaining more SOC while respiring more CO_2 and suggests that NPP has increased due to the DW treatment but not the DL treatment.

The DW treatment especially, and DL to a lesser extent, effectively extend the growing season longer into the dry season by retaining more soil moisture, as evidenced by the more gradual incline to a June/August peak R_s , and a longer tail following that peak (Fig. 1.1). Seasonal differences in R_s and litter decay modeling suggest an overall increase in NPP in this system over two decades of sustained litter additions (Fig. 1.3). Increases in SOC were greater than predicted given the amount of litter added, while at the same time, R_s was greater than predicted. This corroborates Pierson et al.'s (2021b) suggestion that mineral saturation has not yet occurred in this ecosystem, and that there is potential for additional stabilization of SOC on mineral surfaces.

In the early years of this experiment, Sulzman et al. (2005) found weak to nonexistent relationships between soil moisture and respiration and only a slightly stronger correlation with

soil temperature, suggesting that other drivers such as plant phenology and litter quality, and combinations of drivers that include interactions between these and soil moisture and temperature may be better predictors of soil respiration in this ecosystem. Sulzman reported in the early 2000s that volumetric water contents remain at or near saturation in winter months at the DIRT site, indicating that diffusion of CO₂ through soil pores will be highly reduced during those months, resulting in lower Rs rates across all treatments as a function of both lower diffusion and the cooler temperatures that may inhibit microbial activity. Two decades later, my Rs trends follow a similar seasonal pattern across treatments – with highly suppressed winter Rs that is especially pronounced in the NR treatment (Fig. 1.1a).

The somewhat surprising seasonal respiration trend in the NR treatment, where Rs is lower in the winter months compared with all other treatments, but greater Rs in late summer/early fall than the other exclusion treatments (NI and NL), may point to the significant contributions to total Rs from seasonal responses of root and rhizosphere Rs, but also to the potential shifting of microbial metabolism due to changes in resources in the NR plots (Fig.1.1a). Pierson et al. (2021a) reported increases in the more stable form of SOC (mineral-associated organic matter, or MAOM) in the NR plots after two decades of restricted root inputs and suggested that these unexpected gains may be due to the microbial community continuing to metabolize dead roots that persist in these plots. If this is indeed the case, the elevated late summer/early fall NR Rs relative to other exclusion treatments may be a result of the warmer temperatures and relative availability of soil moisture providing ideal conditions for microbial and fungal decomposition of dead roots, while the live roots in the NL plots may be suppressing Rs longer into the fall by taking up any available soil moisture for tree growth and maintenance, and NI treatments are likely experiencing a lack of buffering against temperature and moisture extremes due to the combination of restricted aboveground and belowground inputs and the resultant lack of SOC. Indeed, the NI treatment shows a remarkably steady low CO₂ efflux rate across all seasons (Fig. 1.1).

Other avenues for SOC loss

Given that Pierson et al. (2021b) found that additional detrital litter inputs did not significantly increase SOC stocks in the mineral soil, we provide evidence that this additional litter was relatively quickly metabolized by soil microbes and respired as CO₂. Other avenues for C loss, such as by erosion, wind, or buildup on the soil surface were refuted by Pierson et al. (2021b). Another recent study that measured DOC transport within HJA DIRT plot soils concluded that DL and CTL plot DOC loss did not significantly differ from one another, so it remains unlikely that the additional C in DL plots was lost via DOC leaching (Evans et al., 2020). Previous DIRT site studies also indicated that the DOC leaching component was minimal (Yano et al., 2004; Lajtha et al., 2018).

SOC mineralization as a function of environmental change

Global rises in Rs over recent decades point to sustained SOC losses stimulated by environmental changes that are likely to accelerate with continuing climate feedbacks (Bond-Lamberty & Thomson, 2010; Hashimoto et al., 2015, Bond-Lamberty et al., 2018). Ecosystem changes resulting from increasing air temperatures and changes in seasonal moisture regimes have differing effects on the decomposition processes that affect SOC stabilization and destabilization. For example, changes in tree stomatal conductance in response to moisture limitation affect allocation of photosynthates to roots, in turn influencing root respiration as well as the availability of root exudates to rhizosphere organisms. Climatic shifts that influence the seasonality of moisture will not only result in nonlinear responses to MAOM stability (Heckman et al., 2023), but also the resulting Rs from destabilization of that MAOM.

The nonlinearities that exist among C inputs, ecosystem processes, SOC, and Rs are difficult to represent in process-based forest C cycling models. The assumption that accounting for the quantity and quality (physicochemical properties) of organic inputs will lead to accurate predictions of SOC is continually shown to be an oversimplification (Pierson et al., 2021). At the same time, the avenues by which C is stabilized in soils (i.e. organo-mineral complexation and electrostatic interactions) are not simply reversed to destabilize that C (Bailey et al., 2019);

mineralization of SOC to CO₂ is more nuanced at fine spatial and temporal scales and in response to diverse environmental and physiological drivers. Additionally, changes in seasonal water availability will influence NPP and, in turn, Rs, impacting the ability for forests to act as either sinks or sources of C. I provide evidence that the impact of water availability on C cycling - and particularly on those processes that influence SOC destabilization and Rs - in this temperate PNW forest is likely significantly more than is accounted for in current forest soil C cycling models that are primarily focused on substrate quantity and quality (e.g., Klopatek, 2008), and that those effects can be seen on seasonal and diurnal timescales.

Conclusion

As this region continues to experience intensifying effects of climate change, seasonal moisture limitations are likely to become more pronounced, further limiting NPP and resulting in suppressed Rs because moisture limitations will outweigh any increased microbial and fungal decomposition. However, sustained woody detritus inputs, added at a rate greater than the natural turnover of woody forest biomass, may buffer this effect by increasing the organic soil horizon and retaining more soil moisture during shoulder seasons when trees may otherwise be moisture limited. Though I provide evidence that SOM priming from added litter is no longer occurring in this system, Rs responses to climate changes will be varied due to its disentangled drivers but will most likely follow changes in NPP as a function of soil moisture and the resulting effects on root and rhizosphere activity.

CHAPTER 2: Vegetation and topography as competing drivers of soil C distribution and persistence in HJ Andrews' mid and high elevations

Introduction

Pacific Northwest (PNW) coniferous forests contain vast amounts of above- and belowground C in vegetation and soils. However, estimates of above- and belowground C vary widely across the literature. Estimated soil C stocks to 1 m depth across PNW coniferous forests from one study ranged from around 200 Mg ha⁻¹ to close to 500 Mg ha⁻¹ depending on climate gradients that follow elevation. In that study, C stocks in aboveground living and dead biomass, including the forest floor, were 100 to 260 Mg ha⁻¹ (Gray et al., 2016). Another study estimated total ecosystem carbon (TEC) between 185 and 1200 Mg ha⁻¹, where an average of 63% of that total was in vegetation, 13% in woody detritus, 3% in the forest floor, 7% in the 0–20 cm mineral soil, and 13% in 20–100 cm mineral soil (Homann et al., 2005). A study of PNW forest C in the early 2000s estimated the upper bounds on C storage based on field data of 43 old-growth forest stands across Washington and Oregon (Smithwick et al., 2002). The researchers estimated TEC to 1 m and 50 cm soil depths to distinguish the faster cycling C pools (50 cm to surface) from the slower cycling pools (1 m depth). An area-weighted average for the PNW TEC storage to 1 m was 671 Mg C ha⁻¹, while the area-weighted TEC to 50 cm depth was 640 Mg C ha⁻¹. In that study the Oregon Cascades contained above average TEC: 829 Mg C ha⁻¹ down to 1 m depth and 806 Mg C ha⁻¹ down to 50 cm. While aboveground C stocks in cool, temperate, moist forests such as those of the PNW are a fraction of those in tropical forests (28.5 and 152 Pg C, respectively), belowground C stores are second only to those in Boreal moist forests (210 and 357 Pg C, respectively; Scharlemann et al., 2014). However, spatial heterogeneity in these forest soils is such that field-level estimates are difficult to extrapolate to landscape-scale estimates, as exemplified by the wide range in C estimates above. Drivers of fine-grain variation in soil C are complex and likely differ from drivers of variation at larger scale. There remains a need to identify the mechanisms that determine distribution and retention of SOC in complex terrain that is home to forests known to hold some of the largest terrestrial soil C stocks.

Given that the Pacific Northwest's sizeable soil C pool is highly heterogenous, there is great potential for improvements in estimates of the finer scale spatial distribution of this soil C, in addition to estimates that go beyond bulk soil C and account for the different soil density fractions – mineral associated organic matter (MAOM) and free particulate organic matter (POM). These soil density fractions represent soil C fractions with different turnover rates and a range in resistance to decomposition. POM includes lighter density particulate organics (fragmented plant material), while MAOM is dense material adsorbed to or occluded in microaggregate structures with minerals (Wagai et al., 2020). MAOM-C is the most likely to be better protected from microbial decomposition (although this does not indicate outright chemical recalcitrance) and corresponds to a more slowly cycling C pool (Sollins et al. 2006; Lavellee et al. 2020; Heckman et al., 2022). Due to differences in physical and biochemical properties, these fractions will likely respond differently to environmental drivers and to drivers at different scales. Fine-scale interactions among plants (especially plant roots), soil organisms and minerals help dictate the potential for organic matter sorption and retention, while larger-scale factors like climate and topographic gradients may influence turnover and decomposition of vegetation. Importantly, it has been shown across studies and diverse ecosystems that the majority of MAOM results from microbial processing, and that root exudates serve as a main nutrient substrate for the microbial metabolism that produces those organic compounds that then sorb to minerals (Sollins et al. 2006; Lavellee et al., 2020). The difference, then, in spatial distribution of POM and MAOM C pools may give insight into the biogeochemical drivers that are acting in different topographic positions under different vegetation assemblages.

HJ Andrews Experimental Forest (HJA) exhibits the complex topography and diverse site history typical of Oregon's western Cascades, with steep terrain carved out by glaciers and mass wasting events. It has a varied fire history, with periods of cultural burning lasting into the early 1900s and periods of fire suppression until the early 1980s. Meadows were likely used for sheep grazing during certain historical periods as well. Though there has been some forest encroachment on these meadows, many persist, acting as refugia for pollinators and a diversity of species (Popenoe et al., 1992; Miller and Halpern, 1998; Griffiths et al., 2005).

The complex landforms and landscape features coupled with the land management history (i.e., regions of forest harvest and long-term experimental plots) in HJA cause substantial spatial heterogeneity in aboveground biomass. Large storm events primarily topple larger (older) trees on ridges and upper slopes. Soils in these landscape positions are typically thinner, making them quickly saturate from precipitation and causing trees in those positions to be more vulnerable to disturbance events (Lal, 2005; Overby, 2003). The tallest trees on ridges may be exposed to greater risk from lightning strikes, greater wind gusts, and more snow accumulation, resulting in shorter trees dominating high elevation ridgelines. Tall trees tend to dominate low elevations along valleys because waterways carve out valleys and bring nutrients that then accumulate and build thick soil profiles (Griffiths et al., 2009). These areas tend to be less vulnerable to the moisture limitations of ridges and steep slopes and are more protected from strong winds, so trees in these areas can maximize growth based on available solar radiation. High density young forest stands exhibit characteristics similar to those of mature forests, like closed canopies and high leaf area index (Zald et al., 2016). However, recently disturbed forests have higher nutrient availability than undisturbed forests which has been shown to cause a shift in C-allocation from below- to aboveground; therefore, younger stands should negatively correlate with soil C accumulation (Johnson et al., 1982). As vegetative growth is limited by photosynthetic capacity, S- and W-facing slopes that have greater exposure to solar radiation may result in greater overall biomass (denser stands of smaller trees, but not necessarily more tall trees). However, as slopes steepen, this pattern may diminish since trees will experience greater susceptibility to wind and erosion and more tree mortality. Soil C allocation from above- and belowground sources may become temporally and spatially decoupled from plant metabolism and vegetative decomposition on certain landscape features such as steep slopes, where erosion is a fundamental process. Therefore, plant productivity and soil C pools (POM, MAOM, and bulk SOC) may respond differently to temperature-moisture gradients across topographic features.

An exploration of the spatial scale of variation in forest aboveground living C (ALC) density was performed in HJA using 2008 LiDAR integrated with 702 field plots to map forest ALC density at 25 m grain (Zald et al., 2016). The researchers found that, unsurprisingly, timber harvest was

the most important driver of ALC. Young managed forest stand density was driven by factors influencing site productivity, while old unmanaged forest stand density was driven by site productivity factors and finer scale topographic conditions. A similar study was performed in 2012 in HJA using the same LiDAR and assessed the variation in soil C stocks as predicted by stand dynamics and environmental drivers (Seidl et al., 2012). The researchers used a high-resolution simulation model of landscape dynamics and found that about half of the variation in C stocks was explained by a combination of environmental drivers, while most of the remaining variability was explained by stand structure and composition. Griffiths et al. (2009) studied topographic effects on forest soils by sampling and characterizing 184 sites across HJA. They found that increased elevation strongly correlated with increased soil moisture and increased soil organic matter, and that increase was likely driven by increased precipitation and decreased decomposition rates, but that SOM accumulation on N-facing slopes may be the result of both decreased decomposition rates and increased primary productivity. Elevations were binned into low (<1000 m), medium (1000 – 1500 m), and high (>1500 m) classes and SOM ranged from 18.7% in the low elevation class to 33.2% in the high elevation class. Lower elevation sites tend to exhibit higher productivity than high elevation sites due to the availability of water and the more favorable temperatures for growth. This means that large aboveground biomass does not necessarily correlate with large belowground C stocks, since regions of highly productive forest require a substantial nutrient pool to draw from, and this nutrient pool is made up of decomposing organic matter that releases CO₂ as it is broken down.

The studies outlined above point to the potential for LiDAR data to be used in combination with other spatial and climate data to quantify SOC at meso spatial scale (~1-10 m). If landscape features that can be determined from geospatial data co-vary with stand density and environmental variables, it may be possible to quantify SOC at finer resolution across complex mountainous landscapes. My goals were to assess the relative importance of SOC drivers at 1-10 m scale and to describe how those drivers affected SOC persistence across varied landscape positions and distributions of aboveground biomass. I planned to then use relationships among the most important SOC predictors to then map SOC distributions across HJA, and to compare

my estimated SOC to coarser resolution publicly available SOC datasets (see Chapter 3 for the mapping components and comparisons with landscape scale datasets).

My main research question was: What are the spatial patterns in total soil C, MAOM, POM, and C:N, and how do those relate to the large-scale drivers of vegetation and topographic position?

Hypotheses

- 1) I hypothesized that SOM on ridges and peaks would contain a greater proportion of POM-C:MAOM-C, and that SOM in valleys and depressions would contain comparatively less POM-C:MAOM-C, because the generally thinner, less developed soil profiles of ridges have had less time to experience the conditions for MAOM to form from its precursor, POM.
- 2) Secondly, I hypothesized that MAOM formation, as a primarily root-driven phenomenon, would follow aboveground biomass distributions such that soils enriched in MAOM would tend to occupy the valleys and depressions that not only produce the thick soil profiles that result from erosion and deposition, but have consequently provided the nutrient and soil moisture conditions necessary for growth of large trees with extensive root systems. However, I predicted that meadow sites may prove an exception to this pattern due to multiple scales of biological processes, from historical land management (cultural burning and the practice of grazing sheep in montane meadows) to bioturbation by pocket gophers, as well as the C stabilization provided by deep-rooted grasses.

Methods

HJA Stratification for Site Selection

To control for the varied topographic features and vegetation assemblages that exist in HJA, I performed a series of steps to spatially stratify HJA into a number of representative classes. From among those classes, I chose individual replicate sites that could be accessed by road and trail. Using a combination of data sources gathered from the HJA Data Repository, in addition to

NRCS SSURGO data, PRISM climate data, and derived geomorphon (described below) from the digital elevation model (DEM) as predictor variables, I built random forest (RF) models to predict aboveground biomass (AGB) from 2008 lidar. With the assumption that AGB would be somewhat correlated with SOC, I spatially stratified HJA according to the most important environmental covariate predictors of AGB from the best-performing RF. Distance to stream and elevation were consistently the most important predictors of AGB, but soil sampling is not permitted close to streams given that HJA is a research forest, so I did not include distance to stream as one of the stratification variables. Given that neither of the most important predictor variables was, itself, a driver of variation in SOC, and that each effectively accounted for combinations of other environmental covariates like precipitation, air temperature, and landscape position, I chose sites that covered a wide range in each elevation, slope, aspect, geomorphon class, and AGB. Geomorphon is a fractal approach to represent landform that must be parameterized to the scale of interest, so I tested many search radii to find the best compromise between contiguous area of a single geomorphon class and number of landform classes represented. Using this approach, I proceeded using seven geomorphon classes. I then individually selected potential sampling sites based on site access (distance to roads and trails) and chose sites that covered a wide range in elevation, aspect, and plant cover type, but that were outside of areas that had been previously harvested. I chose sites that were at least 50 m from streams and greater than 100 m from roads, except two alder sites, which were, respectively, 75 m and 20 m uphill from roads. This was due to the difficulty of site access through thick stands of unyielding alder. Out of 50 potential sites, I sampled 30 total due to constraints imposed by the 2020 pandemic, wildfires, and difficulty of site access. Because the intention was to study how environmental covariates drove SOC distributions across complex mountain terrain, I primarily focused my sampling efforts on sites across the varied terrain of Lookout Mountain, with 4 additional sites at each Carpenter Mountain and Frissell, and two sites in alder-dominated high elevation stands ('AL1' & 'AL2'; Fig. 2.1). The Carpenter Mountain and Frissell sites were included as additional pairs of high elevation meadow and forest sites.

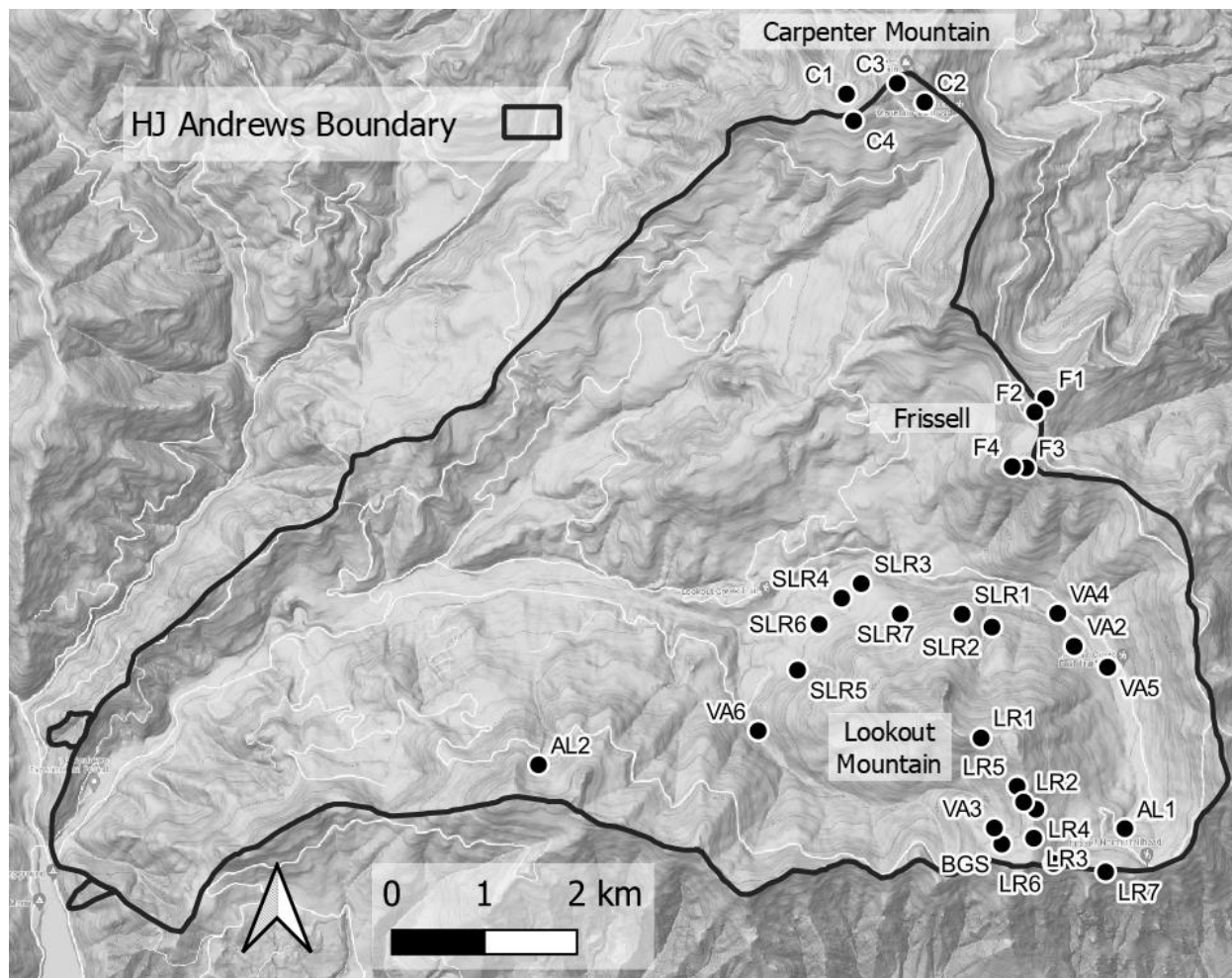


Figure 2.1 Distribution of sampling site locations with HJA Administrative Boundary Layer.

Field Sampling

During the summer of 2020, I sampled two test sites in summit geomorphon positions on Lookout Mountain. At each site I set one 30 m transect between two trees in a meadow and sampled each meter along the middle 15 m of that transect. After measuring the organic horizon depth and removing it, I sampled the 0-15 cm depth by driving a 20 cm long x 5.8 cm diameter PVC pipe into the mineral soil and carefully removing the intact PVC/soil core. The remaining depths of 15-30, 30-50, 50-75, and 75-100 cm were sampled with an electric auger (Landworks Earth Auger) with an attached 5 cm inner diameter core bit. At each meter along the 15 m transect, I sampled each soil depth. I transported the soil back to the laboratory and ran an air-

dried, ground subsample of each soil depth on an elemental analyzer (Elementar Vario Macro Cube; Elementar Analysensysteme GmbH, Langenselbold, Germany) for total organic C and N. Monte Carlo simulations on my C data for each transect at each depth and transect position was then used to determine the predictive power lost by including fewer observations along each transect. From these simulations, I determined that a minimum of 7-12 meters along each transect should be sampled to capture the inherent spatial variation in SOC in the x-dimension. This general distance was further corroborated by Griffiths & Swansons' (2001) transect study of soil properties across HJA, which determined from semivariograms that 5-m spacing provided statistically independent soil samples.

The majority of sampling events for 30 total sites took place between July and September 2021 field campaigns. I located sites using a handheld Garmin InReach GPS and topographic maps. At most sites, I collected a census of vegetation present within a 30 m x 30 m area with the aid of the Seek App by iNaturalist. I set a 15-50 m transect between two trees, if present, or orientated the transect from upslope to downslope if trees were not present. Each of the middle seven meters along the transect was flagged for soil sampling and I took bearings and distances to the nearest large trees to use for site geolocation correction in GIS software. If an organic horizon was present, I measured its depth and removed it to expose the mineral soil. Depending on ease of site access and the rockiness of soil, I sampled soils using either a Landworks Earth Auger or 10-20 cm lengths of beveled PVC driven into the soil. I sampled to at least 30 cm depth unless a restrictive rock layer was present. Few sites were only able to be sampled at depths of 0-10 and 10-20 for this reason, while most were sampled to at least 30 cm, and some included depths 30-50, 50-75, and 75-100 cm. Based on test site results from 2020 sampling and Monte Carlo simulations, I sampled seven transect positions along each transect, spaced 1 m apart, at 20 of the 30 total sites. The remainder of sites included between 3 and 14 total transect positions sampled. I sealed the intact soil-containing PVC cores in airtight bags and transported them back to the lab in coolers.

Bulk density was determined for each soil depth increment with a core sampler (either 5.8 cm diameter PVC pipe or auger core bit) when possible or by excavating a known volume of soil. PVC-sampled soils that were deemed sufficient for bulk density calculations were noted in the field, and any corrections for actual sample depth were measured as the distance between soil depth and top of PVC pipe. Rocks and roots were removed and volumes measured. Root volumes were negligible and were not considered in bulk density calculations, but rock volumes (determined by water displacement) were subtracted from sampling core volumes to estimate bulk density of mineral soil only. For samples that had inaccurate estimates of bulk density (incomplete field samples), bulk density was estimated from the same depth from other samples at the same site.

Lab Analysis

Soils were weighed in the lab before being set out to air dry and sieved to <2 mm. Large rocks and roots were removed and rocks were weighed and set aside for volume estimates using water displacement. Air dried soils were weighed for use in bulk density calculations. A subsample of each dried soil depth sample from each transect (n=500+), was ground in preparation for elemental C and N analysis. Organic C and N content from the 2020 samples were determined using an Elementar Vario Macro Cube (Elementar Analysensysteme GmbH, Langenselbold, Germany) at Oregon State University's Soil Health Lab. C and N content for the remaining samples were determined using a LECO CHN elemental analyzer at the National Forage Seed Production Center (ARS-USDA) on Oregon State University's campus. Accuracy of the C analysis was confirmed by >90% accuracy of included standard reference samples and >90% consistency in the analysis results between sample replicates.

Composite mineral soil samples were made for each depth increment by combining an equal mass of each depth along a single transect to achieve one sample per depth per transect for soil density fractionation, as it was not feasible to density fractionate every individual sample. Soil density fractionation was performed on 30 g composited subsamples of < 2 mm mineral soil for each transect depth to separate the soils into light and heavy fractions. Soils were weighed into

conical centrifuge tubes with 50 mL of sodium polytungstate (SPT) solution at a density of 1.85 g cm^{-3} . Centrifuge tubes were vigorously shaken by hand, then placed on a shaker table for two hours. The resulting slurry was then centrifuged to separate the light fraction ($<1.85 \text{ g cm}^{-3}$) from the rest of the soil material. The light fraction was aspirated into a collection vessel, and 50 mL of SPT was added back to the centrifuge tube. The tube was shaken vigorously by hand for one minute, then centrifuged again. The light fraction was aspirated into the same tube, and the same process repeated once more to ensure that all of the light fraction material was removed. The light fraction SPT mixture was filtered through a Whatman GF/F filter to separate the solid material from the SPT. Light fraction solids were gently scraped into a Mason jar and dried in an oven at 60°C until constant weight was maintained. The heavy fraction solids remaining in the centrifuge tube were washed and centrifuged three times with deionized distilled water to remove SPT, before being scraped into a Mason jar and placed in the oven with the light fraction samples. Once dry, light and heavy fractions were weighed, then ground for C and N analysis.

Data Analysis

Measured SOC values were interpolated using weighted averages to harmonize all data to the same depths, which was necessary due to some field samples that varied in the depth increment recovered as a function of restrictive rocks and roots. Actual sampled depths were always noted in the field and used to correct for bulk density of samples. If any depth in a given sample was in the range I interpolated to, it was included in that depth range bin. The range of depths that went into each bin was recorded and the dataset was repeated the number of times needed to complete each depth set. The harmonized depths were: 0-10, 10-20, 20-50, 50-75, 75-100 cm.

Statistical differences in SOC and fraction C were determined using one-way ANOVAs with site or site classification (vegetation type or landform position) as the explanatory variable. Post-hoc Tukey HSD tests were used to determine significant differences between sites grouped into one of two pairings of environmental covariates: meadow and forest, or ridge and valley. Sites were categorized into the ridge and valley classes only if they were forested, as meadow sites showed

significantly different soil properties and meadows were only present on ridges and sideslopes, not in valleys. Alder sites were excluded from the comparisons because they were significantly different than any other sites in any of the groupings. ANOVAs and post-hoc tests were performed separately for each fraction (POM and MAOM) and soil depth increment (0-10, 10-20, 20-50, 50-75, 75-100 cm) combination, as well as for site-level comparisons with depths grouped. Statistical differences were defined as significant at $\alpha = 0.05$. Data analysis, statistical analysis, and data visualization were performed in Deepnote (2021) using R coding language (R Core Team, 2021). GIS analysis was performed in Deepnote and QGIS (2009).

Results

The 30 sites included in this study occupied a variety of landscape positions – from valleys to slopes and ridges – and covered a range of vegetation assemblages (alder stands, old growth Douglas fir-Western hemlock, Pacific silver fir and mountain hemlock, and meadows). Sites covered a range of topographic positions, with most sites concentrated on Lookout Mountain but capturing the varied aspect, slope, and elevations present across the more mountainous regions of HJA. Across sites, elevation ranged from 780 m to 1550 m and slopes ranged from 4% to 40%.

SOC trends in valley and ridge sites

Forested ridge and valley sites showed similar trends of decreasing SOC concentration with depth, with ridge sites containing a greater, but statistically nonsignificant, SOC concentration than valley sites (Fig. 2.2). Although ridge sites tended to have greater C concentration than valley sites, this trend ceased below 50 cm depth. Ridge SOC concentrations varied from 61.4 ± 15.0 mg C g⁻¹ soil in the bottom depth to 145.5 ± 16.2 mg C g⁻¹ soil in the upper depth, while valley sites contained SOC concentrations between 54.8 ± 9.6 in the bottom depth to 125.2 ± 23.6 mg C g⁻¹ in the upper depth. Ridge and valley sites contained similar SOC stocks in the fine earth soil fraction to 1 m depth (561.7 ± 26.3 and 530.3 ± 16.9 Mg ha⁻¹, respectively) that were not statistically significantly different ($p > 0.05$; Fig. 2.3). The ratio of mean C to N differed between valley and ridge sites, with valleys containing more C:N than ridge sites, although those differences were not statistically significant ($p > 0.1$; Fig. 2.4). Valley site mean C:N ranged

between 22.1 ± 1.6 and 29.9 ± 4.0 , while ridge site mean C:N ranged between 21 ± 6.3 and 23.9 ± 2.3 .

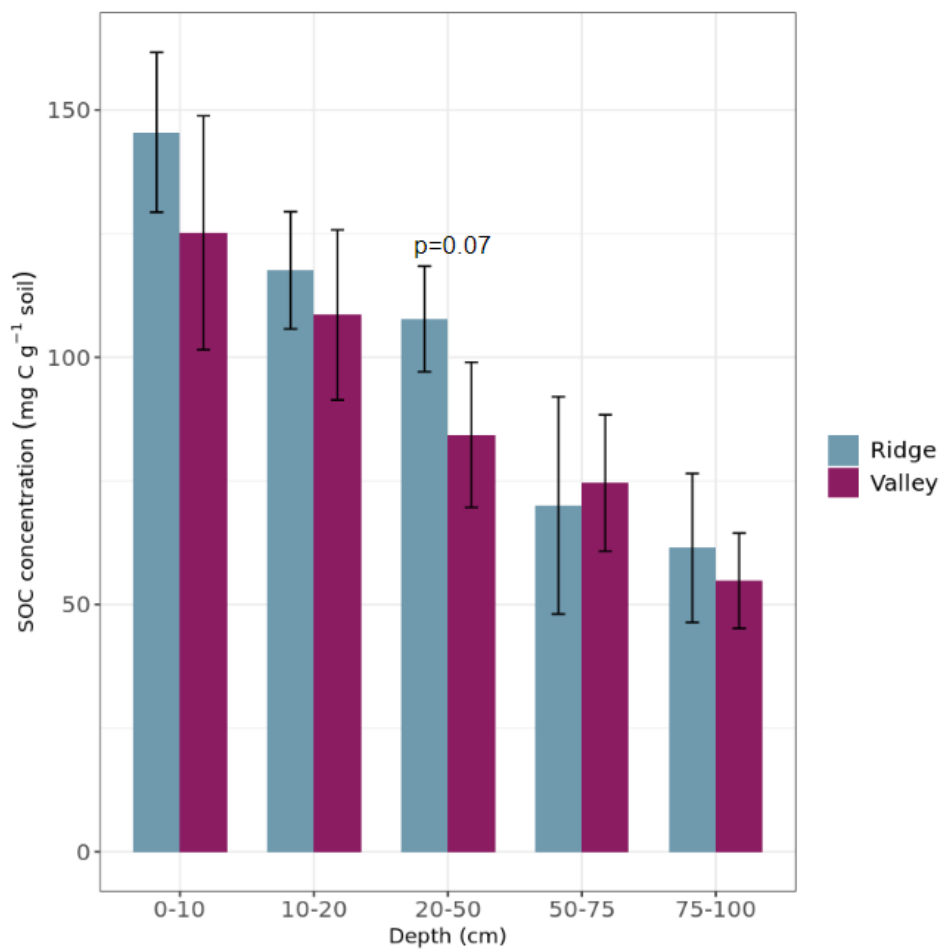


Figure 2.2 Mean SOC concentration by depth in ridge and valley sites \pm SE of the mean.

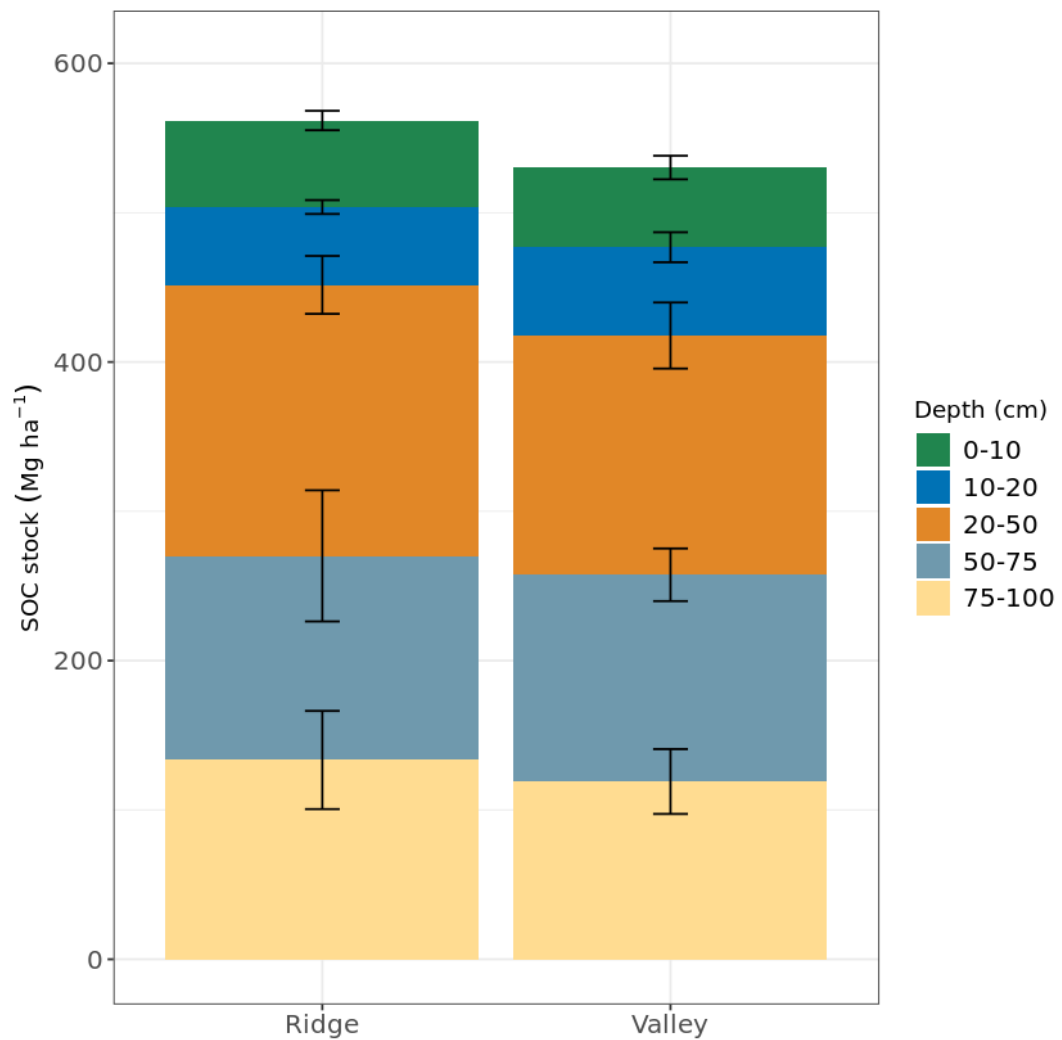


Figure 2.3 Mean SOC stocks of the fine earth fraction in forested ridge and valley sites ± 1 SE of the mean by soil depth increment.

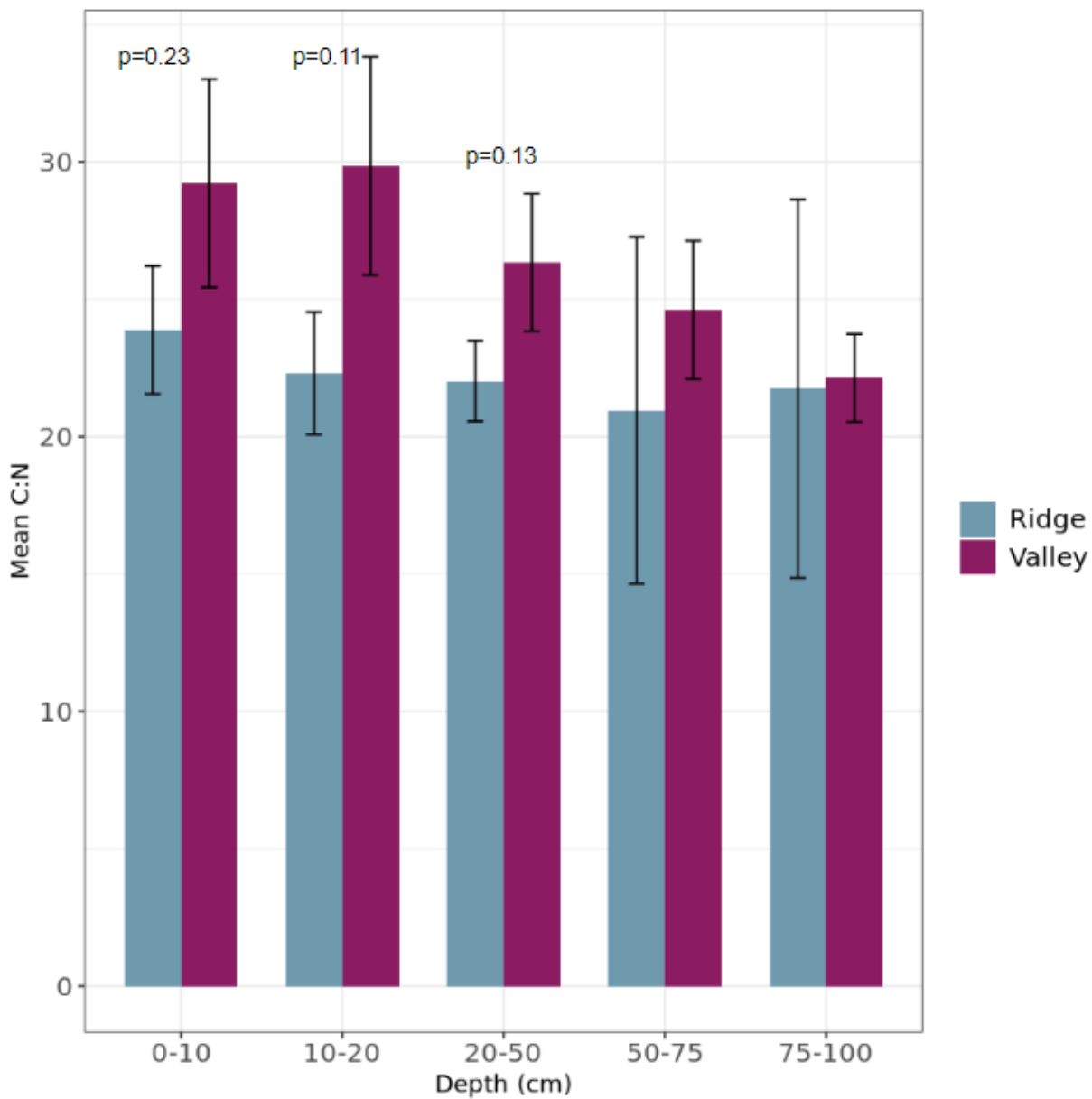


Figure 2.4 Mean C:N ratio in ridge and valley sites by soil depth. Error bars represent ± 1 SE of the mean.

SOC trends in forest and meadow sites

Mean soil C concentration decreased by depth and was consistently less in meadow than in forest sites, although both cover types contained about the same C concentration at the 75-100 cm depth (54.1 ± 9.2 and 54.8 ± 9.6 mg C g⁻¹ soil, respectively; Fig. 2.5). Mean soil C concentration by depth was not statistically significantly different between cover types ($p > 0.1$ for all depths). In the top 0-10 cm depth, mean soil C concentration was 118.8 ± 10.3 mg C g⁻¹ soil in forest sites and 95.4 ± 13.8 mg C g⁻¹ soil in meadow sites. However, SOC stocks were slightly greater in meadow sites due to higher soil bulk density across depths in meadows versus forest sites (Fig. 2.6; Table 2.1). Meadow sites contained mean SOC stocks to 1 meter depth of 552.4 ± 19.8 Mg ha⁻¹, while forests contained 518.5 ± 13.9 Mg ha⁻¹. Ratios of C to N were strikingly different between forests and meadows, with forests containing a much greater proportion of C to N than meadows ($p < 0.01$; Fig 2.7). While forest C:N decreased with depth – from 29.5 ± 0.72 in the top depth to 23.4 ± 1.2 in the deepest depth – meadow C:N was quite similar across all depths (14.6 ± 0.35 – 15 ± 0.19).

Table 2.1 Soil bulk density (Db) by depth in vegetation and topographic position classes.

Db (g cm⁻³) §				
Soil Depth (cm)	Valley 5 sites	Ridge 7 sites	Meadow 9 sites	Forest 18 sites
0-10	0.44 (±0.03)	0.41 (±0.04)	0.56 (±0.04)***	0.41 (±0.02)
10-20	0.54 (±0.03)	0.45 (±0.03)	0.65 (±0.05)**	0.51 (±0.02)
20-50	0.65 (±0.04)*	0.55 (±0.02)	0.70 (±0.05)	0.61 (±0.02)
50-75	0.76 (±0.04)	0.78 (±0.01)	0.87 (±0.08)	0.76 (±0.04)
75-100	0.87 (±0.02)	0.87 (±0.01)	0.94 (±0.05)	0.87 (±0.02)

§ ± 1 SE of the mean; * Differences in Db by depth between pairs of vegetation or topographic position classes were statistically significant ($\alpha = 0.05$).

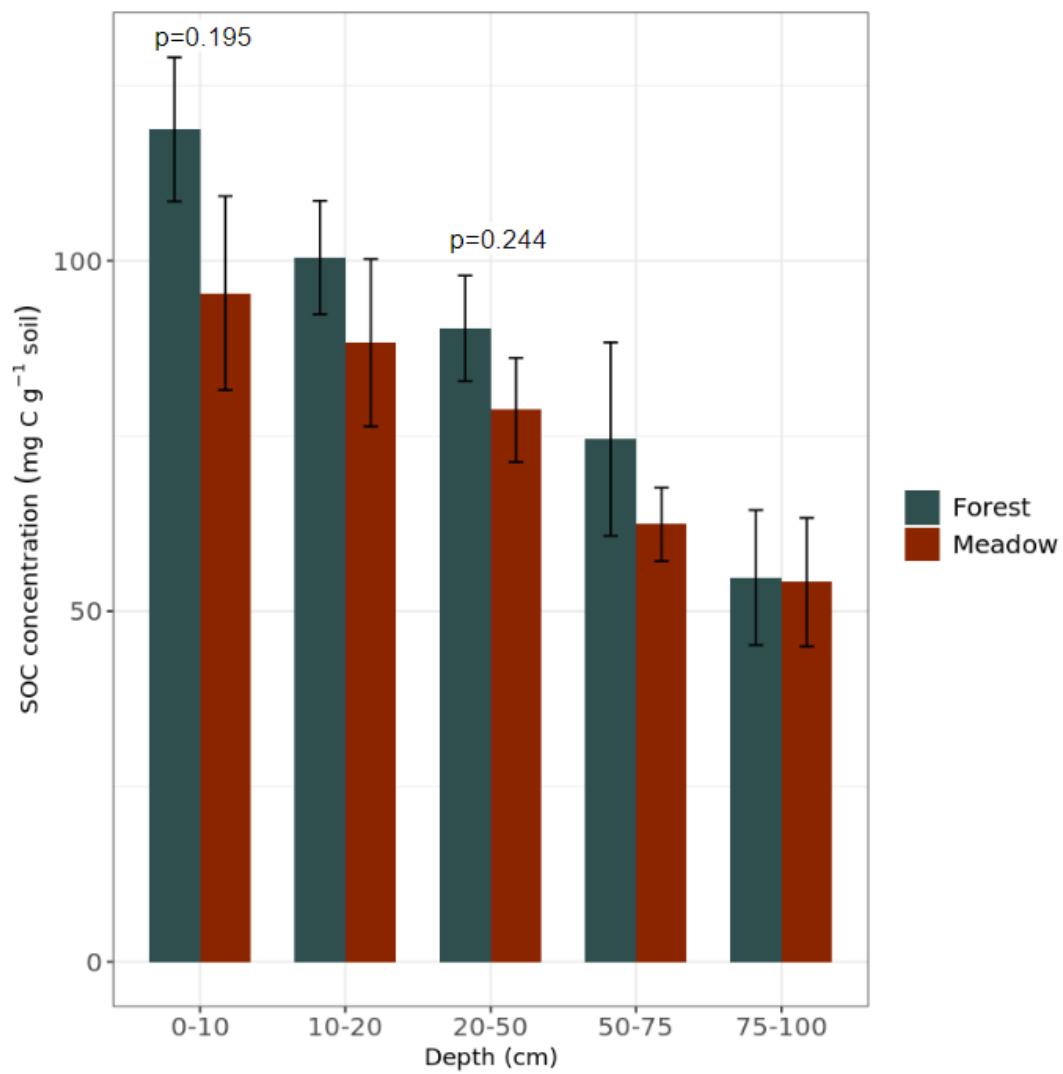


Figure 2.5 Mean SOC concentration by depth and cover type \pm 1 SE of the mean.

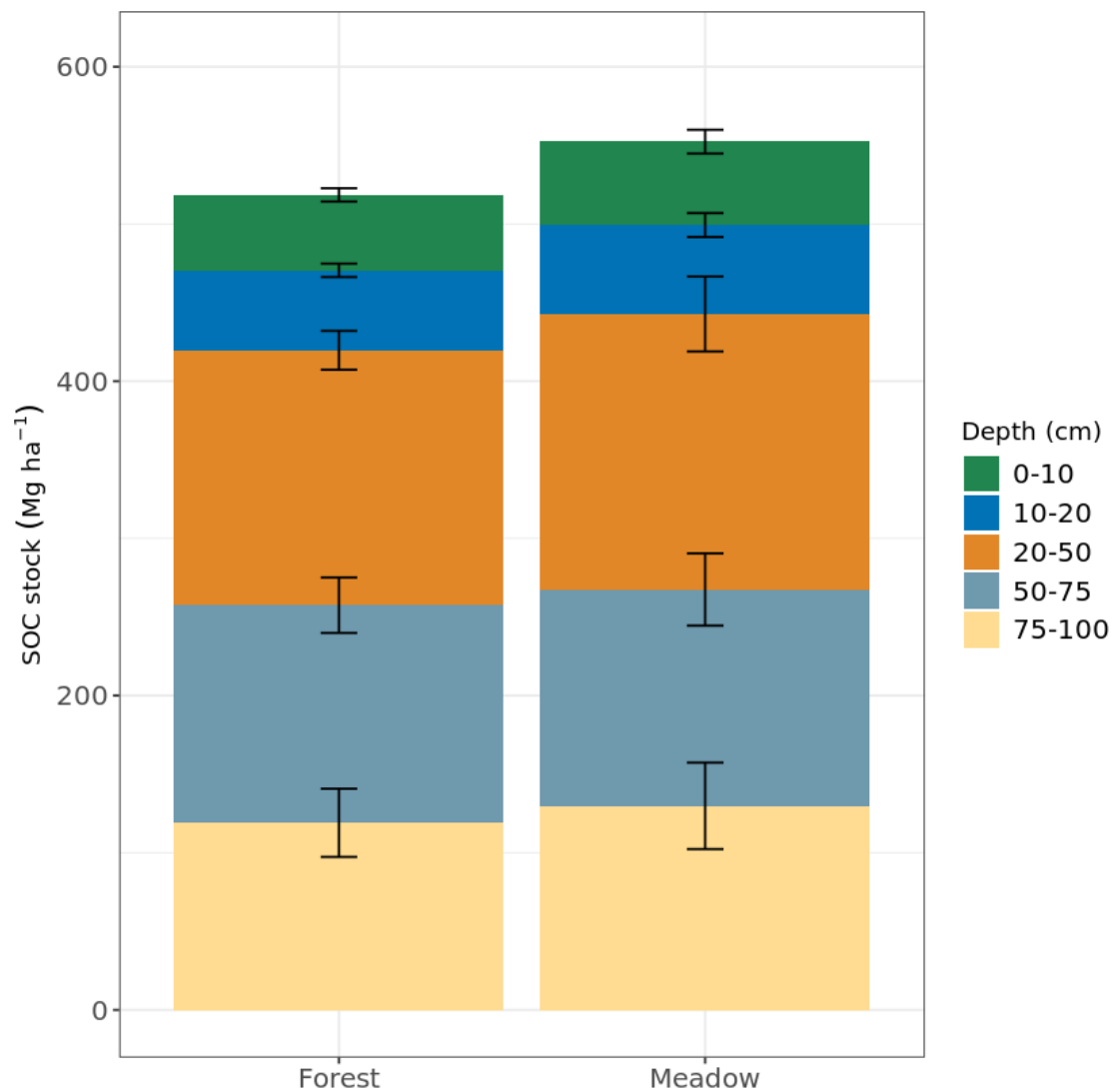


Figure 2.6 Mean SOC stock in the fine earth fraction by cover type \pm 1 SE of the mean per soil depth increment.

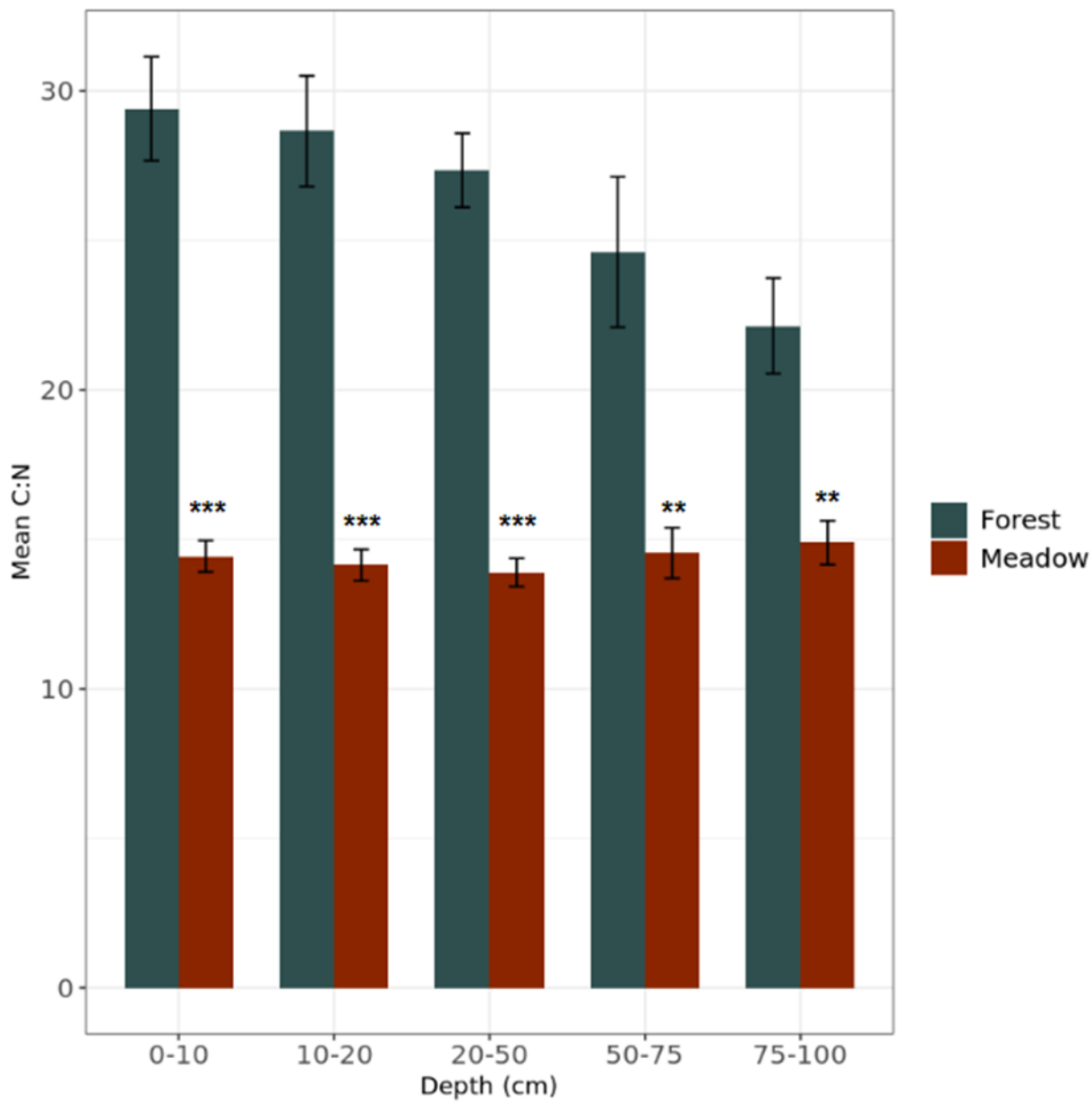


Figure 2.7 Mean C:N for forest and meadow sites by depth ± 1 SE of the mean. *** represents $p < 0.001$ and ** represents $p < 0.01$ at $\alpha = 0.05$.

Site level differences by soil density fraction

The proportion of MAOM-C relative to total soil C increased with depth and was significantly different between ridge and valley sites at the 20-50 cm depth only ($p=0.046$; Fig. 2.8). Below 50 cm depth, the ratio of MAOM-C to total soil C was greater than the other depths, but more similar between valley and ridge sites. The ratio ranged from a low of 0.14 ± 0.03 at the surface depth of ridge sites, to a high of 0.52 ± 0.11 at the 75-100 cm depth of ridge sites. In forest and meadow sites, there was significantly greater MAOM-C relative to total soil C in the meadow sites at depth increments between 0 and 50 cm ($p<0.05$; Fig. 2.9). Mean meadow site MAOM-C proportion ranged from 0.28 ± 0.03 in the surface depth to 0.58 ± 0.09 in the 75-100 cm depth, while mean forest site MAOM-C proportion ranged from 0.19 ± 0.02 in the 0-10 depth to 0.52 ± 0.03 in the 75-100 cm depth.

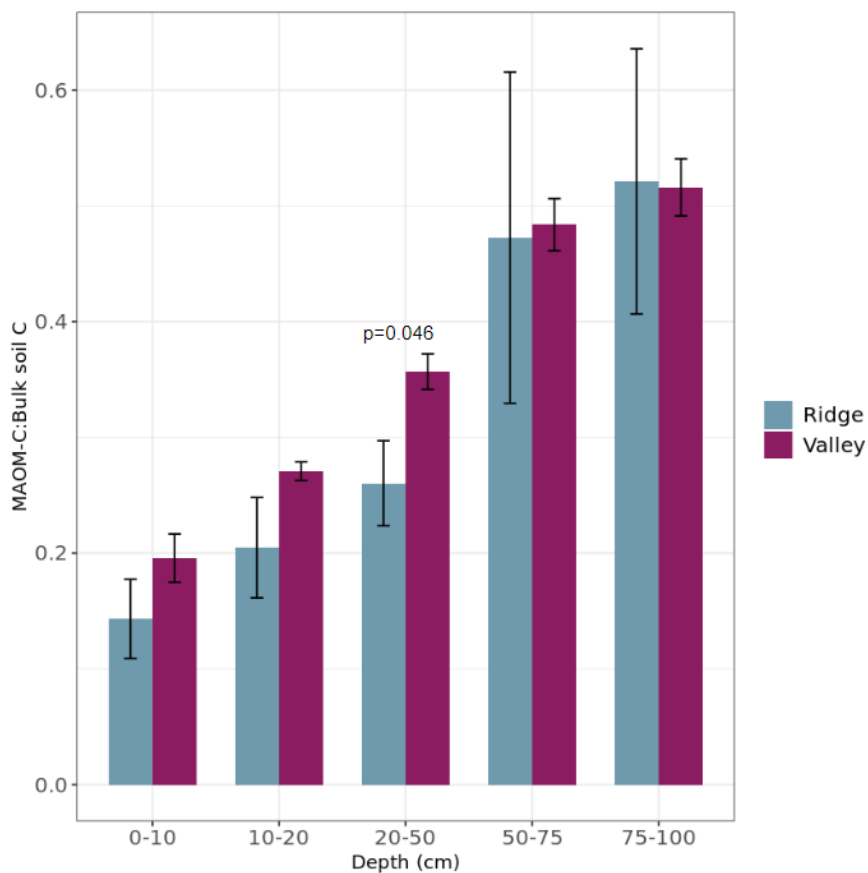


Figure 2.8 The proportion of mean MAOM-C to bulk soil C by depth in ridge and valley sites \pm 1 SE of the mean.

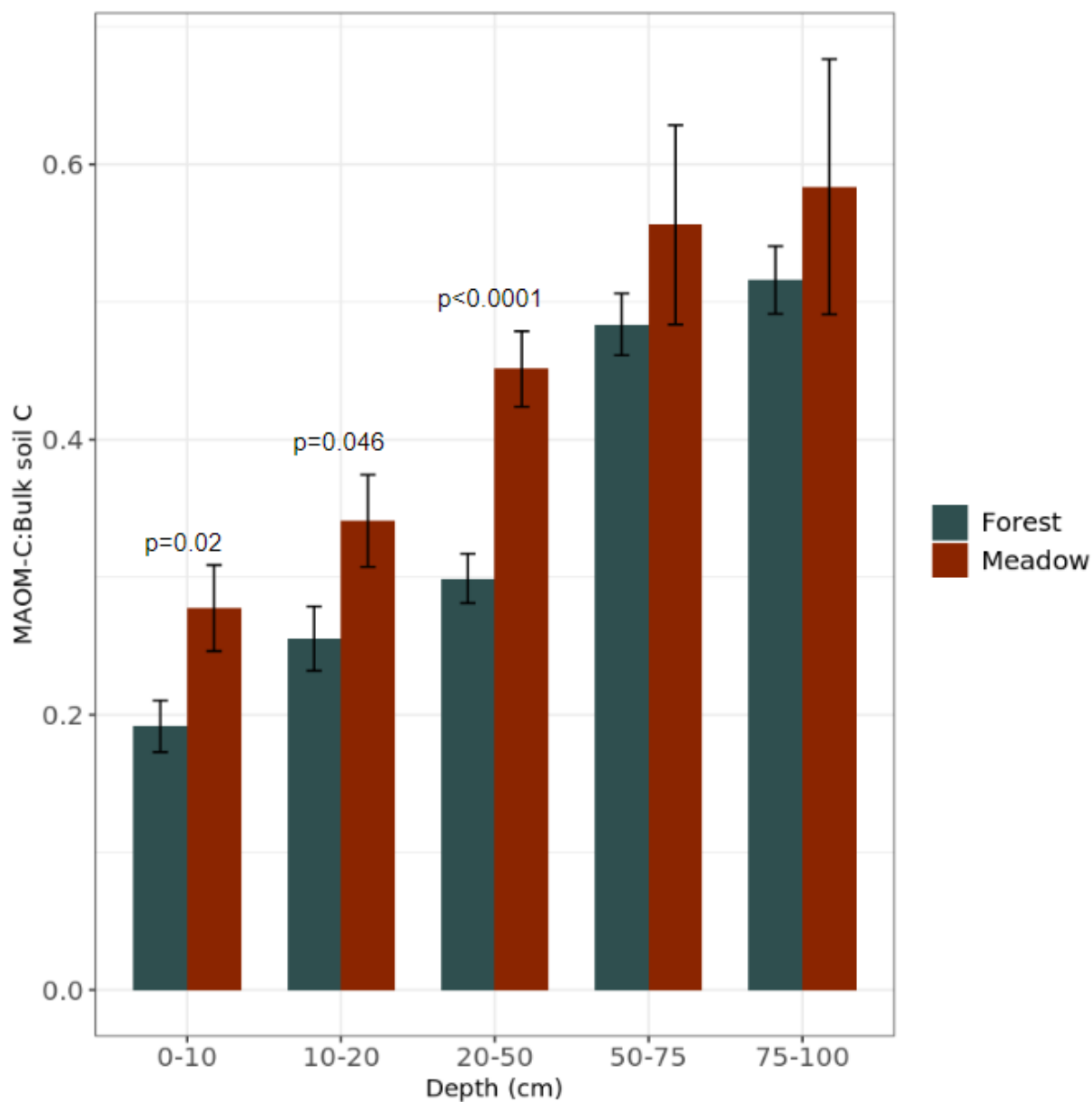


Figure 2.9 The proportion of mean MAOM-C to bulk soil C by depth in forest and meadow sites ± 1 SE of the mean.

Across depths (except 75-100 cm), the MAOM-C concentration of valley sites was greater than the MAOM-C concentration of ridge sites, although differences were not statistically significant

($p > 0.05$; Fig. 2.10). In ridge soils, mean MAOM-C ranged from 15.6 ± 1.1 mg C g⁻¹ bulk soil in the 0-10 cm depth to 25.4 ± 0.58 mg C g⁻¹ soil in the 75-100 cm depth. In valley soils, mean MAOM-C concentration was 20.6 ± 2.24 in the 0-10 cm depth but was greatest in the 50-75 cm depth at 31.1 ± 10.8 mg C g⁻¹ soil. In forest soils, the mean MAOM-C concentration was generally lower than it was in meadows, although the only statistically significant difference between the two was in the 20-50 cm depth ($p = 0.002$; Fig. 2.11). In meadows, mean MAOM-C concentration ranged from 21.7 ± 2.23 mg C g⁻¹ soil in the 0-10 depth to 32.3 ± 3.44 in the 20-50 cm depth, before declining slightly in the 50-100 cm depth to around 29 mg C g⁻¹ soil. In forests, mean MAOM-C concentration varied between 17.8 ± 1.1 mg C g⁻¹ soil in 0-10 cm and 31.1 ± 10.8 mg C g⁻¹ in the 50-75 cm depth.

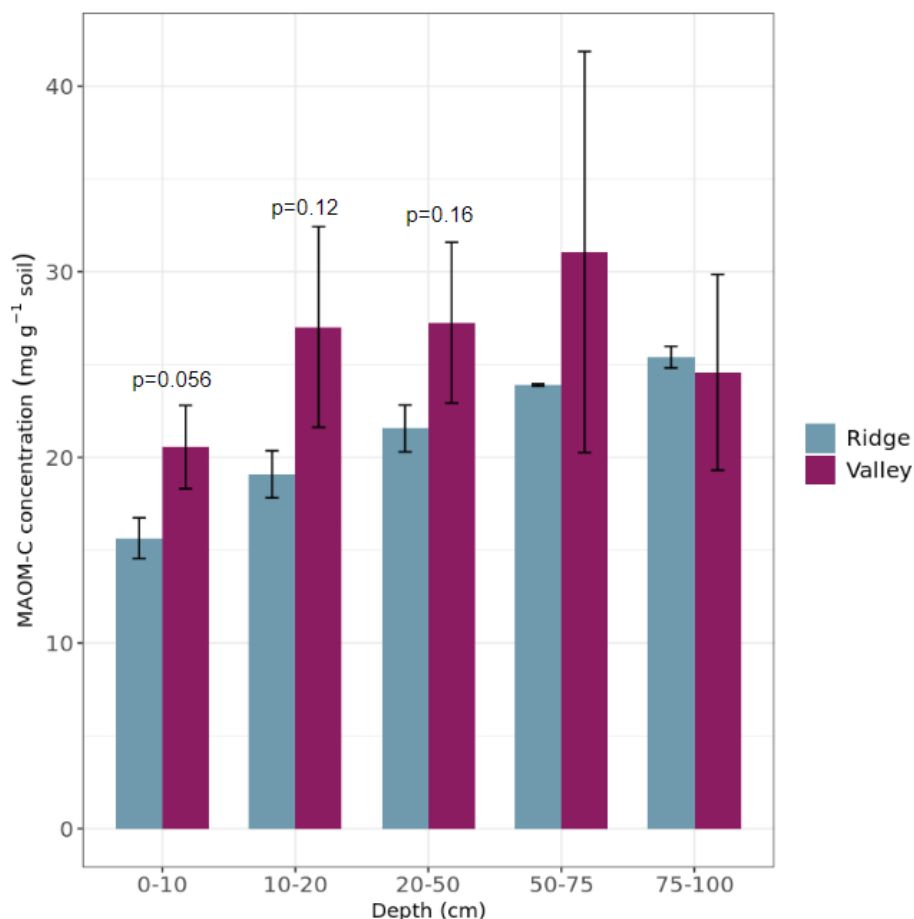


Figure 2.10 Mean C concentration of the MAOM soil fraction as a proportion of bulk soil mass in ridge and valley sites, ± 1 SE of the mean.

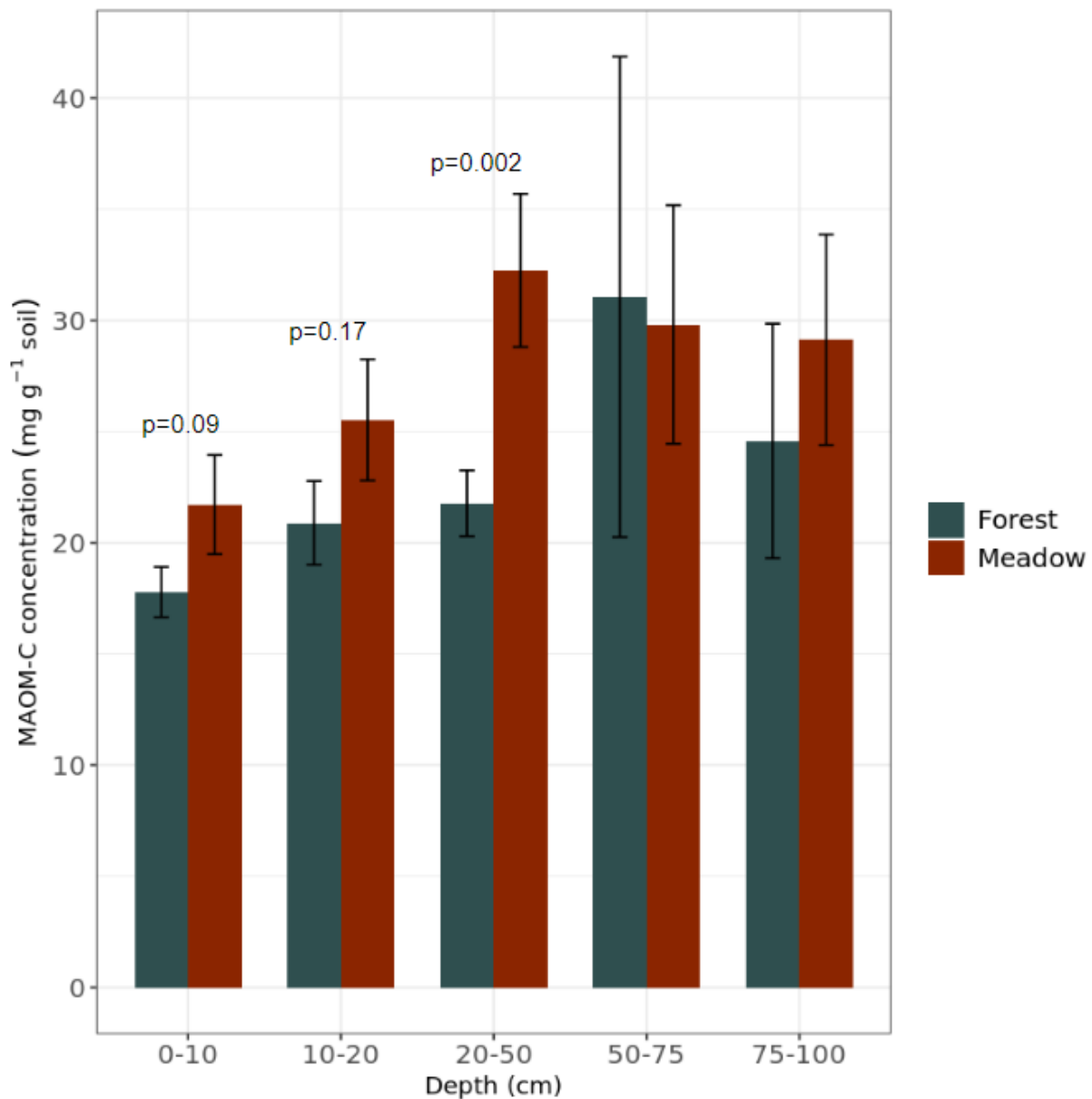


Figure 2.11 Mean C concentration of the MAOM soil fraction as a proportion of bulk soil mass in forest and meadow sites, ± 1 SE of the mean.

The mean C concentration of the POM fraction as a proportion of bulk soil C declined sharply with depth in ridge and valley sites (Fig. 2.12). The 20-50 cm depth was the only depth increment where there were statistically significant differences between the POM-C concentrations of ridge and valley sites (respectively, 72.3 ± 6.7 and 48.0 ± 6.1 mg C g⁻¹ soil;

$p=0.018$). Ridge sites contained 111.3 ± 13.9 mg POM-C g^{-1} soil in 0-10 cm depths and 25.6 ± 10.7 mg POM-C g^{-1} soil in the 75-100 cm depth, while valley sites contained between 93.7 ± 21.9 and 22.5 ± 3.9 mg POM-C g^{-1} soil in their upper and lower depths. Forest POM-C concentration was generally greater than that of meadows, except in the 75-100 cm depth, where they were similar (Fig. 2.13). Forest POM-C concentrations were statistically significantly greater than those of meadow sites in the 20-50 cm depth (57.1 ± 4.5 and 37.9 ± 2.5 mg POM-C g^{-1} soil, respectively; $p=0.008$). Across depths, forest POM-C ranged from 22.5 ± 3.9 to 87.9 ± 9.6 mg POM-C g^{-1} soil, while meadow POM-C ranged from 23.7 ± 9.0 in the 75-100 cm depth to 64.4 ± 11.5 mg POM-C g^{-1} soil in the 0-10 cm depth. The ratio of POM-C to MAOM-C was greater in the ridge sites than the valley sites and declined in both cover types with depth (Fig. 2.14). Below 50 cm, ratios were similar between the two cover types, while above 50 cm, there was significantly more POM-C to MAOM-C in 20-50 cm and 10-20 cm depths ($p<0.05$). Forests contained significantly greater POM-C:MAOM-C compared with meadows in the 20-50 cm depth ($p=0.002$), and also contained greater POM-C in the 0-10 and 10-20 cm depths, but those differences were not statistically significant.

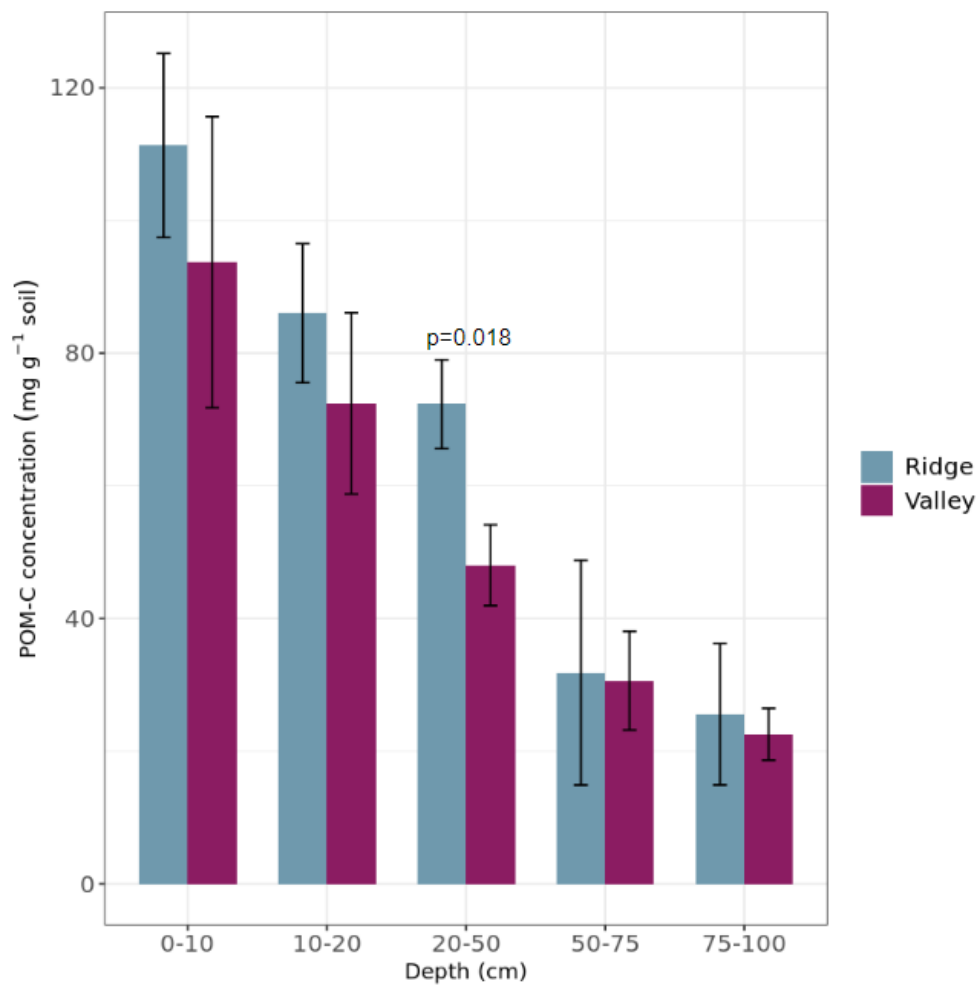


Figure 2.12 Mean C concentration of the POM soil fraction as a proportion of bulk soil mass \pm 1 SE of the mean in ridge and valley sites.

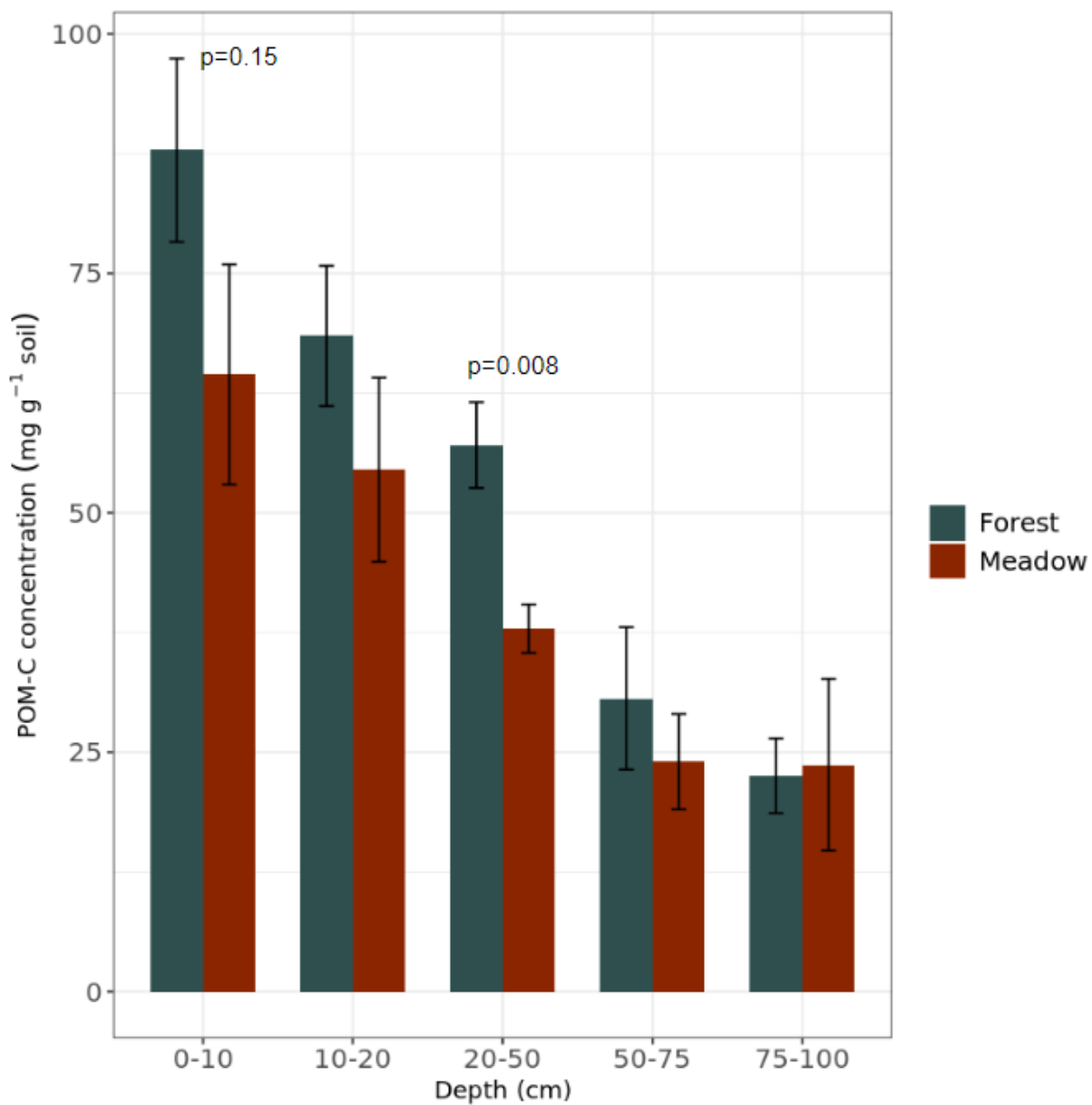


Figure 2.13 Mean C concentration of the POM soil fraction as a proportion of bulk soil mass \pm 1 SE of the mean in forest and meadow sites.

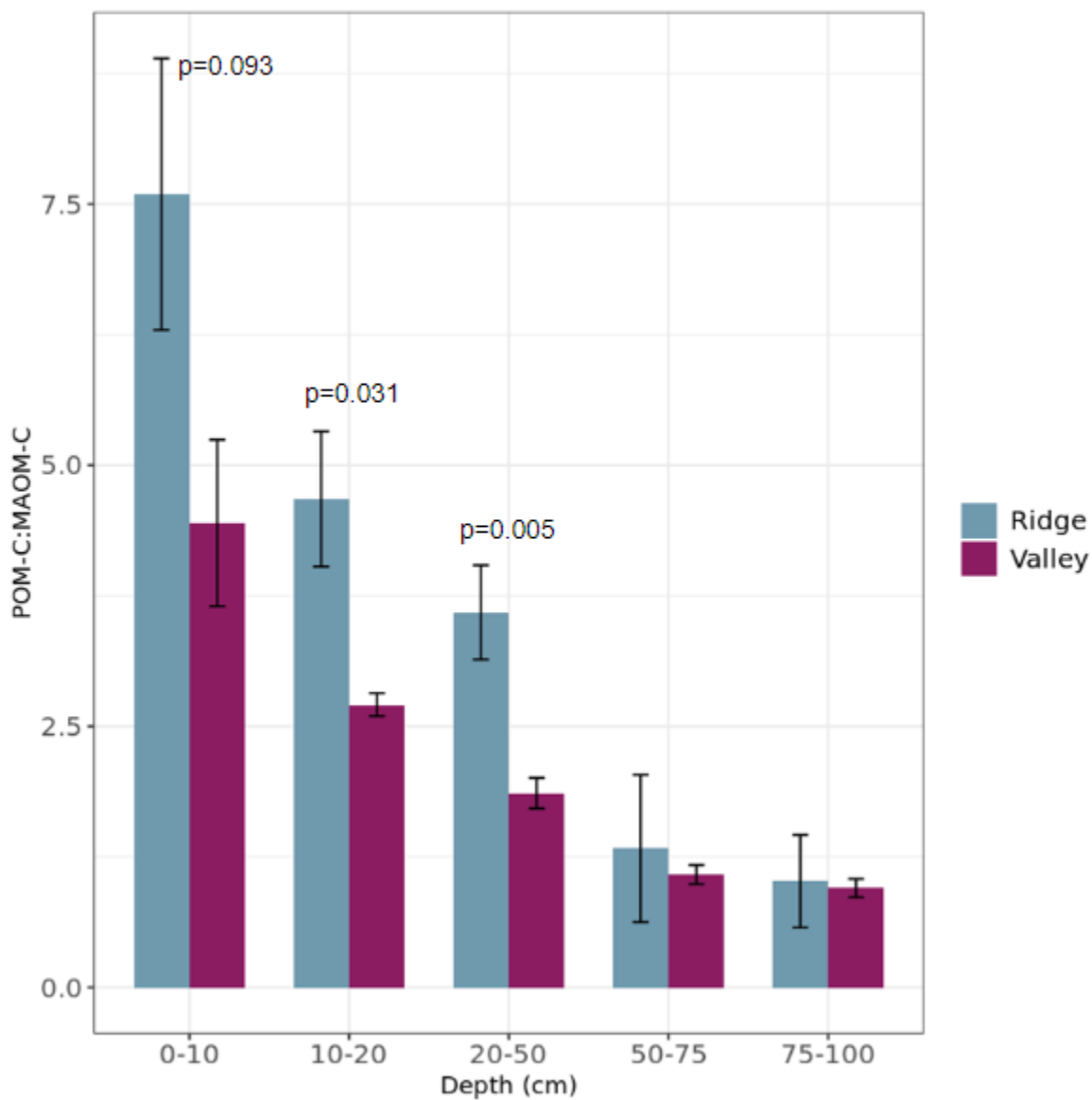


Figure 2.14 Ratio of mean POM-C to MAOM-C \pm 1 SE of the mean in ridge and valley sites.

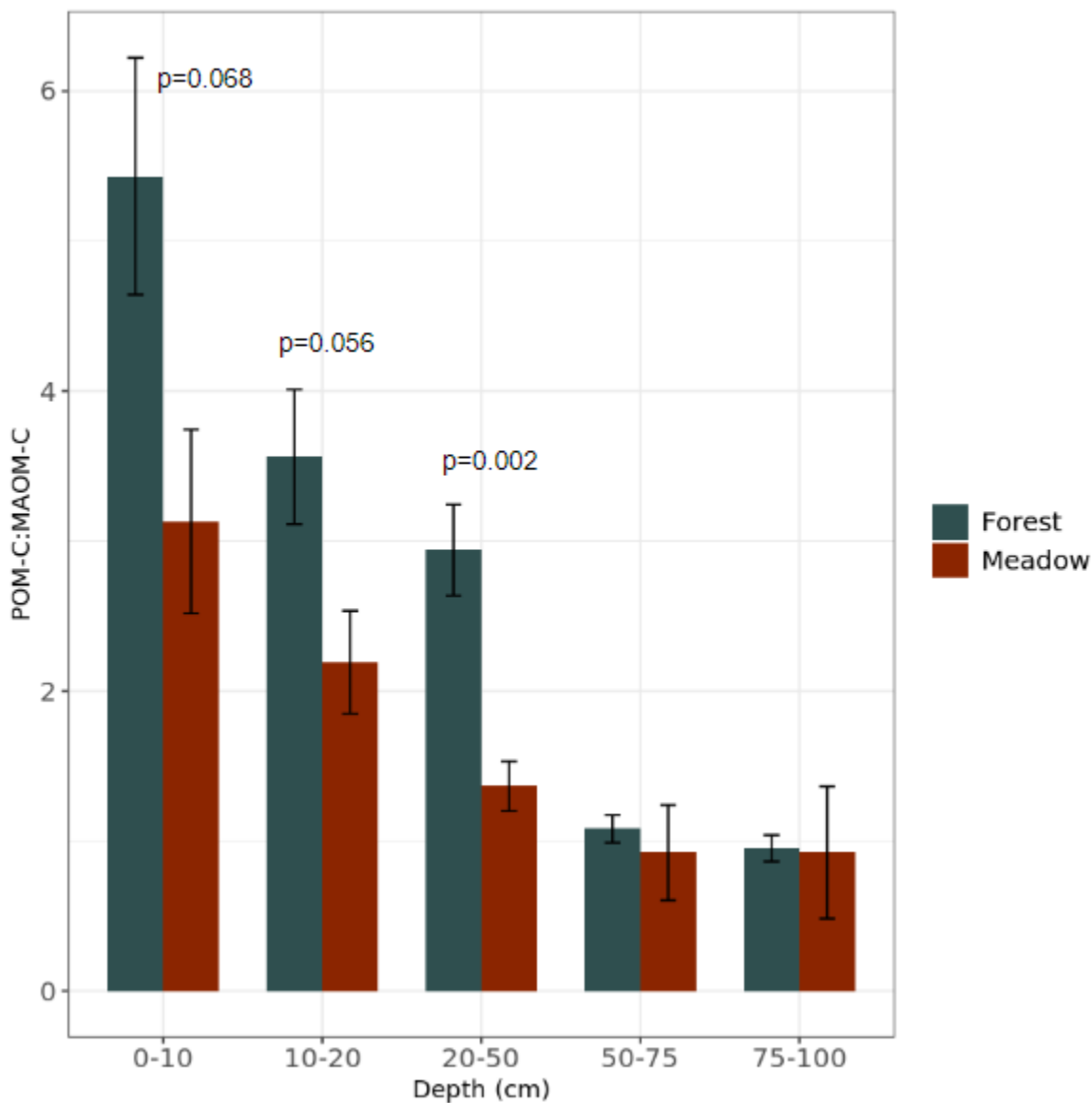


Figure 2.15 Ratio of mean POM-C to MAOM-C \pm 1 SE of the mean in forest and meadow sites.

Discussion

My first hypothesis that (1) SOM on ridges and peaks would contain proportionally more POM-C than MAOM-C, and (2) SOM in valleys and depressions would contain comparatively less POM-C, was supported by my data (Fig. 2.14). Although not statistically significant at $\alpha = 0.05$ at all soil depths, POM-C did represent a greater proportion of total soil C than did MAOM-C in

ridge sites versus valley sites in depths above 50 cm, and was statistically significantly greater in the 10-20 cm and 20-50 cm depths. My second hypothesis, that regions of high aboveground biomass would correspond to regions of high MAOM-C, was somewhat supported by my data (Fig. 2.15). When I compared forested sites to meadow sites, the ratio of POM-C to MAOM-C was greater at soil depths between 0 and 50 cm, but was only statistically significantly greater in the 20-50 cm depth. My additional hypothesis about meadow sites containing more MAOM-C than would be expected based only on the amount of aboveground biomass was somewhat supported, given that the ratio of MAOM-C to bulk soil C was greater in the meadow sites than in the forest sites (Fig. 2.9). Meadows contained statistically significantly greater MAOM-C: Bulk soil C in all depths between 0 and 50 cm. Below that, meadows still contained a greater proportion of MAOM-C to total soil C but the difference was not statistically significantly different.

Across bulk C, C fractions, and C:N, the 20-50 cm depth was frequently the depth that showed the most significant differences between C by cover type and by topographic position. I attribute this to the 20-50 cm zone being a region of active root growth, rhizosphere activity, and animal activity, given that nutrients are plentiful and soil moisture is more abundant than in deeper depths.

The lack of statistically significant differences between C stocks by topographic position or cover type was surprising. Although not statistically significant, the differences in those C stocks could still be considered substantial if one considers the magnitude across the entirety of HJA. If ridges do in fact contain a mean SOC of 560 Mg ha^{-1} , and valley sites contain a mean of 530 Mg C ha^{-1} , there could be greater implications for loss of that substantial ridge C stock with continued climate change effects, particularly if ridges and high elevation areas are warming at a faster rate than lower elevation areas. Another concerning trend is that ridges contained a greater proportion of POM-C, which is considered a more ephemeral C pool. Warming temperatures

could differentially impact this more vulnerable C pool and cause additional soil C loss via microbial respiration.

Previous studies from HJA and other westside Cascade forests corroborate the low N status of these forests (e.g., Boyle et al., 2008; Pierson et al., 2021b). The significant differences between ratios of C to N in forests and meadows, with forests containing a much greater proportion of C:N than meadows (Fig 2.7), indicates that the forested areas are typically N-limited. This is in large part due to the abundance of woody detritus that contains a much greater C:N than the relatively smaller needle litter detritus input with a smaller ratio of C:N. In these forests, relative aboveground litter production is lower and the proportion of fine roots to coarse roots is greater due to the need for a tree to expand its search radius for soil N. Turnover of these fine roots is also reduced relative to forests that are less N-limited and that have increased ecosystem productivity (Nadelhoffer et al., 1985; Lajtha et al., 2018). While forest C:N decreased with depth, meadow C:N was quite similar across all depths. The relatively constant C:N in meadow soils with depth could be an artifact of the bioturbation by pocket gophers (family Geomyidae), which are abundant in these meadows. As the gophers burrow, they effectively mix the soil layers, creating more homogenous soil properties across depths. The lower C:N ratio in meadows could be attributed to a number of factors. SOM inputs in meadows consist of a lesser proportion of woody detritus (material that has a high C:N) because the vegetation mostly consists of graminoids, forbs, and beargrass (*Xerophyllum tenax*). Additionally, turnover of fine roots may be greater in these areas and may support microbial populations that have a larger proportion of bacteria relative to fungi. Bacteria are generally believed to require more N per unit biomass than fungi (Fierer et al., 2009). The diversity of plant species in meadows may also result in diverse root exudates, which would support microbial diversity and microbial biomass accumulation (Chen et al., 2019). Finally, nitrogen-fixing host species like lupines are found in some HJA meadows, and their presence will increase the soil N concentrations.

The difference between the meadow mean SOC stock of about 552 Mg and the forest mean SOC stock of about 519 could also be considered substantial despite the lack of statistical significance (Fig. 2.6). Meadows occupy a relatively small proportion of the entire HJA, yet they contain unique biodiversity and support pollinator species. The encroachment of forests into meadows could not only disrupt the unique ecosystem functions of meadows, but could also promote loss of C and N as trees mine nutrients from these soils. Griffiths et al. (2005) studied soil properties as related to conifer invasion of high elevation meadows in HJA and found that N was more available in meadow soils than in forest soils. By studying microbial enzyme activity, they found that the microbial population likely changed in response to tree invasion into meadows due to changes in available substrates. They concluded that the observed changes to soil properties happened quickly after forests begin to invade meadows and that trees quickly became the dominant force in biogeochemical cycling in these areas. This trend of forest invasion of high elevation meadows has implications for C and N cycling in these areas and is particularly concerning with respect to pollinator diversity loss and stable soil C loss in an era of global change. These trends are discussed further in chapter 3.

CHAPTER 3: Multi-scale spatial patterns in soil carbon distribution across complex mountain terrain

Introduction

Global soils serve as a storage reservoir of over two-thirds of terrestrial carbon, but soil carbon distribution in complex mountain terrain differs from the soil carbon gradients seen in flatter and more homogenous landscapes. Soil landscape mapping techniques that were developed for application in agricultural settings or natural resource management are less effective at capturing spatial variance in SOC in mountainous terrain that contains more edge features and greater spatial variation in SOC over short distances. Edge features in steep, highly variable terrain will cause abrupt changes in soil properties, which would otherwise tend to manifest as more gradual changes along a catena (Rahbek et al., 2019). Sampling and statistical analysis techniques must be able to account for spatial heterogeneity and sharp transitions in meter-distance soil properties. We can take advantage of recent advances in geospatial and computing technologies, as well as machine learning (ML) algorithms, to more accurately assess soil landscapes at fine spatial scale.

Currently available mapped products of landscape-scale SOC differ widely in their predictions and distributions of predicted soil C. While some of this uncertainty is an artifact of inherent spatial heterogeneity of soils, much can also be attributed to the constraints on effective field sampling. Soil sampling methods vary – from digging pits to augering and extracting cores – but each method is time-intensive relative to the amount of spatial variation that can be captured per sampling event. As a consequence, it is a common practice to composite soils sampled from nearby locations, with the compositing distance and number of samples being chosen somewhat arbitrarily by the person sampling. By effectively hiding the inherent variability in soil properties by compositing, even less is known about the finer scale spatial variation in soils. While this may be less important for studies of landscape-scale processes, it becomes more consequential when studying processes that interact at multiple spatial scales (Dufour et al., 2006). For instance, in mountain terrain like that present in the mid and high elevations of HJA, climatic gradients

interact with vegetation distributions, parent material, and soil organisms to produce vastly different soil properties within tens of meters (Griffiths et al., 2009). Edge features created by steep terrain and mass movements produce highly heterogeneous spatial distributions of soil organic matter, which are not well captured in current publicly available mapped soil products (e.g., SSURGO). In this study, my objective was to create a soil C map of HJA that effectively captured the spatial variation caused by the interaction of biogeochemical processes acting at multiple spatial and temporal scales. My research question was: How do soil C distributions vary across complex mountain terrain in response to small- and large-scale biogeochemical processes? To further explore the effect of spatial resolution on SOC estimates, I also compared my SOC estimates with those from other studies and publicly available spatial data.

Methods

Spatial and climate data sources

Data accessed and downloaded from the HJA repository were provided by the H.J. Andrews Experimental Forest and Long-Term Ecological Research (LTER) program, administered cooperatively by Oregon State University, the USDA Forest Service Pacific Northwest Research Station, and the Willamette National Forest. This material is based upon work supported by the National Science Foundation under the grant LTER8 DEB-2025755. Data used in RF models are described below and referenced in Table 3.1.

HJA dataset ‘TV062: Plant Community Typing (2009 update), Andrews Experimental Forest’ is a spatial data layer containing 23 forest communities that were classified through a combination of similarity analysis, stand ordination, and ground-truthed reconnaissance plots (Hawk & Schulze, 2010). This was used as the vegetation polygon layer. LiDAR (2008) derived products from 1 m spatial resolution data were used from dataset ‘GI010: Lidar data (August 2008) for the Andrews experimental forest and Willamette National Forest study areas’ (Spies, 2016). The derived product, aboveground biomass (AGB), was used in RF models as a predictor variable for

SOC from the dataset ‘TV080: Aboveground Live Biomass (2008), Andrews Experimental Forest (Spies, 2015). We used the elevation model from dataset ‘GI003: 10 Meter Digital Elevation Model (DEM) Clipped to the Andrews Experimental Forest, 1998’ (Lienkaemper & Valentine, 2005). Slope and aspect spatial layers were also derived products from the 2008 LiDAR. For roads and trails, I used dataset ‘GI007: Transportation network system including trails, road construction history, and gates for the Andrews Experimental Forest, 1952-2011’ (Lienkaemper & Schulze, 2014). The stream network from dataset ‘HF013: Stream network from 1997 survey and 2008 lidar flight, Andrews Experimental Forest’ was used to match the 10 m DEM (Lienkaemper & Johnson, 2016) and was used as a predictor variable in RF models as ‘distance to nearest stream (m)’.

Climate data were interpolated from 133 locations in HJA using the PRISM model (Daly, 2020). Monthly 1981-2010 normals were generated at 800 m spatial resolution for precipitation, mean minimum daily temperature, mean maximum daily temperature, mean daily temperature, daytime temperature mean, vapor pressure deficit (VPD) minimum, and maximum VPD. These normals were then summarized to annual estimates. I applied an inverse distance weighting to the mean value of the ten nearest neighbor pixels to spatially summarize all PRISM climate data.

Geomorphon (terrain form) mode, minority, and variety (between 1 and 3 classes of geomorphon) at 30 m spatial resolution were used as predictor variables in RF models. Geomorphons are calculated using a machine vision fractal approach that calculates a comprehensive set of idealized landforms that are independent of the size, relief, and orientation of the actual landform. This larger set of landforms is binned into ten representative landforms: flat, peak, ridge, shoulder, spur, slope, hollow, footslope, valley, and pit (Jasiewicz & Stepinski, 2013).

Table 3.1 Sources of data and associated spatial resolution.

Category	Environmental covariate	Dataset	Variable(s)	Spatial Resolution
Climate	Precipitation	PRISM	mean annual precipitation (in) from monthly normals between 1981 and 2010	800 m
	Temperature	PRISM	mean daily, mean daily minimum, and mean daily maximum temperature, and mean daytime temperature (degrees F) annualized from monthly normals between 1981 and 2010	800 m
	Vapor pressure deficit (VPD)	PRISM	VPD minimum, maximum	800 m
Physical	Aspect	HJA DEM from LiDAR	mean aspect, SD, CV	10 m
	Slope	HJA DEM from LiDAR	mean slope percent, SD, CV	10 m
	Geomorphon (terrain form)	Generated in R using opensource code (Jasiewicz & Stepinski, 2013)	geomorphon mode, minority, and variety*	30 m
	Elevation	HJA DEM	mean, SD, CV	10 m
	Distance to	HJA LiDAR	mean distance to nearest	10 m

	stream	(Lienkaemper & Johnson, 2016)	stream (m)	
Biological	Aboveground biomass (AGB)	HJA LiDAR (Spies, 2016)	mean AGB (Mg ha ⁻¹), SD, CV	10 m
	Vegetation assemblages	HJA Plant Community Typing (Hawk & Schulze, 2010)	polygons of 23 classes of vegetation assemblage	NA

*Number of different geomorphons at a site – between 1 and 3.

Statistical Models and Mapping Methods

Random forest (RF) was chosen as a data-driven modeling technique because of its ability to handle both categorical and continuous data from large datasets, ability to output an ordered list of variable importance allowing the user to tune models by adjusting covariates, robust decision tree framework, unbiased error estimates, and widely accepted (and growing) use in digital soil mapping at the landscape scale (Breiman, 2001; Wang et al., 2022). RF models were developed to predict percent SOC from a suite of variables derived from GIS and climate data. Models were used to predict transect level and site level variables (described in Chapter 2), using the default parameters for RF. I used the environmental covariates described in Table 3.1 to predict those variables, in addition to depth increments (top and bottom soil sample depths in cm) used in field sampling. Eighteen separate RF models were built to predict C, N, C:N, bulk density (mean, standard deviation, and coefficient of variance for each), light and heavy fraction C (POM and MAOM, respectively), and light and heavy fraction mass proportions. Models were either built on transect-level data or data summarized to the site level for comparison. The same parameters and predictor variables were used for all models so that model performance and variable importance was comparable between models. I created a 5 m buffer around each transect position location and summarized pixel values for all data to all buffered point locations. I then created a 10 m x 10 m grid across HJA to summarize all RF-generated data to, then created rasters from the gridded data.

Cross-Validation

When I assessed spatial autocorrelation in SOC and environmental covariates, I found that SOC within sites at the 1 m transect level was more autocorrelated than was SOC by depth across sites. Summarizing variables from the transect to the site level would not effectively address this issue since autocorrelation would still exist between environmental covariates and site level data. To address the potential issue of sample and covariate autocorrelation, I cross-validated the three main RF models (that predicted C, N, and C:N) using a bootstrapped approach. For each RF model, I randomly selected one individual site's data to leave out of the training dataset and to then predict on. For the remaining individual sites, I randomly selected one C value from a random depth at a random transect position to leave out of the training dataset, then used that bootstrapped dataset to predict that set of random values in validation. This approach was designed to prevent any possible overfitting of the RF model in any dimension (within site, by depth, and between samples and environmental covariates). Bootstrapped distributions from cross-validation are included in each inset plot for the variable importance plots.

I performed additional cross-validation by testing my modeled predictions against a large set of soil samples from an unrelated research project in HJA performed by Robert P. Griffiths in the late 1990s (Griffiths et al., 2019). Griffiths sampled the 0-10 cm depth of soils at 0.5 km intervals along all accessible HJA roads and recorded a total of 183 sites. They report soil organic matter (SOM) percent for all samples, which I converted to approximate SOC percent by multiplying by the commonly accepted conversion factor of 0.5 that represents the stoichiometric proportion of C in organic matter (Pribyl, 2010). This conversion factor was close to the reported values of needle (46% C) and woody (47 % C) litter C measured by Pierson et al. (2021b) in the HJA DIRT site. While I intentionally avoided sampling near roads due to the known edge effects of road construction and road features (e.g., concentrated areas of runoff and localized erosion, vegetation differences resulting from disturbance and tree gaps, etc.), Griffiths intentionally sampled along roads – presumably for ease of site access. I recognize that a cautious approach to interpreting similarities between the two datasets is warranted due to known differences in sampling design but argue that general comparisons can still be made. I built an RF on Griffiths'

SOM data using the same environmental covariates from my original RF to compare model performance between my RF and the Griffiths RF.

Comparison with other soil products

Publicly available SOM data were downloaded from datasets available in Google Earth Engine for comparison with my predicted C stocks. A conversion factor of 0.5 was used for conversion of SOM to SOC, as with the Griffiths data above. Soil depth increments varied among datasets, so data were harmonized to the same set of depths as were used in all other analyses (0-10, 10-20, 20-50, 50-75, 75-100 cm) by taking a weighted average. NRCS Soil Survey (SSURGO) data were downloaded from ‘Web Soil Survey’ using a shapefile of the HJA boundary for the AOI. Other datasets were downloaded from Google Earth Engine databases and included “Soil Grids” and “Polaris” data products. The original Soil Grids, first released in 2014, predicts global soil properties on a 1 km grid. It was updated to “SoilGrids250m” in 2017 and algorithms were updated from linear models to tree-based machine learning models, so the predictions are now primarily data-driven (Hengl et al., 2017). They report that extensive covariates derived from remote sensing data were used for these modeling efforts, including variables such as MODIS EVI, monthly precipitation and landform classes. Hengl et al. (2017) found in their cross-validation that their predictions for SOC tended to underestimate the overall mean with wide prediction intervals. Based on this, the researchers caution against using their predictions for detailed spatial modeling. The Soil Grids dataset was thus chosen as a coarse resolution (250 m spatial resolution) comparison product. Polaris Probabilistic Soil Properties is a USGS 30 m spatial resolution map of soil properties that covers the contiguous United States. Polaris data were developed using ML on high-resolution GIS data to remap the SSURGO database. Its developers claim that it offers solutions to some of the weaknesses in SSURGO data. Those weaknesses cited include the practice of gap-filling where soils were not mapped using data from the surrounding regions and the artificial discontinuities produced where political boundaries exist. Polaris was thus chosen as a finer resolution (30 m) data comparison product.

Results

RF model results for predicting SOC

When all predictor variables were included in the random forest model for prediction of percent C, the variance explained by the model was 86.6% (Fig. 3.1). I grouped covariates in physical, climate, and biological groupings to examine the relative proportion of variation explained by each set of covariates. The variance explained was scaled between zero and one to maintain interpretability between predictors used in each random forest. Depth was the most important covariate in predicting soil C, closely followed by mean elevation (physical drivers – though it could be argued that elevation more closely represents a combination of climate variables in the form of a moisture and temperature regime gradient). Mean daily maximum temperature was the next most important predictor, with distance to nearest stream explaining nearly as much variation. The first biological driver in order of variable importance was aboveground biomass (AGB), which explained almost half as much variation in soil C as did depth. The vegetation assemblage groupings consistently came up as the least important predictors, explaining almost none of the variation in soil C, and were excluded from the final model. Similarly, the landscape position variable, geomorphon, was not an important predictor of soil C, but was slightly more predictive than was vegetation assemblage.

As described in the methods section, it was necessary to perform a rigorous cross-validation of each RF model by strategically leaving out sets of data and predicting them using a bootstrapping approach. While the bootstrapped model explained much less variation overall ($R^2=0.29$), it showed a strong correlation with the full model (0.54 correlation coefficient) and regressed quite similarly to both the full model and the 1:1 line (Fig 3.1 inset plot).

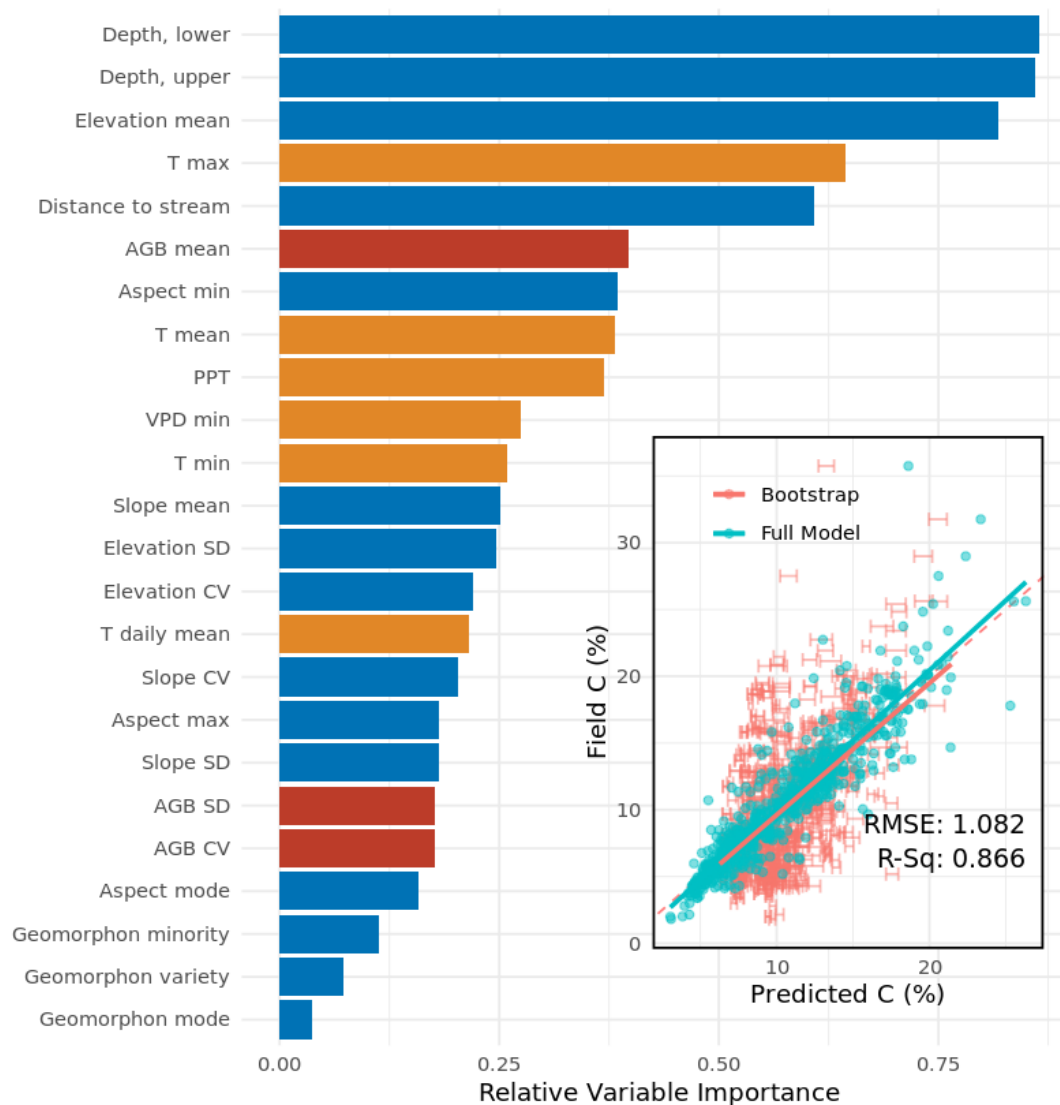


Figure 3.1 Variable importance plot for RF prediction of soil C % with an inset plot of the regression of the predicted model versus the measured data and the goodness of fit of the cross-validated bootstrapped model. Colors represent covariate groupings, with blue representing physical variables, red representing biological variables, and yellow representing climate variables.

Using the same predictor variables, I built an RF model to predict soil C stock (Mg ha^{-1}) in the fine earth fraction of 1 m depth of soil, but excluded depth as a predictor variable (Fig. 3.2). This was to isolate depth as a predictor from the rest of the environmental covariates, given that depth alone explained a large proportion of the variance in soil C and may overwhelm the effect of

other important predictors. With depth excluded, the RF model explained 65 percent of the variance in soil C stock. This indicates that depth alone explains about 20 percent of the total variance in soil C when the full model is compared with the constrained model. With depth excluded, the remaining ranking of variable importance was quite similar, except that precipitation increased in relative importance as an explanatory variable.

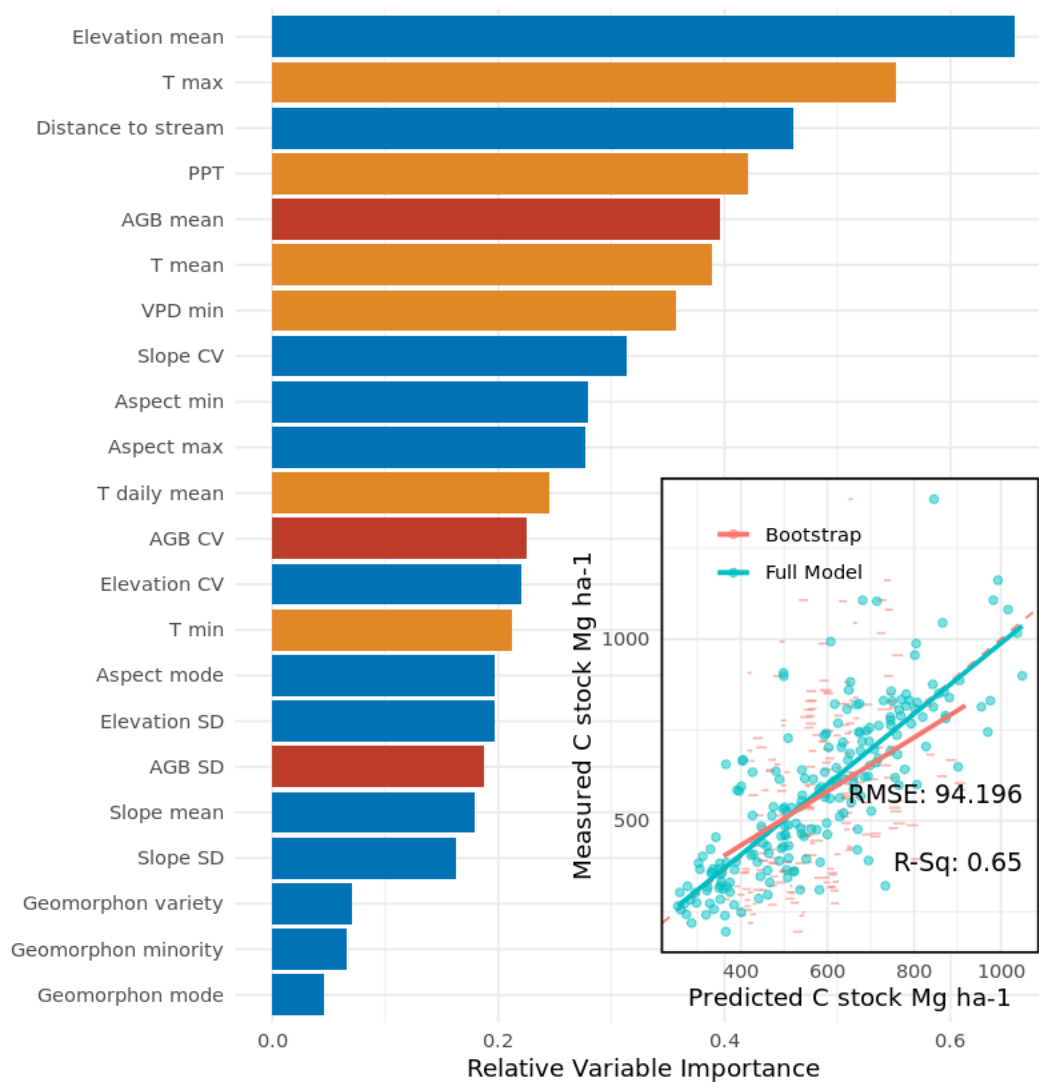


Figure 3.2 Variable importance plot for RF prediction of soil C stock to 1 m depth, excluding depth as a predictor variable, with an inset plot of the regression of the predicted model versus the measured data and the goodness of fit of the cross-validated bootstrapped model. Colors represent covariate groupings, with blue representing physical variables, red representing biological variables, and yellow representing climate variables.

RF modeling results for prediction of N

The same covariates were used in an RF model to predict organic N, with a similar, but not the same, set of predictors coming up as the most important (Fig. 3.3). Depth was comparatively less important than were elevation, mean daily maximum and mean daily temperature, and distance to nearest stream. The goodness of fit of the full model was high ($R^2 = 0.95$, RMSE = 0.047), and although the cross-validation with the bootstrapped data showed much greater variance, the regression was still close to that of the full model and the 1:1 line. The split between the variance explained by the most important predictor, mean elevation, and the next two most important predictors, mean daily maximum temperature and distance to nearest stream, was much greater than in the C model.

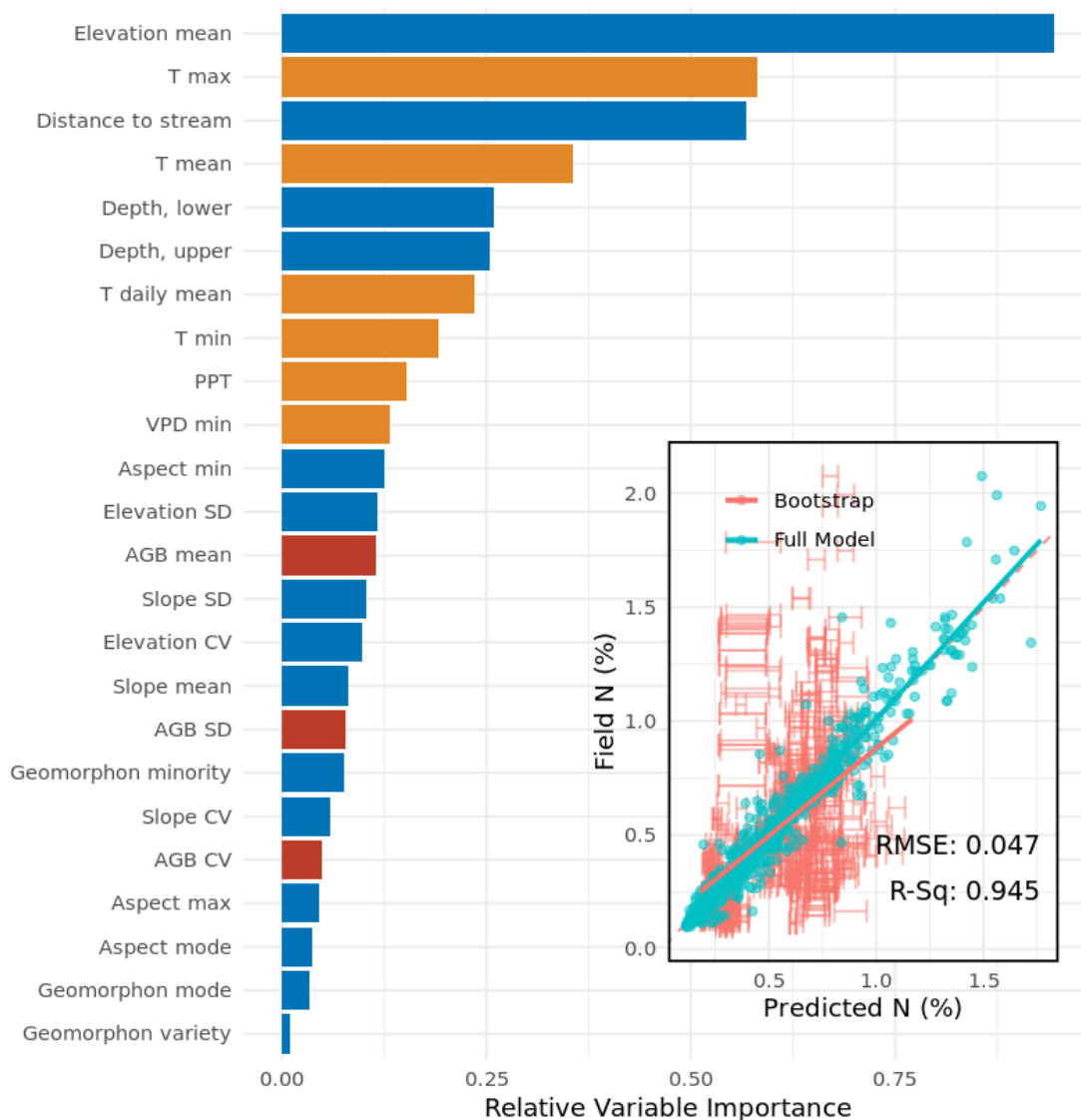


Figure 3.3 Variable importance plot for RF prediction of soil N with an inset plot of the regression of the predicted model versus the measured data and the goodness of fit of the cross-validated bootstrapped model. Colors represent covariate groupings, with blue representing physical variables, red representing biological variables, and yellow representing climate variables.

RF model results for prediction of C:N

As with the other RF models, I used the same covariates to predict the C:N and the model was, again, highly predictive of my measured C:N data ($R^2 = 0.97$; Fig. 3.4). Depth was not an important predictor in this model, given that C:N did not differ by depth.

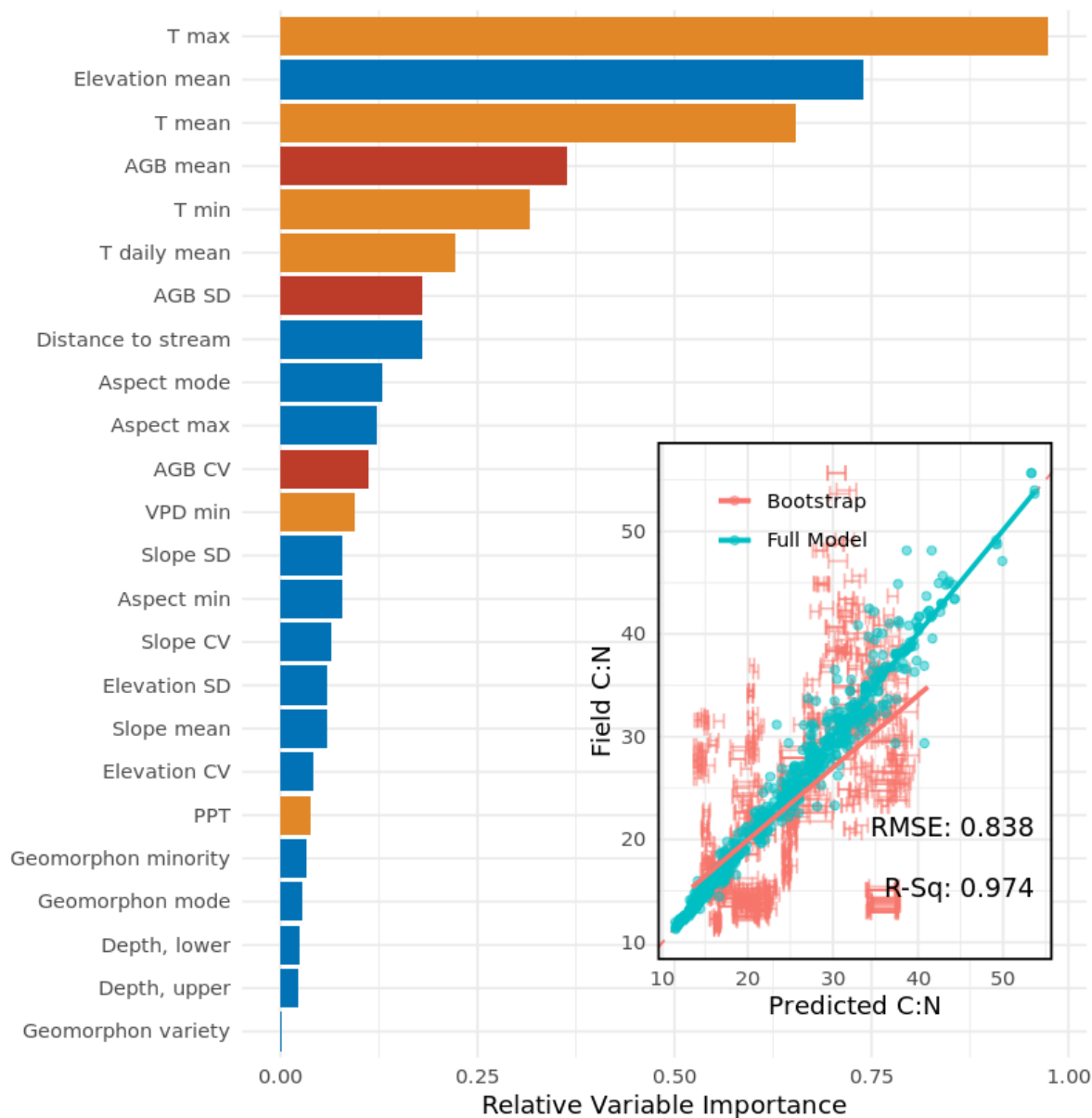


Figure 3.4 Variable importance plot for RF prediction of soil C:N with an inset plot of the regression of the predicted model versus the measured data and the goodness of fit of the cross-validated bootstrapped model. Colors represent covariate groupings, with blue representing physical variables, red representing biological variables, and yellow representing climate variables.

Mapped products from RF predictions at 100 m² spatial resolution

Across HJA, predicted soil C concentration ranged from 67 to 250 mg C g⁻¹ soil in the 0-10 cm depth increment (Fig. 3.5). Soil C concentrations appeared to follow a strong elevation gradient, with lower C concentrations generally in lower elevation areas and higher C concentrations in high elevation areas (see Fig. 3.6). There was a strong positive trend between closer proximity to stream and greater soil C, especially within about 50 m of a stream. The highest elevation ridges on Carpenter Mountain and Lookout Mountain (~1600 m) show high C concentrations concentrated on the ridge itself that quickly decrease with descending elevation off each side slope of the ridge, until a headwater begins for each stream network and the C concentration quickly increases again (Fig. 3.7). In the 75-100 m depth, C concentration is decreased to between 44 and 161 mg C g⁻¹ of soil and appears less correlated with elevation and more correlated with distance to stream than in the surface depths (Fig. 3.8). There is a pattern of speckling present at the deeper depths, where spatial variation in soil C concentration is high at short distances, which could be attributed to greater uncertainty in soil C estimates at that depth.

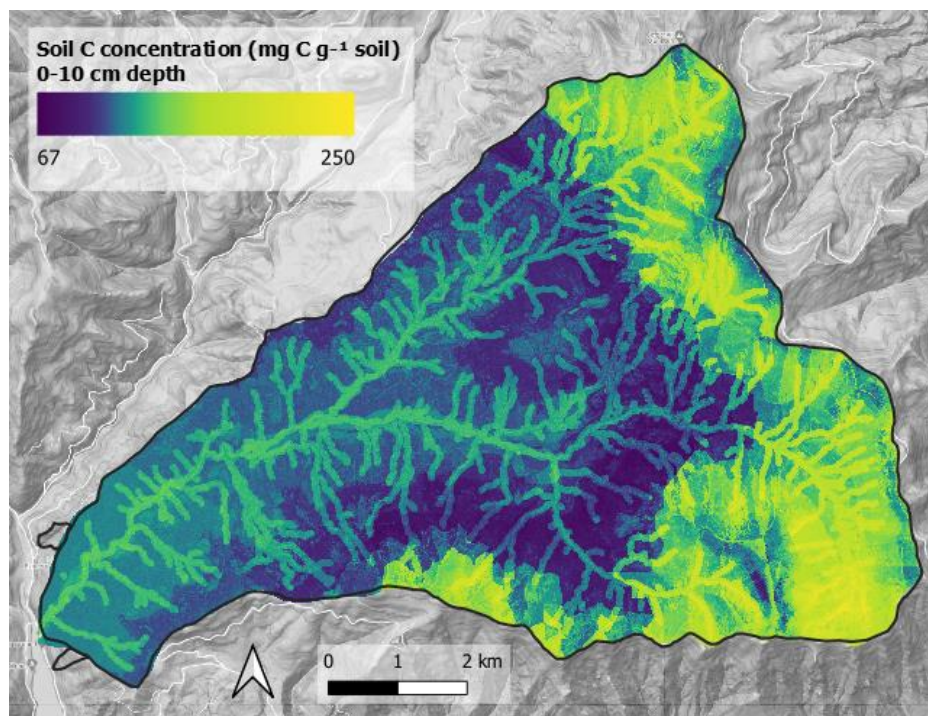


Figure 3.5 Spatial distribution of predicted soil C concentration across HJA in the 0-10 cm soil depth increment at a 10 m x 10 m pixel size.

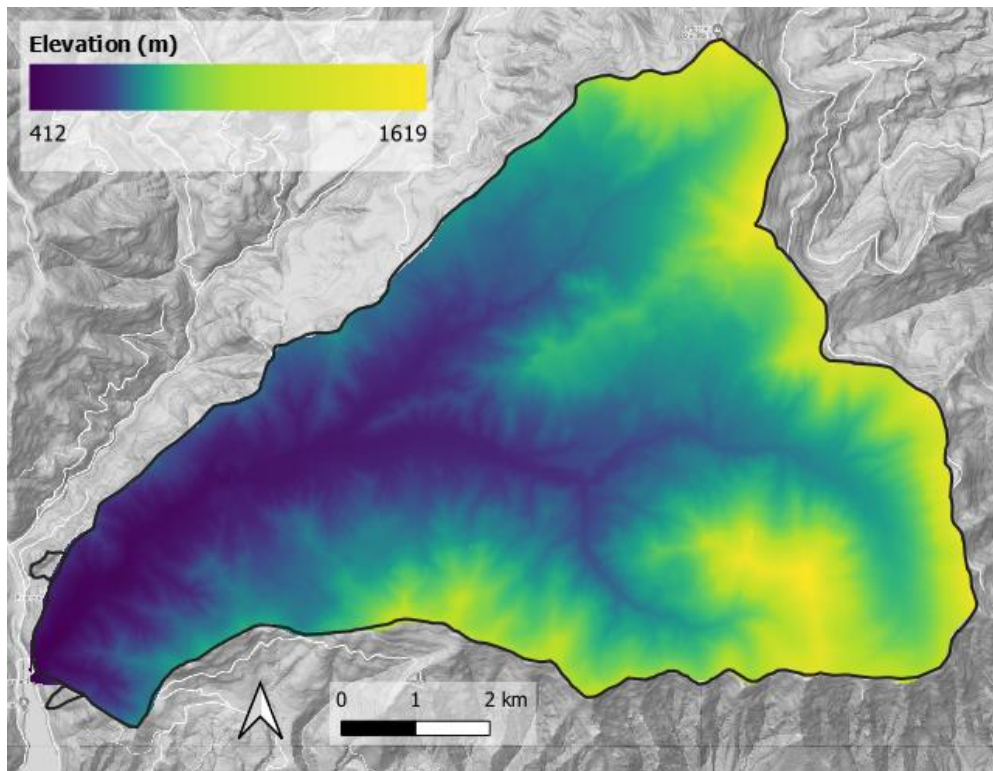


Figure 3.6 Elevation map of HJA in meters.

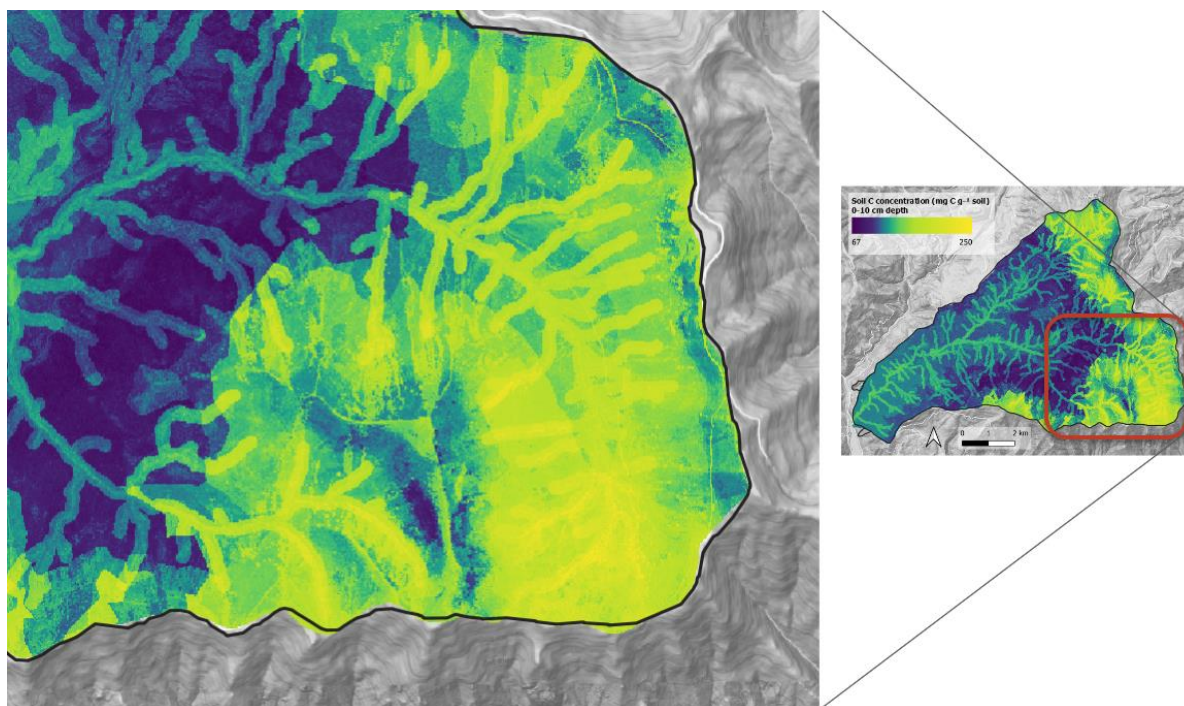


Figure 3.7 Lookout Mountain region enlarged to show patterns in soil C concentration at finer spatial scale.

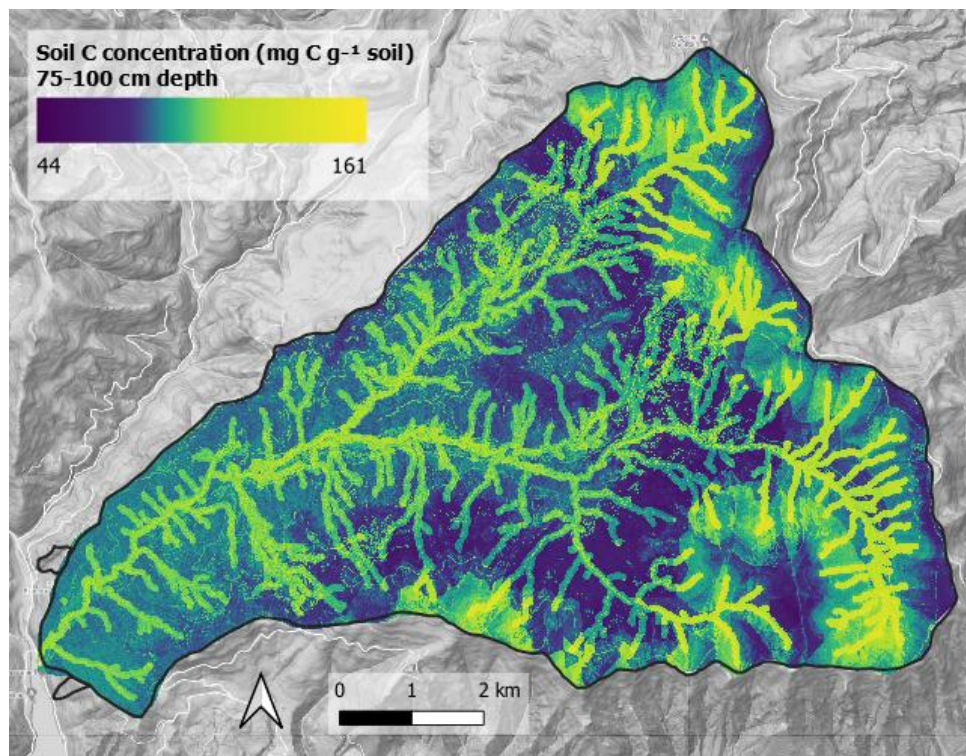


Figure 3.8 Map of predicted soil C concentration across HJA in the 75-100 cm depth increment at 10 m x 10 m spatial resolution.

Predicted soil N concentrations follow similar broad-scale spatial patterns to those of soil C, with greater N at high elevations and following waterways (Fig. 3.9). The gradient N follows is somewhat smoother than the C gradient, which showed more fine-scale spatial patterning in comparison. The N gradient distinctly follows elevation bands, with the highest N concentrations predicted between 1100 and 1300 m elevation. There's a decrease in N above and below these elevations, and below 1100 m, distance to stream appears to replace elevation as the dominant driver of N distributions.

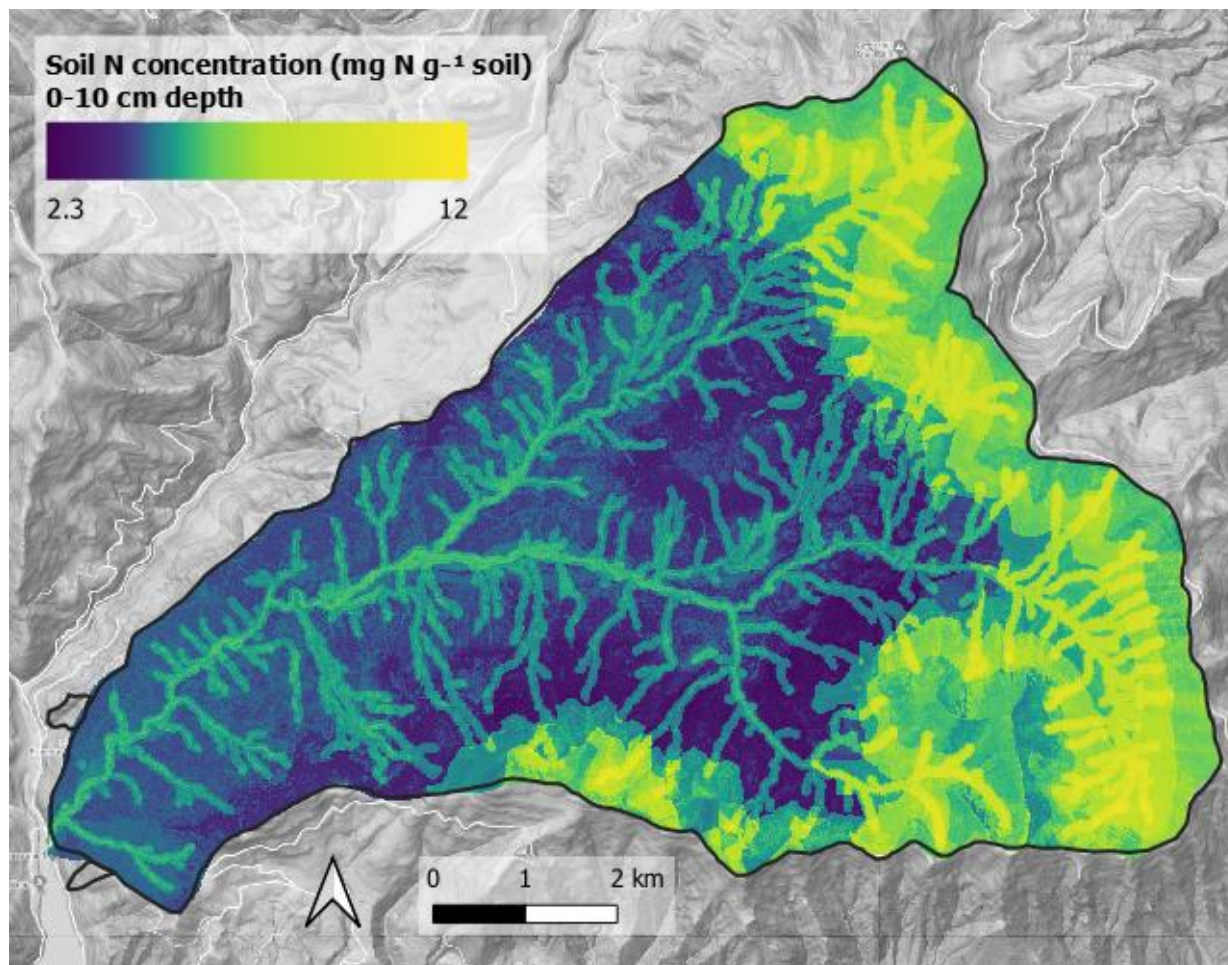


Figure 3.9 Map of predicted soil N concentration in the 0-10 cm depth increment across HJA.

The predicted C:N shows different spatial patterns than either the C or the N map alone, with finer scale spatial patterns becoming evident (Fig. 3.10). Aboveground biomass distributions and areas of disturbance (forest harvest and mass movements) are much more apparent in the C:N map. At a larger scale, the C:N ratio is greatest in lower elevation areas but decreases with closer proximity to stream. Higher elevation areas have a distinctly low C:N, especially along ridges, as do areas of disturbance. C:N ranges from a low of 13.7 at high elevation to a high of 36.6 in lower elevation vegetated regions. C:N stayed constant with depth.

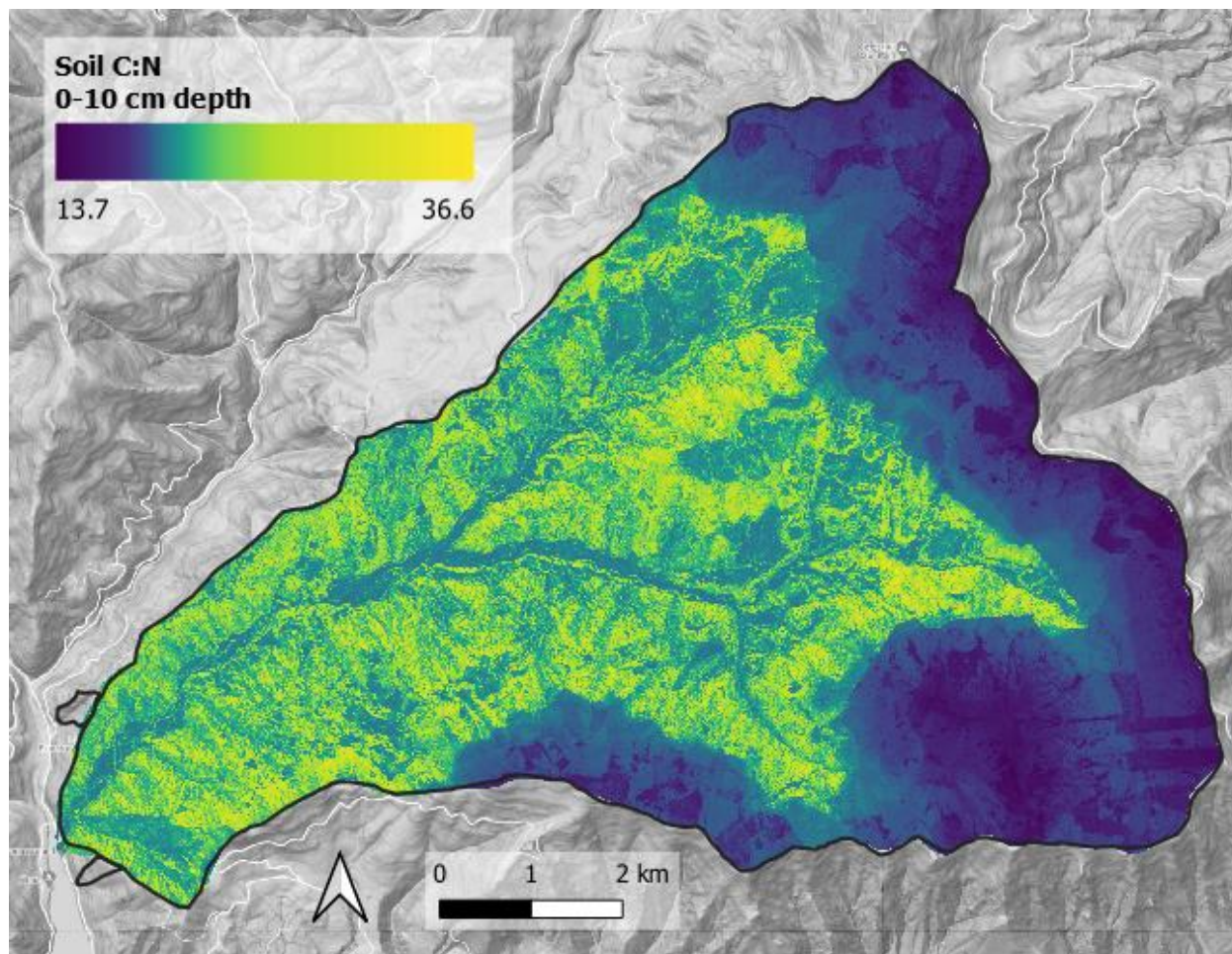


Figure 3.10 Map of predicted soil C:N in 0-10 cm depth increment across HJA.

Predicted soil C stock followed similar trends to those of mapped soil C concentration but showed an even greater positive trend associated with streams and showed similarly strong associations with particular high elevation bands (1100-1300 m; Fig. 3.11). The side slopes and foot slopes of Lookout Mountain and other highly sloped areas showed the smallest C stocks (a low of 218 Mg ha^{-1} in the fine earth fraction to 1 meter depth), while flatter regions and valleys had the greatest soil C stocks (to a high of 873 Mg ha^{-1}).

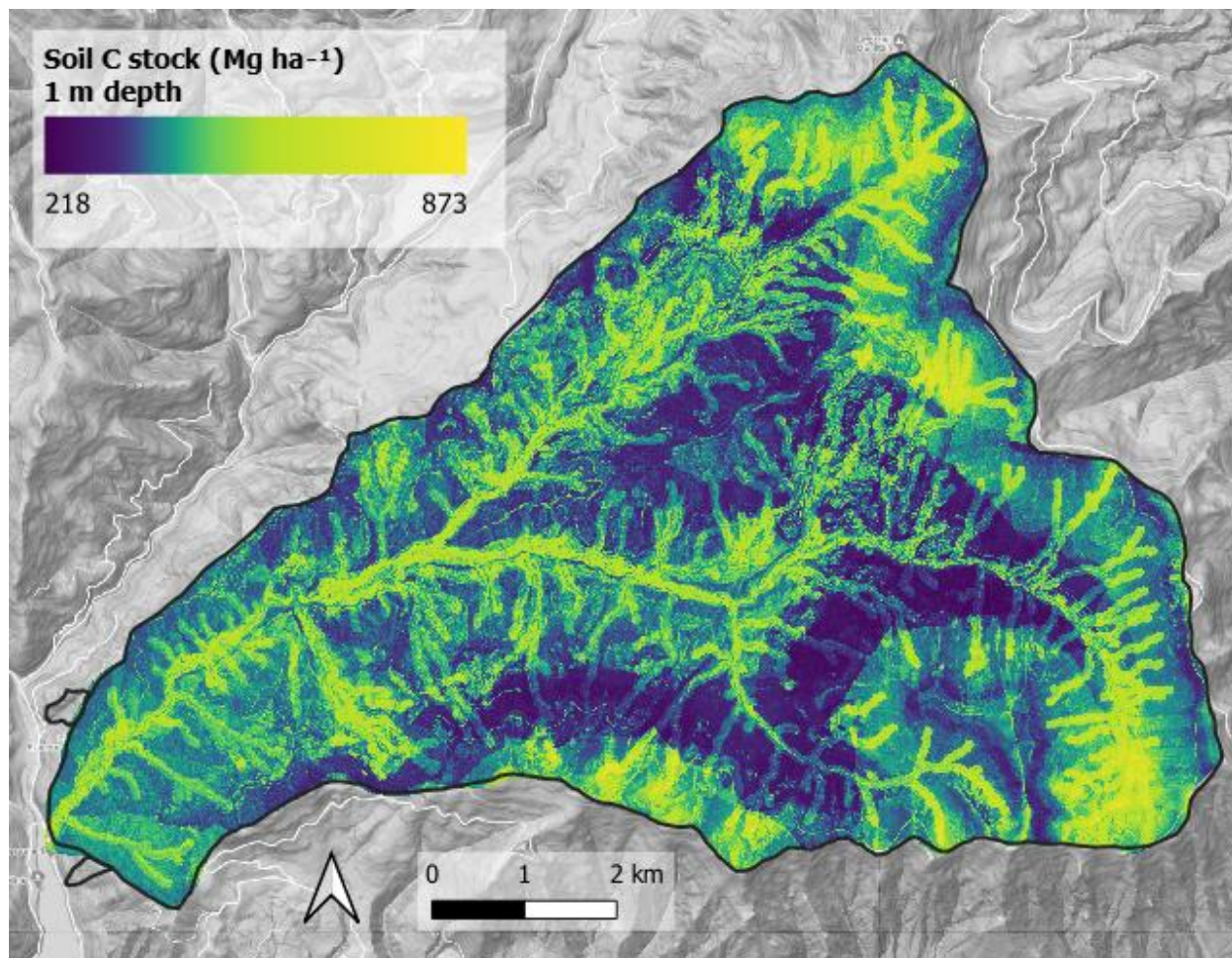


Figure 3.11 Map of predicted soil C stock to 1 m depth across HJA.

Predicted POM-C concentration in the 0-10 cm depth ranged from 43.8 to 195 mg g⁻¹ soil (Fig. 3.12) and 21 to 160 mg g⁻¹ soil in the 75-100 cm depth (Fig. 3.13). There were strong correlations between greater POM-C concentration, close proximity to stream, and higher elevations. Predicted MAOM-C concentration showed a strikingly different distribution than did POM-C (Fig. 3.14). In the 0-10 cm depth, MAOM-C varied between 13.7 and 36 mg g⁻¹ soil, while in the 75-100 cm depth, the mean concentration was only slightly greater – varying between 14.8 and 41 mg g⁻¹ soil (Fig. 3.15). Distance to stream was much less influential to the MAOM-C concentration than to the POM-C concentration. MAOM-C instead followed an

elevation gradient, where it was greatest in the flattest valleys below 800 m elevation, but increased sharply again in certain areas above 1400 m elevation.

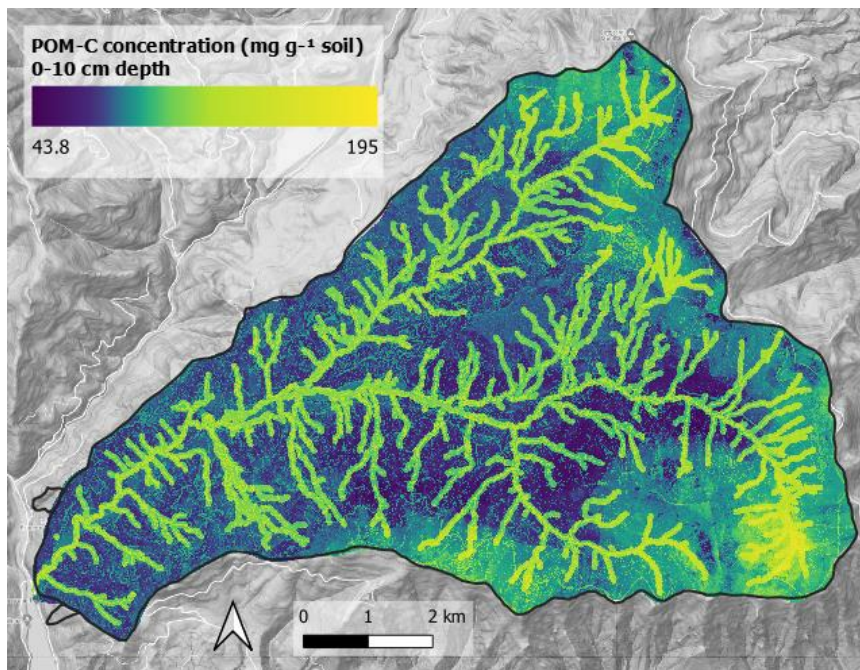


Figure 3.12 Map of predicted POM-C concentrations across HJA in the 0-10 cm soil depth increment.

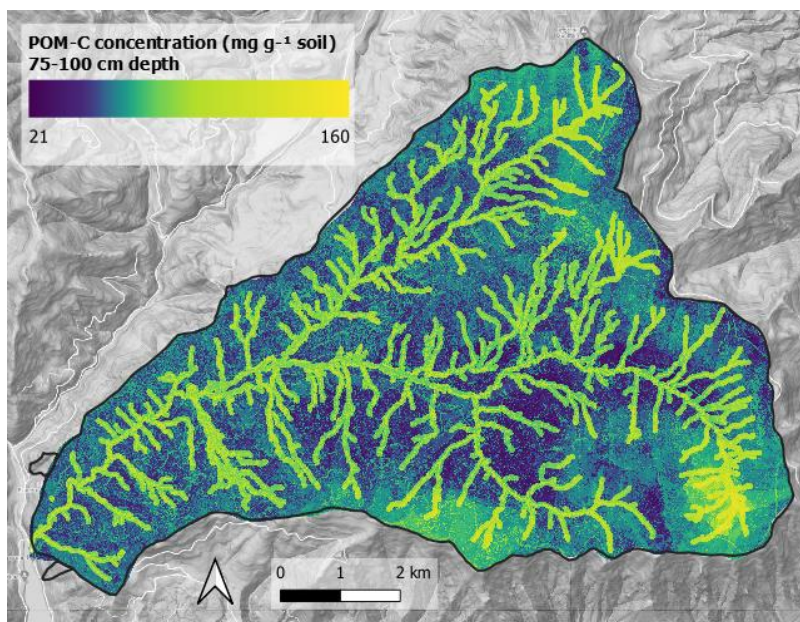


Figure 3.13 Map of predicted POM-C concentration in the 75-100 cm soil depth across HJA.

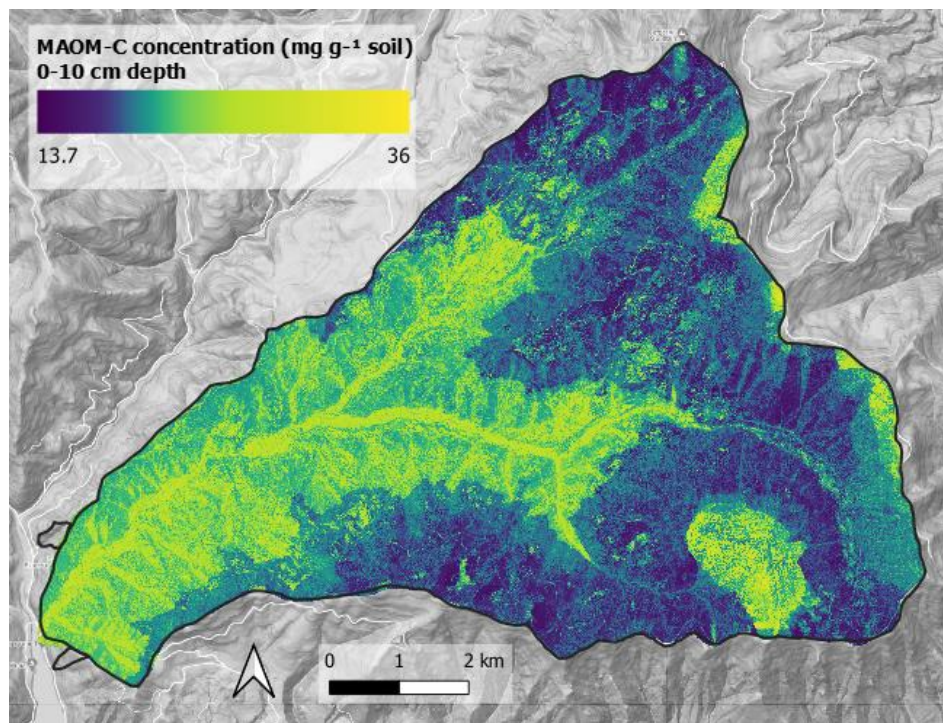


Figure 3.14 Map of predicted MAOM-C concentration in the 0-10 cm depth increment across HJA.

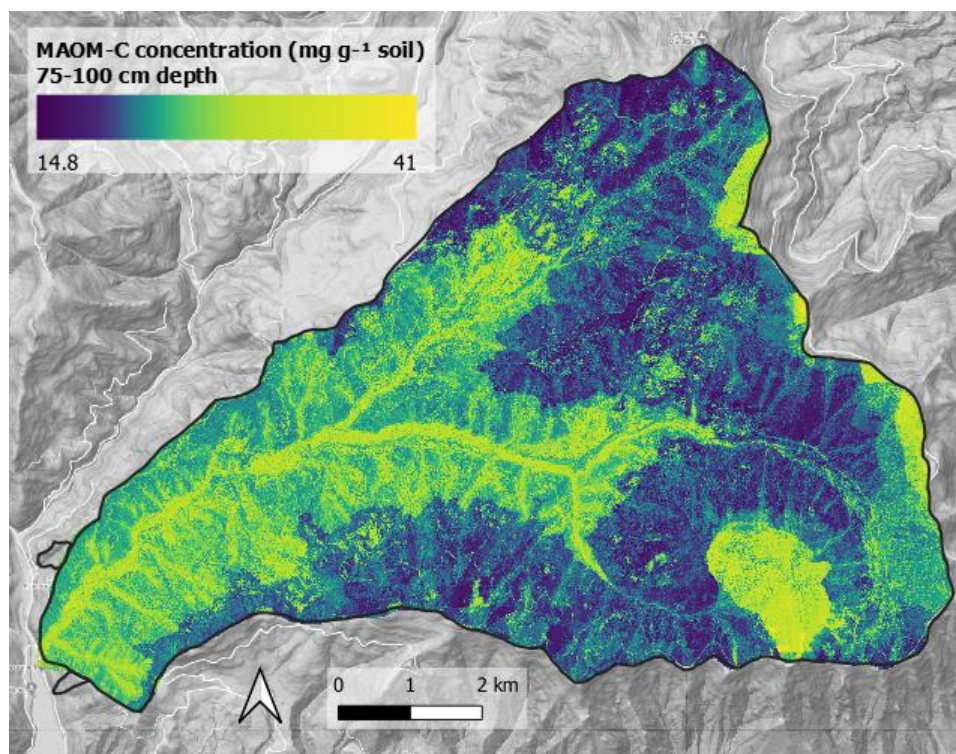


Figure 3.15 Map of predicted MAOM-C concentration in the 75-100 cm depth across HJA.

A cross-validation of my RF model using Griffiths' data

I used the same covariates in an additional RF model to test its accuracy in regions of HJA where I had not sampled (mostly lower elevations and regions that had been harvested previously). The most important predictors in the Griffiths model were climate variables (temperature and precipitation), and distance to stream came up as explaining a negligible amount of the variation in SOM. The correlation coefficient between Griffiths' measured and predicted SOM was 0.57, compared with the correlation coefficient between Griffiths' model predictions and our measured SOC (divided by 0.5 to convert to SOM) of 0.41. A linear regression of Griffiths' model predictions versus measured data produced a statistically significant $p < 0.01$ at the 0.05 alpha level, with an R^2 of 0.32. The Griffiths model was less predictive of my data, with an R^2 of 0.16 ($p < 0.01$). However, when the models are regressed against each other, they predict similarly and are close to the 1:1 line (Fig. 3.16).

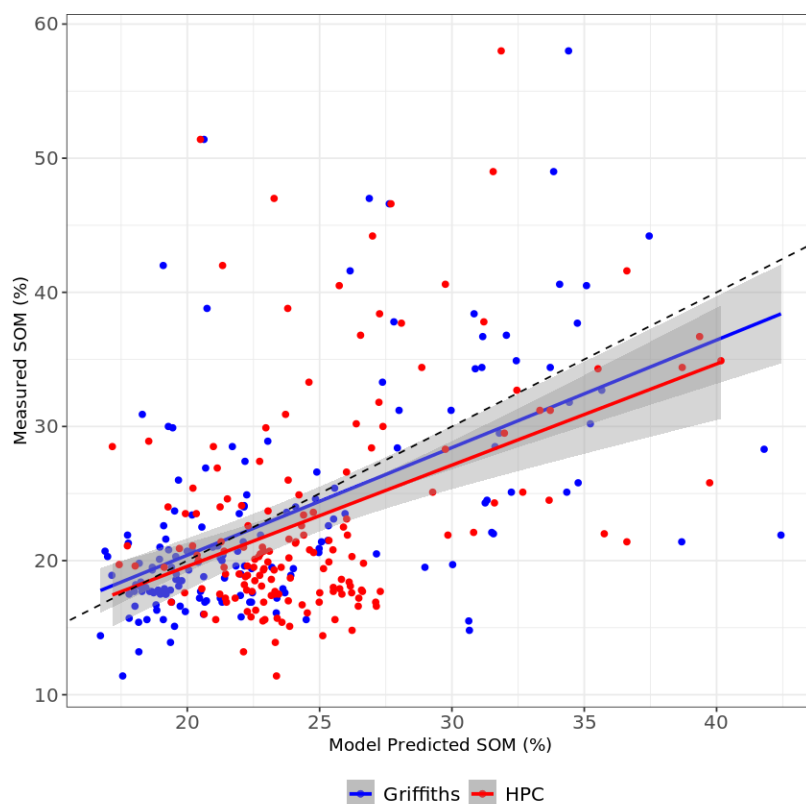


Fig. 3.16 RF model prediction comparison between my RF-predicted SOM and measured SOC (converted to SOM; 'HPC') and between my RF-predicted values and Griffiths' measured SOM.

SOC stock comparisons with publicly available datasets

When SOC stock predictions across HJA were compared between my model and publicly available datasets, there was some overlap between SOC predictions from all four datasets, but the range of estimates varied widely between them (Fig. 3.17). The estimates from my RF model were higher, and Polaris data were the lowest, with SSURGO and Soil Grids in between. There was little agreement between my modeled results and Polaris when the data were regressed against each other (Fig. 3.18), more agreement with Soil Grids (Fig. 3.19), and much less with SSURGO (Fig. 3.20). When I tested the strength of correlation between each of the datasets and my data, I found the strongest correlations between my RF-modeled data and Soil Grids (Fig. 3.21; $\text{corr}=0.31$), a negative correlation with SSURGO (-0.49), and no meaningful correlation with Polaris (0.05). My site-level and transect-level measured data showed a similar degree of correlation with Soil Grids as my RF-modeled data, but greater correlation with Polaris than did my modeled data (between 0.24 and 0.3) in the 0 - 10 cm depth. In the 0 - 100 cm depth, correlation among the above pairs was similar – between 0.23 and 0.35 . The SSURGO soil C in 0 - 10 cm was negatively correlated with all other datasets, but in the 0 - 100 cm depth increment, SSURGO was positively correlated with my site-level and transect-level data (correlation coefficients of 0.34 and 0.23 , respectively).

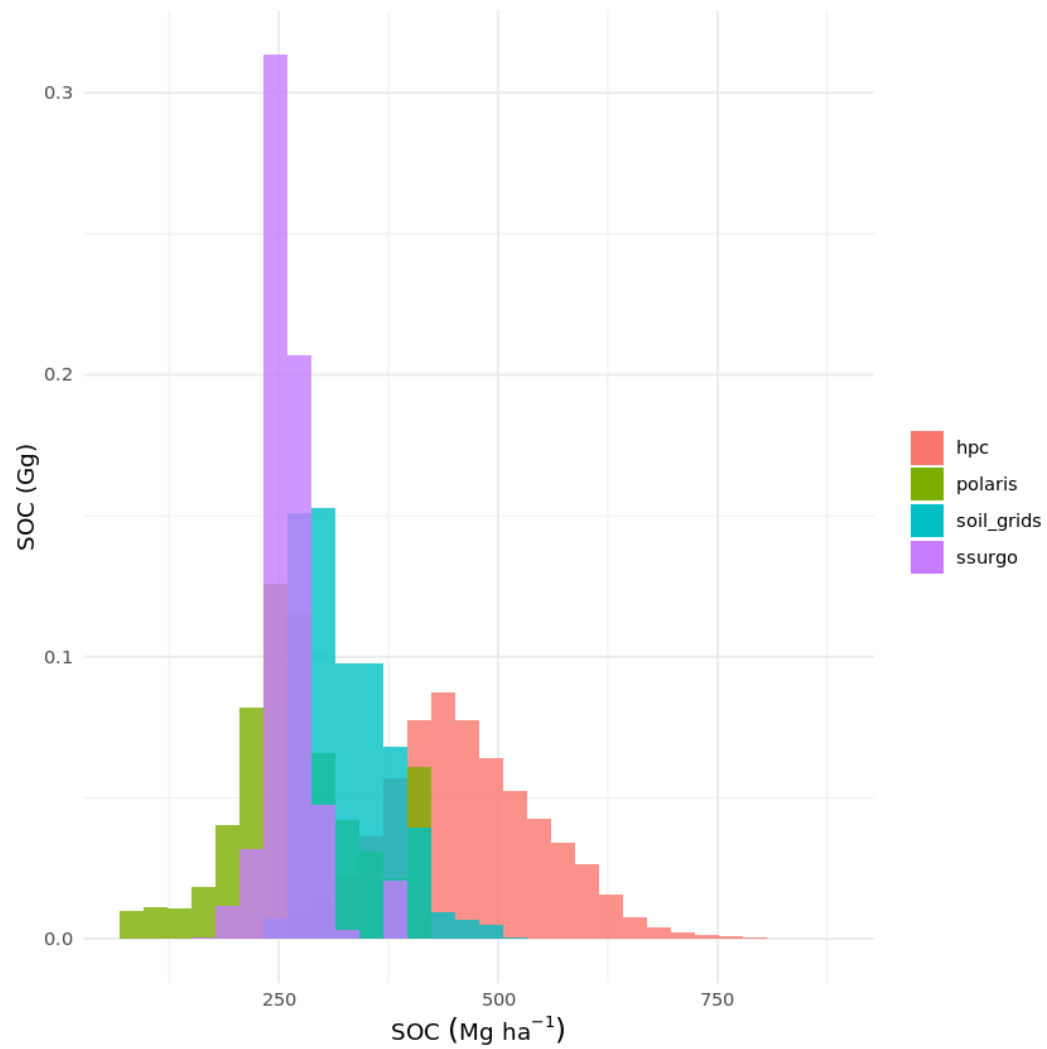


Figure 3.17 Range in distribution of estimated SOC in the top 1 m of soil for HJA.

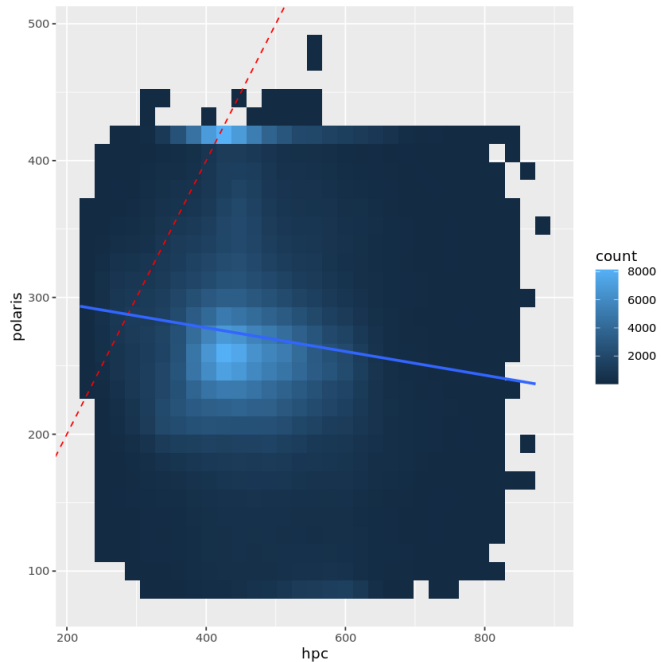


Figure 3.18 Regression of my RF-predicted soil C stock ('hpc') and the Polaris estimated C stock.

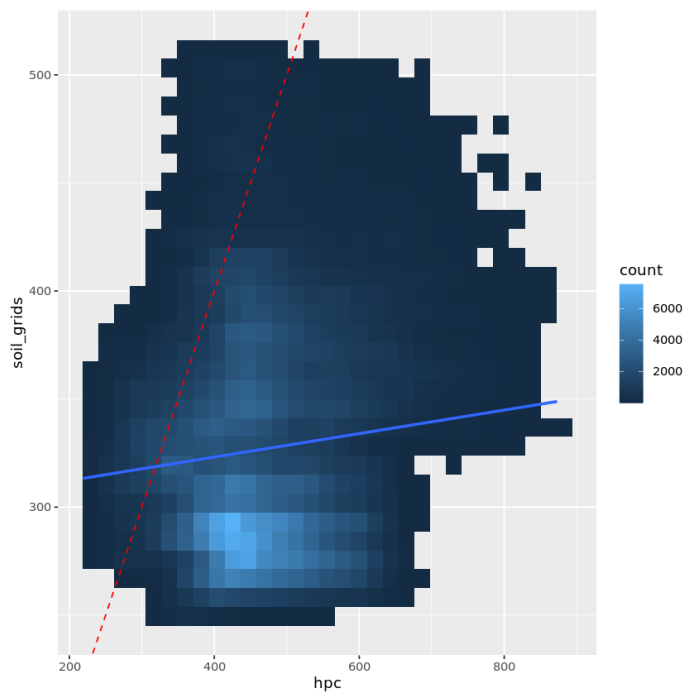


Figure 3.19 Regression of my RF-predicted soil C stock ('hpc') and the Soil Grids estimated C stock.

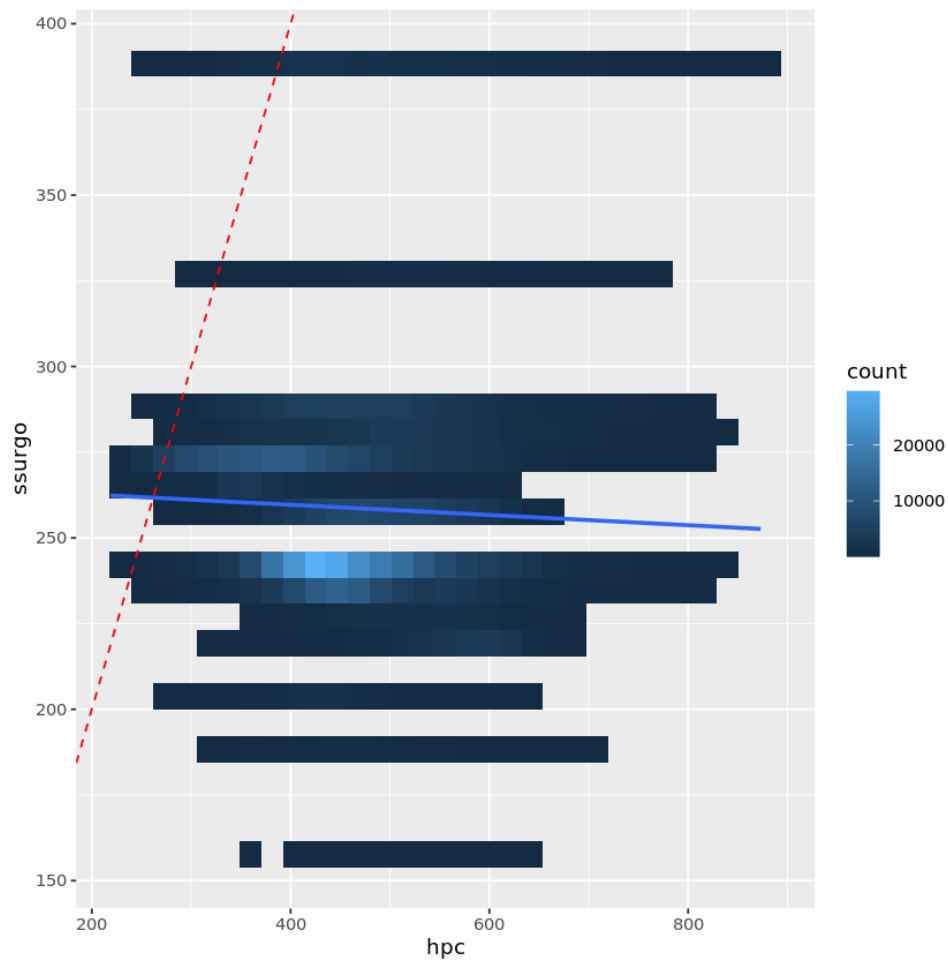


Figure 3.20 Regression of my RF-predicted soil C stock ('hpc') and the SSURGO estimated C stock.

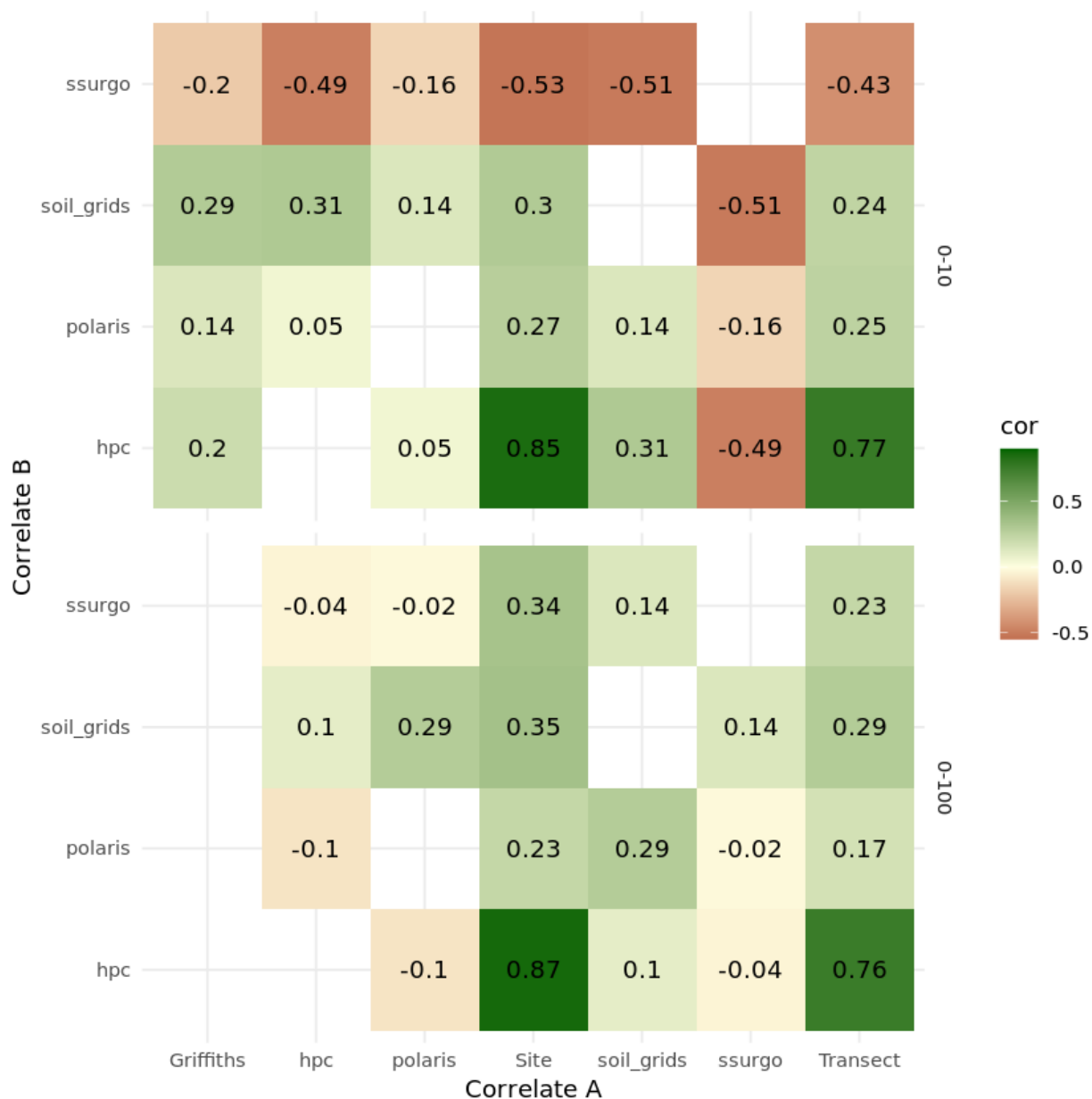


Figure 3.21 Correlation matrix for comparisons among publicly available datasets and my site-level (“Site”), transect-level (“Transect”), and RF-predicted (“hpc”) data, as well as another dataset generated by Robert Griffiths (“Griffiths”) from soil sampling 0-10 cm along HJA roads in the late 1990s. The top matrix contains correlation coefficients for 0-10 cm depth soil C predictions and the bottom matrix contains correlation coefficients for 0-100 cm depth soil C predictions.

Discussion

C and N trends with selected covariates

The predictors I had previously assumed would have the greatest influence on soil C and N distributions – chiefly vegetation and topographic position – were alone less influential than climate variables and proximity to water source, although they certainly contributed to variability in C and N distributions. To further explore some of the trends in significant covariates, I performed a series of regressions relating different drivers to SOC, soil N, and C:N, discussed and presented below.

A regression of SOC stock and distance to nearest stream shows a threshold distance that seems to be the most influential to SOC stock at around 50 m from a stream (Fig 3.22). At that distance, greater SOC stocks are associated with closer distance to stream. Beyond 50 m, SOC drops off precipitously as distance increases; the distribution appears to be bimodal at > 50 m and < 50 m, which appears to be the critical distance for influence of water source on SOC.

When mean daily maximum temperature is plotted against SOC stock, there appears to be some structure in the data that may describe the relationship between decomposition and plant productivity as a function of temperature (Fig 3.23). Plant productivity decreases with temperature, as does decomposition, but not at the same rate. The pattern in Fig 3.23 may be indicative of the point at which decomposition exceeds the rate of productivity – around 13°C , with decomposition becoming more important and starting to outweigh plant productivity around 14°C . The temperature trends could indicate that the rate of decomposition decreases more quickly than the rate of plant productivity with decreasing temperature. These temperature bands appear to correspond to elevation bands when mapped (as with the N data described below).

The SOC stock shows a negative relationship with slope – likely indicative of the erosion that happens as slope increases (Fig 3.24). This is an important process in HJA, where steep slopes

are common and snowmelt and heavy rainfall cause erosion from hillsides and deposition along the edges of river valleys.

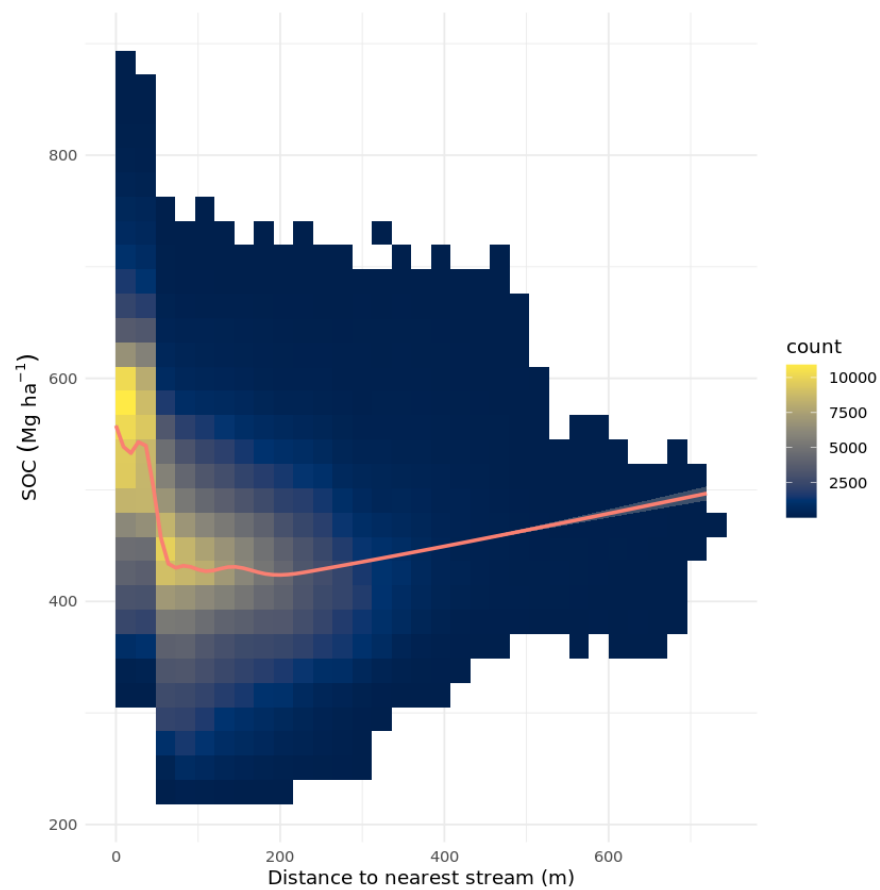


Figure 3.22 Relationship between SOC stock and distance to nearest stream across HJA.

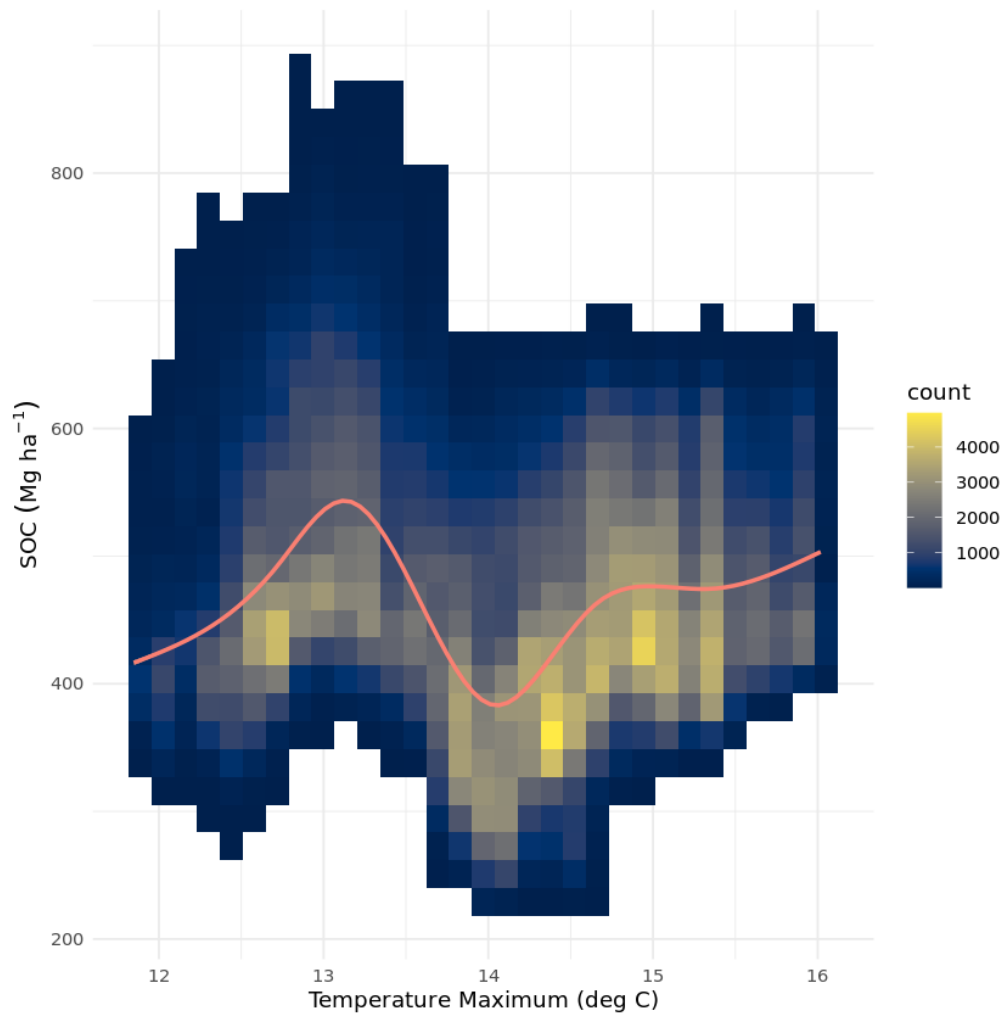


Figure 3.23 Relationship between SOC stock and mean daily maximum temperature across HJA.

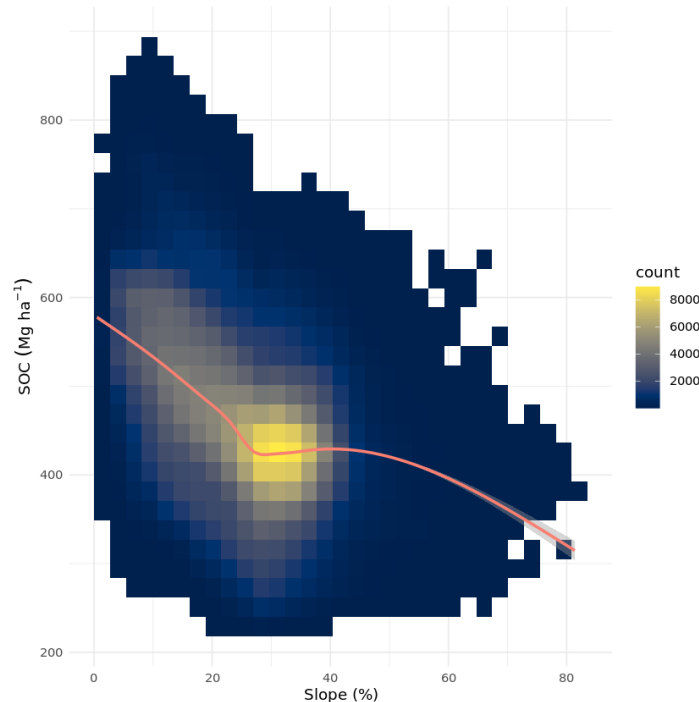


Figure 3.24 Relationship between SOC stock and percent slope across HJA.

A regression of elevation and soil N stock shows distinct banding at at least three distinct N thresholds (Fig. 3.25). These N bands appear to decrease slightly with increasing elevation, and are strongest at low N ($\sim 8\text{-}10 \text{ Mg ha}^{-1}$), indicating that there is a strong influence of elevation (which produces temperature and moisture gradients) on N. A regression of temperature and N shows the same trend but reversed – as daily maximum temperature increases, so does N (Fig. 3.26). To explore these N thresholds further, I plotted N stocks across HJA with thresholds that I identified as peaks in the temperature and elevation data (Fig. 3.27). I found that there was indeed a strong elevation gradient, where below $\sim 1100 \text{ m}$, N stock was $\leq 11 \text{ Mg ha}^{-1}$, and above that elevation, N stocks increased substantially to $15\text{-}20 \text{ Mg ha}^{-1}$, and $>22 \text{ Mg ha}^{-1}$ if within 50 m of a stream and above 1100 m. Although soil N distributions are expected to follow N-fixing vegetation types like red alder (*Alnus rubra*), these patterns were not evident at the landscape scale in HJA. However, they were present in the site-level data presented in chapter 2. Red alder is known to be a pioneer species that establishes quickly after landscape disturbance, so it is

possible that the finer scale N distributions that are evident along roads and along streams (regions of greater soil N concentrations) are a result of alder presence.

There was some structure present in the data when C:N was regressed against aboveground biomass, but the pattern was not consistent across the landscape (Fig. 3.28). There appeared to be two significant groupings of high and low C:N that produced a somewhat bimodal distribution of C:N at relatively low biomass ($\sim 300\text{-}400 \text{ Mg ha}^{-1}$), where one grouping had low C:N (<25) and a larger grouping had higher C:N (30-38). This could be due to differences in vegetation type or forest harvest history. When C:N was classified into groupings of low C:N (18-25) and high C:N (28-37) and mapped across HJA, the groupings strongly followed an elevation-driven temperature gradient, with low C:N at the low-temperature, high elevations, and high C:N in the lower-elevation, higher temperature regions (Fig. 3.29; Fig 3.30). This pattern was mainly influenced by N, as it showed the same pattern as N when plotted (Fig. 3.16), except that the influence of distance to stream was not identifiable in the C:N map. While distance to stream was a less influential driver of C:N based on the map, suggesting that other drivers overwhelmed its influence, a regression of distance to stream versus C:N corroborated the significant influence of 50 m distance to stream as a strong peak in the distribution (Fig. 3.31). At distances of 100-200 m, the influence of stream on C:N substantially decreased. Within 50 m of a stream, the majority of the distribution centered around a C:N of 30-35, indicating that higher C and lower N were correlated with distance to stream. However, there was also a lower C:N peak between 20 and 23 that suggested that lower C and higher N could also be associated with closer proximity to stream in certain areas. These areas were determined to be high elevations near the heads of streams based on the N map (Fig. 3.27). The C:N versus AGB and C:N versus distance to stream plots (Fig. 3.28 and Fig 3.31) show similar bimodal distributions, but in the peak at lower C:N, the ratio of C to N is much lower with lower AGB than it is with close proximity to stream. This suggests that moisture availability may be more influential to C:N than is the amount of biomass.

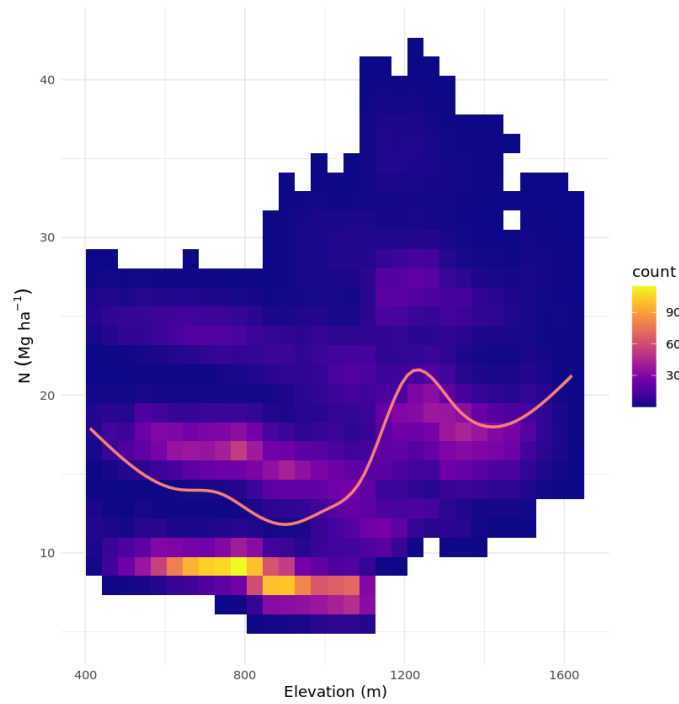


Figure 3.25 Relationship between elevation and soil N across HJA.

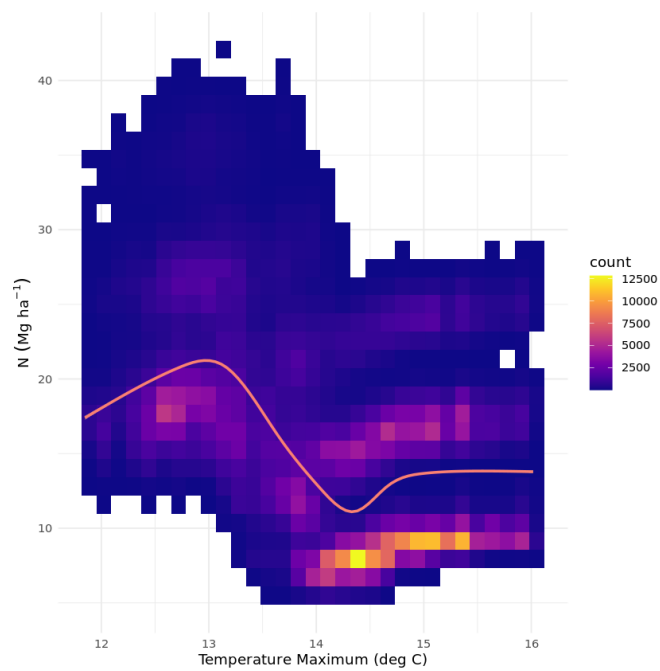


Figure 3.26 Relationship between mean daily maximum temperature and soil N across HJA.

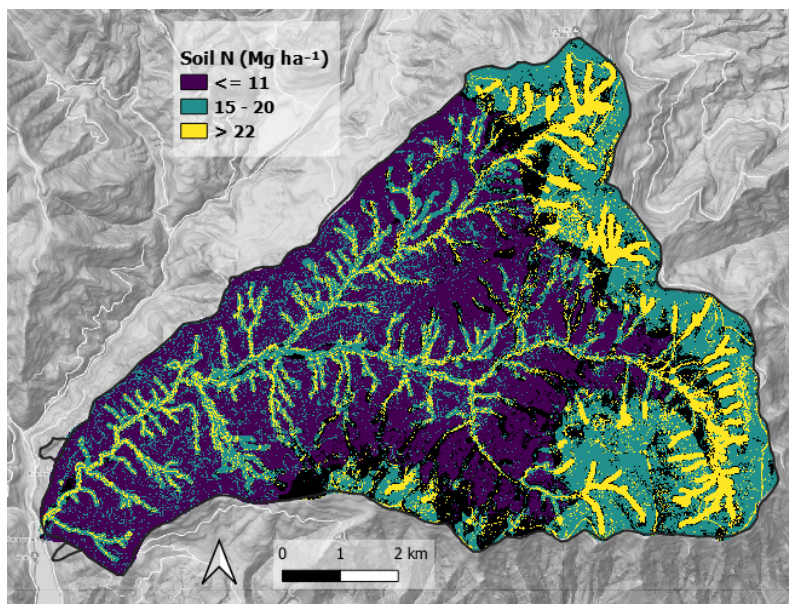


Figure 3.27 Map of predicted N stock to 1 m soil depth across HJA, classified and visualized by natural breaks in the data.

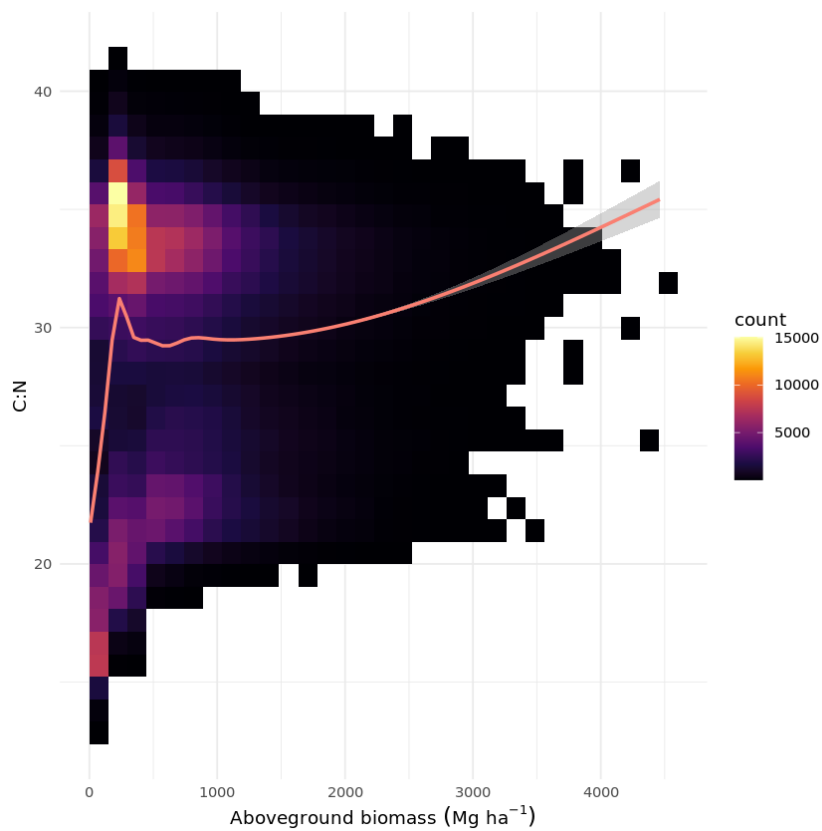


Figure 3.28 Relationship between aboveground biomass (AGB) and C:N across HJA.

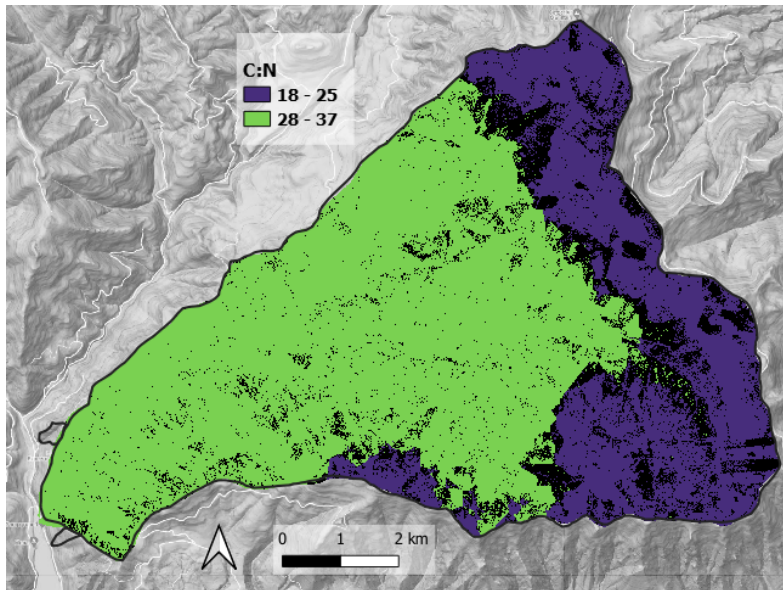


Figure 3.29 Map of C:N across HJA in the 0-10 cm depth increment, visualized by significant peaks in the C:N data.

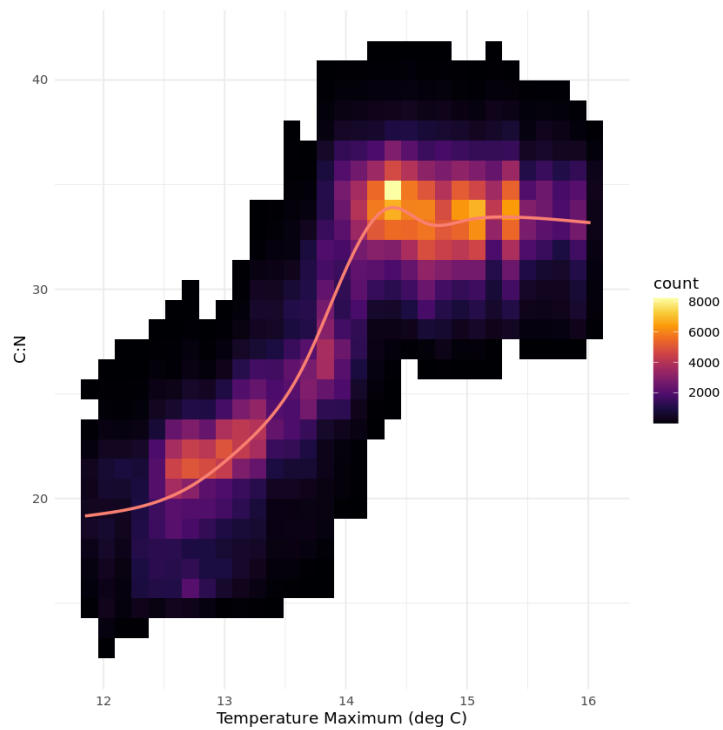


Figure 3.30 Relationship between mean daily maximum temperature and C:N across HJA.

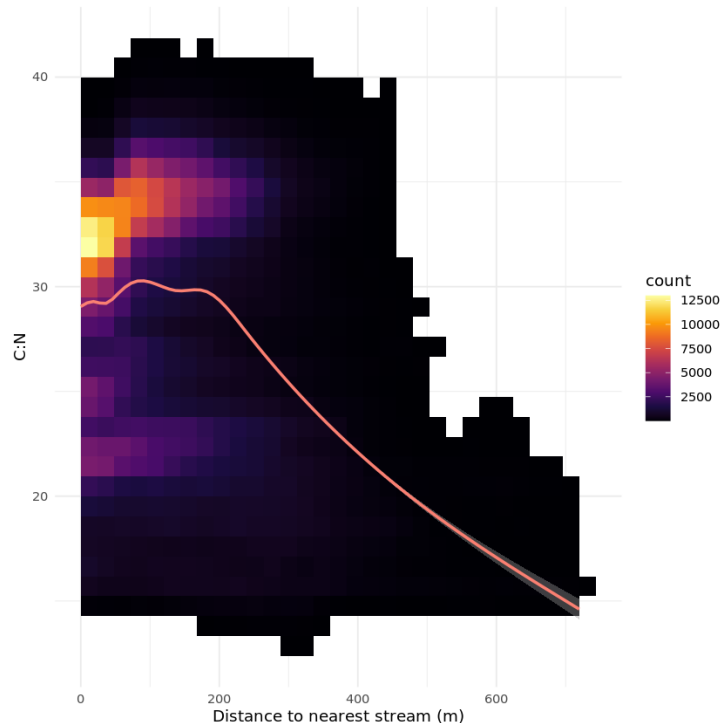


Figure 3.31 Relationship between mean distance to nearest stream and C:N across HJA.

Large- and small-scale spatial patterns

On a global scale, temperature and precipitation represent the dominant controls on SOC cycling (Post, 1982), while vegetation, topography, and parent material may become more significant drivers at increasingly smaller spatial scale. The strong elevation gradients present in HJA can be used as a proxy for temperature and moisture thresholds and point to the overwhelming influence of climate at the km and even 10-50 m scale. The abrupt edges at particular elevation bands, such as 1100 to 1300 m, show critical thresholds where temperature and moisture become limiting to biological activity and to the biogeochemical processing of nutrients that results. Despite the strong influence of climate at different elevations in HJA, proximity to a water source (a smaller, meso-scale driver) is a dominant driver of C and N distributions, outcompeting climate in certain areas (e.g., high elevation watershed heads and low elevation valleys). Other drivers thought to be significant predictors of soil C and N were less so – surprisingly, AGB, vegetation assemblage, and topographic position were much less predictive than expected. Of those three, AGB was perhaps the most important, but was always secondary or tertiary to other predictors at

the landscape scale. Topographic position showed some significance in that high slopes were important for nutrient loss and transport from an area, and aspect could be seen as influential in the E-W ridge divide on Lookout Mountain, where N concentrations were greater on the W-facing slope than the E-facing slope (Fig. 3.9). This could be a function of higher productivity on the W aspect, which experiences less seasonal moisture limitation than does the E aspect.

In agreement with previous studies in HJA and other cool, temperate forests, soil C and N increased with elevation (Post et al., 1985; Hart & Perry, 1999; Griffiths et al., 2009; Jenny, 2012). Organic matter resulting from primary productivity at high elevations is retained because the cold temperatures limit microbial activity (Paul, 2014). In a soil transfer experiment at HJA, Hart & Perry (1999) transferred soils from high elevations to low elevations and vice versa and found that the soils originally from the high elevation sites had more than doubled soil net N mineralization and nitrification rates when transferred to the low elevation sites, while soils transferred from the low to high elevation sites resulted in greatly reduced N mineralization and nitrification. This evidence further supports the conclusion that high elevations in Oregon's central Cascades support greater soil C and N storage than similar low-elevation sites as a function of temperature limitations on C and N mineralization at high elevations.

Mineralogical influences

While clay content has long been used as the principal modifier of SOM turnover rates in biogeochemical models due to its ability to sorb organic matter and promote aggregation, recent research efforts have pointed to the flaws in this simplistic representation and have instead cited the importance of specific physicochemical properties (Rasmussen et al., 2018). In humid, forested regions, an abundance of Fe and Al can be a strong predictor of SOM as both can bind organic matter. Rasmussen et al. showed that short range order (SRO) minerals and Ca may be more important drivers above pH 5.5, while lower pH (as in HJA soils) favors organo-metal complexation as the dominant factor. In HJA, the prevalent steep slopes prevent accumulation of clays in many areas, but moderately sloped regions and valleys are able to collect deep residual and colluvial, clay-rich soils. However, clay content tends to decrease with elevation if it is

below a weathering threshold since coarse, young volcanic material has not had sufficient time to develop significant secondary clay minerals (Osterloh, 2018).

Additional trends with elevation: Persistent snowpack and Andisol formation

Osterloh's (2018) research in the Oregon Cascades suggests that snow and high annual precipitation (exceeding 150 cm) is highly influential in the formation of andic properties and Andisols, perhaps outweighing the influence of parent material as the most important factors for Andisol formation. He states that the rapid weathering caused by high levels of precipitation removes the soluble, base-forming cations from the soil, causing the less mobile Fe and Al to become oversaturated in the soil solution, thus forming short-range order (SRO) minerals. In his study, SRO minerals increased with elevation, meaning that the presumed capacity for C sorption increased with elevation. The prevalence of andic properties including SRO minerals were positively associated with elevations above 1000 m. Precipitation typically falls in the form of snow above elevations of 1200 m and can persist from December through April in the highest elevations. Mountainous regions are already experiencing decreased seasonal snowpack as a result of anthropogenic climate change. A recent review predicted a decline of 25% in snow water equivalent across the western US in the next 50 years (Siirila-Woodburn et al., 2021). With only a 2°C increase in winter temperatures, much of this snow is at risk of converting to rainfall (Nolin & Daly, 2006). As persistent snow lines increase in elevation and move further North in latitude, there may be fewer regions that have the conditions necessary for Andisol formation – and for the soil C storage that comes along with andic properties.

Distributions of POM and MAOM

Mineralogy is expected to be an important driver of not only bulk C distributions, but also MAOM-C distributions. Parent material and soil texture are significant drivers of MAOM-C, since the underlying mineralogy is necessary for interaction and potential for sorption with organic matter. To perhaps a lesser extent, vegetation and climate influence MAOM-C distribution. Clays and phyllosilicate materials with large surface area bind organic matter, forming soil aggregates. Plant roots provide labile C exudates to the microbial community in the rhizosphere, and those microbes aid in the aggregation processes.

I investigated the potential relationship between SSURGO mapped clay percent, MAOM-C, mapped rocks, wetlands and meadows, and soil bulk density to attempt to explain the distribution of MAOM-C across HJA (Figs. 3.32-3.36). As expected, there was a strong correlation between soil bulk density and MAOM-C (Fig. 3.34; Fig. 3.35). The higher bulk density along the ridge of Lookout Mountain was in agreement with the high prediction of MAOM-C in that area. Interestingly, as an aside, the prediction of greater bulk density in Watershed 1 of HJA (lower left corner of Fig. 3.34) would appear to agree with its harvest history (clearcut), particularly compared with the lower bulk density in its paired old growth Watershed 2 to the right of it. However, the mapped clay did not entirely agree with the MAOM-C distribution. There were low elevation areas in valleys that contained both greater clay content and greater MAOM-C, but the high MAOM-C content on the top of Lookout Mountain was not reflected by a high clay content – at least as predicted by SSURGO. When I plotted MAOM-C concentration as a function of clay percentage, I found some correlation between moderate clay concentration and moderate MAOM-C concentration (Fig. 3.32). The high bulk density along the ridge of Lookout Mountain did not entirely explain the distribution of MAOM-C, which covered a wider area on top of the mountain. The abundance of mapped “rocks, cliff, talus, steep tag alder patches” and wetlands and dry meadows on top of Lookout Mountain (Fig 3.36) could help further explain the MAOM-C in that area, since the alder patches and meadows are very likely higher soil N areas, and higher soil N correlates with a greater microbial community abundance for processing the organic compounds that form MAOM (in opposition to greater fungal abundance, which would tend to process a greater proportion of C and not lead to MAOM formation, according to current understanding).

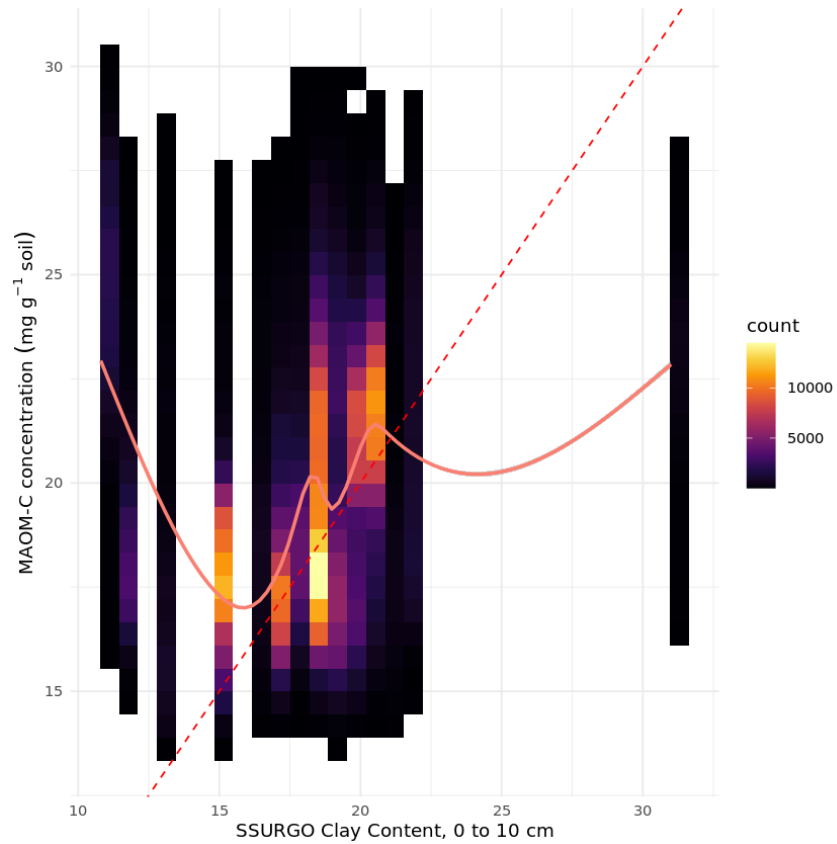


Figure 3.32 Relationship between MAOM-C concentration and SSURGO clay content in the 0-10 cm soil depth increment.

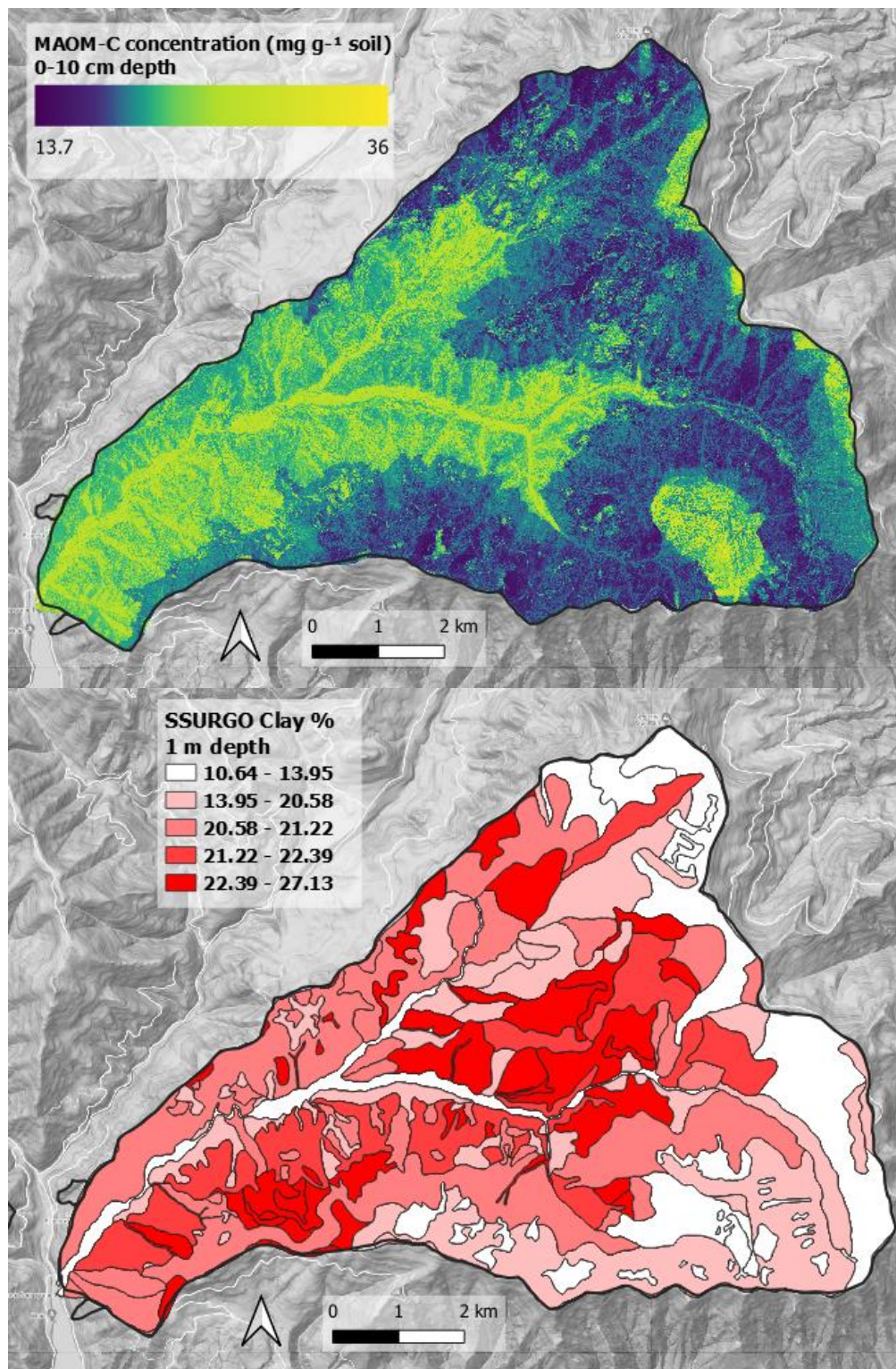


Figure 3.33 Map of SSURGO estimated clay percentage across HJA to 1 m depth (bottom) paired with MAOM-C concentration (top) for visual comparison.

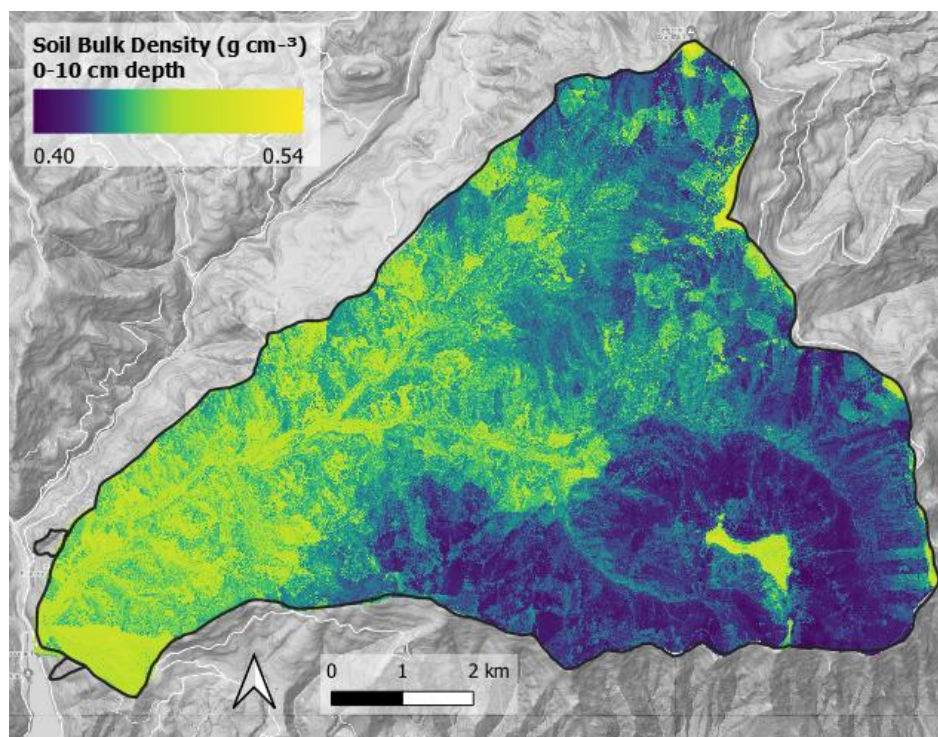


Figure 3.34 Map of soil bulk density at 0-10 cm depth increments across HJA.

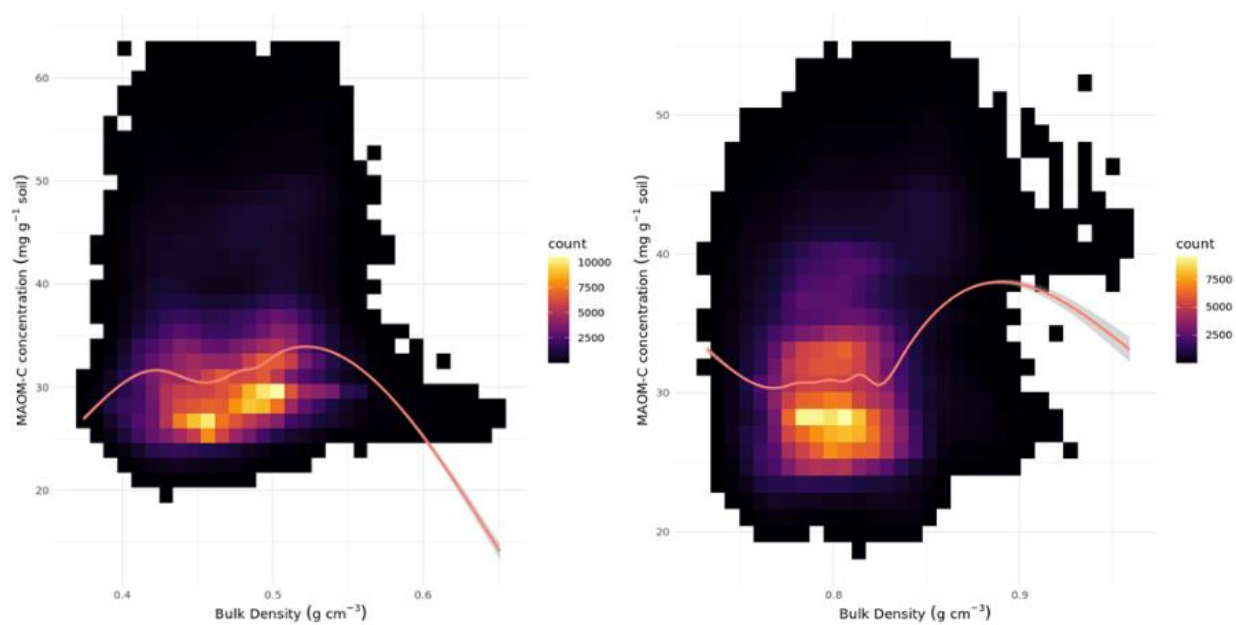


Figure 3.35 Relationship between bulk density and MAOM-C concentration in the 0-10 cm soil depth increment (left) and 75-100 cm depth increment (right).

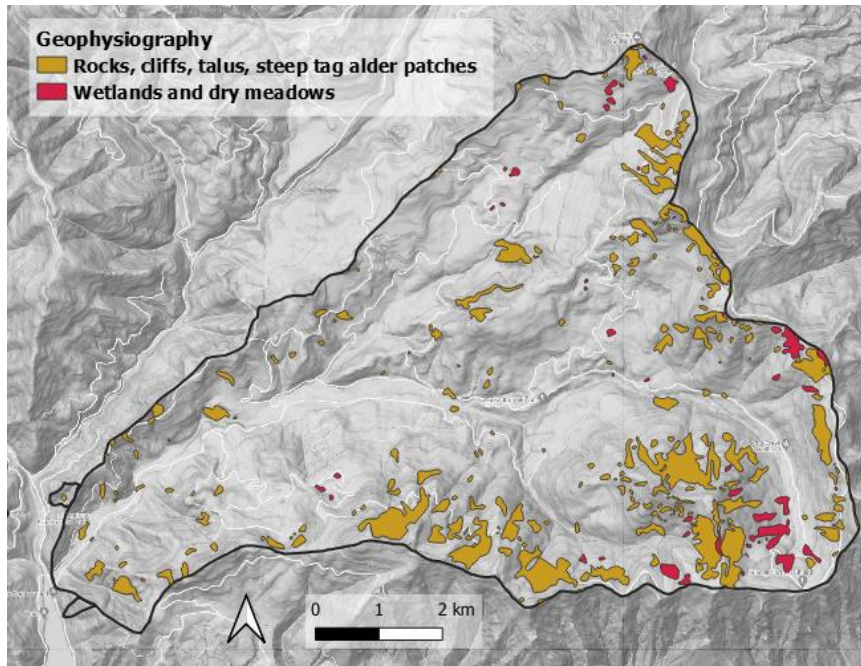


Figure 3.36 Mapped rocks, cliffs, talus, steep tag alder patches, wetlands, and dry meadows across HJA.

Climate has long been recognized as a primary driver of soil C and N distributions (Jenny, 1961). Jobbágy & Jackson (2000) noted in a meta-analysis of global SOC stocks that the relative distribution of SOC with depth had a slightly stronger association with vegetation than with climate, but that the opposite was true for the absolute amount of SOC. In their analysis, total SOC increased with clay content and precipitation, and decreased with temperature. In shallow depths, climate was the primary driver, while in deeper depths, clay content was the dominant predictor of SOC. However, Rasmussen et al. (2018) showed that it is not just the amount of clay that is important for C interactions in soil, but the types of clays present, as well as the acidity and soil moisture regime. Rasmussen demonstrated that in acidic soils in humid temperate forests, Al- and Fe- complexes are the most important predictors of SOC, while in drier environments and with increasing pH, short-range order (SRO) minerals, Ca, and total clay emerged as more important drivers.

Torn et al. (1997) suggested that the non-crystalline amorphous Al and Fe hydroxides that accumulate in weathered soils may retain SOC for millenia. The 1:1 silicate clays are associated with shorter SOC timescales due to their more limited sorptive capacity than the larger surface area 2:1 silicate clays. Since weathering of volcanic parent material proceeds from metastable, non-crystalline mineral formation over the first ~150,000 years to accumulation of more stable crystalline minerals after that, the capacity for C sorption should follow a similar timeline (greater capacity in younger volcanics but decreasing over time on a millennial scale). As the volcanics weather, they transform from the Andisols known for their high C retention to Oxisols with a lower capacity to stabilize C.

Transitions from seasonal snowpack to precipitation in the form of rainfall may be expected to increase the proportion of POM-C:MAOM-C in Cascade Mountains if there are commensurate increases in primary production and decomposition at high elevations that cause increased mineralization of C and N. Heckman et al. (2021) found that persistence of all C pools decreased with increasing mean annual temperature throughout the soil profile, while persistence increased with increasing wetness index in subsurface soils (30-176 cm). In their study, MAOM-C in surface soils (<30 cm) increased more strongly with increasing wetness index than did POM-C, but both pools showed decreased response to wetness index at depth. They conclude that climate showed a strong influence on soil C properties, and that there was risk of loss of soil C from protected pools in areas with decreasing wetness.

Future work

Although my RF models are highly predictive in their current state, there is much room for improvement through additional field sampling across the lower elevations of HJA and the mid elevations of Lookout Mountain, and through model refinement using additional and/or improved predictor variable datasets. Additional sampling would lend greater confidence to model estimates in areas that were not sampled and could be used to validate future models. I was surprised to find that the vegetation assemblages were not at all predictive of soil C, and I hypothesize that this is an artifact of the map not being truly representative of the spatial

distribution of vegetation across HJA. An improved vegetation assemblage map or a spectral data source like NDVI could be used instead, since it is well-established that vegetation type will influence soil C and N. Another improvement could be a data source that has high resolution parent material and mineralogy estimates across HJA. This could be used to better understand MAOM-C distributions across the region. Additional field sampling could aid this effort. Data sources that reach beyond the bounds of HJA could help elucidate the patterns of high C and high N (and consequently low C:N) along ridges, as the ridges mainly occupy the outskirts of the mapped area, and, as a consequence, there are relatively few E-facing slopes to investigate. A final recommendation would be to obtain a high-resolution soil depth map that includes cobble and boulder estimates. Although they occupy a relatively small proportion of the entire HJA, it could be useful to mask out the rock outcrops and rockfall areas as regions that do not contain soil C. Likewise, cobble, boulder, and smaller rock fragment estimates in soils would help accurately predict soil C area-based estimates. Overall, the increasingly higher resolution GIS datasets, coupled with increased computing power and ML techniques, if coupled with intensive field sampling, offer great promise to the enumeration of soil properties and understanding of biogeochemical cycling.

BIBLIOGRAPHY

- Adachi, M., Ishida, A., Bunyavejchewin, S., Okuda, T., & Koizumi, H. (2009). Spatial and temporal variation in soil respiration in a seasonally dry tropical forest, Thailand. *Journal of Tropical Ecology*, 25(5), 531-539.
- Andrews, J.A., Harrison, K.G., Matamala, R, Schlesinger, W.H. (1999). Separation of root respiration from total soil respiration using carbon-13 labeling during free-air carbon dioxide enrichment (FACE). *Soil Sci Soc Am J* 63:1429–1435.
- Bache, S. M., & Wickham, H. (2021). magrittr: A Forward-Pipe Operator for R [Computer software]. Version 2.0.1. URL <https://CRAN.R-project.org/package=magrittr>.
- Bahn, M., Schmitt, M., Siegwolf, R., Richter, A., & Brüggemann, N. (2009). Does photosynthesis affect grassland soil-respired CO₂ and its carbon isotope composition on a diurnal timescale?. *New Phytologist*, 182(2), 451-460.
- Bailey, V. L., Pries, C. H., & Lajtha, K. (2019). What do we know about soil carbon destabilization? *Environmental Research Letters*, 14(8), 083004. <https://doi.org/10.1088/1748-9326/ab2c11>.
- Baston, D. (2022). exactextractr: Fast Extraction from Raster Datasets using Polygons. R package version 0.9.1. <https://CRAN.R-project.org/package=exactextractr>.
- Beaudette, D., Skovlin, J., Roecker, S., Brown, A. (2023). soilDB:Soil Database Interface. R package version 2.7.7. <https://CRAN.R-project.org/package=soilDB>.
- Bernard, L., Basile-Doelsch, I., Derrien, D., Fanin, N., Fontaine, S., Guenet, B., ... & Maron, P. A. (2022). Advancing the mechanistic understanding of the priming effect on soil organic matter mineralisation. *Functional Ecology*.
- Bivand, R.S. and Wong, D.W. S. (2018) Comparing implementations of global and local indicators of spatial association *TEST*, 27(3), 716-748. URL <https://doi.org/10.1007/s11749-018-0599-x>.
- Bond-Lamberty, B., Bailey, V. L., Chen, M., Gough, C. M., & Vargas, R. (2018). Globally rising soil heterotrophic respiration over recent decades. *Nature*, 560(7716), 80-83.
- Bond-Lamberty, B. & Thomson, A. M. (2010). Temperature-associated increases in the global soil respiration record. *Nature* 464, 579–582.
- Bowden, R. D., Nadelhoffer, K. J., Boone, R. D., Melillo, J. M., & Garrison, J. B. (1993). Contributions of aboveground litter, belowground litter, and root respiration to total soil

- respiration in a temperate mixed hardwood forest. *Canadian Journal of Forest Research*, 23(7), 1402–1407. <https://doi.org/10.1139/x93-177>.
- Bowling, D. R., McDowell, N. G., Bond, B. J., Law, B. E., & Ehleringer, J. R. (2002). 13 C content of ecosystem respiration is linked to precipitation and vapor pressure deficit. *Oecologia*, 131, 113-124.
- Boyle, S. A., Yarwood, R. R., Bottomley, P. J., & Myrold, D. D. (2008). Bacterial and fungal contributions to soil nitrogen cycling under Douglas fir and red alder at two sites in Oregon. *Soil Biology and Biochemistry*, 40(2), 443-451.
- Breiman, L. (2001). Random forests. *Machine learning*, 45, 5-32.
- Carbone, M. S., & Trumbore, S. E. (2007). Contribution of new photosynthetic assimilates to respiration by perennial grasses and shrubs: residence times and allocation patterns. *New Phytologist*, 176(1), 124-135.
- Chen, C., Chen, H. Y., Chen, X., & Huang, Z. (2019). Meta-analysis shows positive effects of plant diversity on microbial biomass and respiration. *Nature communications*, 10(1), 1332.
- Crow, S. E., Lajtha, K., Bowden, R. D., Yano, Y., Brant, J. B., Caldwell, B. A., & Sulzman, E. W. (2009). Increased coniferous needle inputs accelerate decomposition of soil carbon in an old-growth forest. *Forest Ecology and Management*, 258(10), 2224-2232.
- Crow, S. E., Lajtha, K., Filley, T. R., Swanston, C. W., Bowden, R. D., & Caldwell, B. A. (2009). Sources of plant-derived carbon and stability of organic matter in soil: implications for global change. *Global Change Biology*, 15(8), 2003-2019.
- Crowther, T. W., Todd-Brown, K. E., Rowe, C. W., Wieder, W. R., Carey, J. C., Machmuller, M. B., ... & Bradford, M. A. (2016). Quantifying global soil carbon losses in response to warming. *Nature*, 540(7631), 104-108.
- Davidson, E. A., Belk, E., & Boone, R. D. (1998). Soil water content and temperature as independent or confounded factors controlling soil respiration in a temperate mixed hardwood forest. *Global change biology*, 4(2), 217-227.
- Daly, C. (2020). PRISM 30-Year Normals. PRISM Climate Group at Northwest Alliance for Computational Science and Engineering, Oregon State University. <https://prism.oregonstate.edu/normals/>.
- Deepnote (2021). Deepnote. Available: <https://deepnote.com>.

- Dixon, J. J. (2003). Applying GIS to soil geomorphic landscape mapping in the Lookout Creek Valley, western Cascades, Oregon. *S., Crops and Soil Science, Oregon State University, Corvallis.*
- Dorman, M. (2023). ngeo: k-Nearest Neighbor Join for Spatial Data. R package version 0.4.7. <https://CRAN.R-project.org/package=ngeo>.
- Dowle, M, Srinivasan, A (2022). data.table: Extension of `data.frame`. R package version 1.14.4. <https://CRAN.R-project.org/package=data.table>.
- Dufour, A., Gadallah, F., Wagner, H. H., Guisan, A., & Buttler, A. (2006). Plant species richness and environmental heterogeneity in a mountain landscape: effects of variability and spatial configuration. *Ecography*, 29(4), 573-584.
- Ekblad A. & Högberg, P. (2001). Natural abundance of ^{13}C in CO_2 respired from forest soils reveals speed of link between tree photosynthesis and root respiration, *Oecologia* 127:305– 308.
- Evans, L. R., Pierson, D., & Lajtha, K. (2020). Dissolved organic carbon production and flux under long-term litter manipulations in a Pacific Northwest old-growth forest. *Biogeochemistry*, 149(1), 75-86.
- Fierer, N., Carney, K. M., Horner-Devine, M. C., & Megonigal, J. P. (2009). The biogeography of ammonia-oxidizing bacterial communities in soil. *Microbial ecology*, 58, 435-445.
- Fogel, R., & Cromack Jr, K. (1977). Effect of habitat and substrate quality on Douglas fir litter decomposition in western Oregon. *Canadian Journal of Botany*, 55(12), 1632-1640.
- Gao, Q., Zhao, P., Zeng, X., Cai, X., & Shen, W. (2002). A model of stomatal conductance to quantify the relationship between leaf transpiration, microclimate and soil water stress. *Plant, Cell & Environment*, 25(11), 1373-1381.
- Gray, A. N., Whittier, T. R., & Harmon, M. E. (2016). Carbon stocks and accumulation rates in Pacific Northwest forests: role of stand age, plant community, and productivity. *Ecosphere*, 7(1), e01224.
- Griffiths, R. (2019). Effects of topography on soil characteristics in the Andrews Experimental Forest, 1998. Long-Term Ecological Research. Forest Science Data Bank, Corvallis, OR. [Database]. Available: <http://andlter.forestry.oregonstate.edu/data/abstract.aspx?dbcode=SP020>. <https://doi.org/10.6073/pasta/891259b761f1e4ccbbbadd528d19adb>.

- Griffiths, R., Madritch, M., & Swanson, A. (2005). Conifer invasion of forest meadows transforms soil characteristics in the Pacific Northwest. *Forest Ecology and Management*, 208(1-3), 347-358.
- Griffiths, R. P., & Swanson, A. K. (2001). Forest soil characteristics in a chronosequence of harvested Douglas-fir forests. *Canadian Journal of Forest Research*, 31(11), 1871-1879.
- Han, M., & Jin, G. (2018). Seasonal variations of Q10 soil respiration and its components in the temperate forest ecosystems, northeastern China. *European Journal of Soil Biology*, 85, 36-42.
- Hanson, P. J., Edwards, N. T., Garten, C. T., & Andrews, J. A. (2000). Separating root and soil microbial contributions to soil respiration: a review of methods and observations. *Biogeochemistry*, 48(1), 115-146.
- Harmon, M.E., Franklin, J.F., Swanson, F.J., Sollins, P., Gregory, S.V., Lattin, J.D., Anderson, N.H., Cline, S.P., Aumen, N.G., Sedell, J.R., Lienkaemper, G.W., Cromack, K., Jr., and Cummins, K.W. (1986). Ecology of coarse woody debris in temperate ecosystems. *Adv. Ecol. Res.* 15. pp. 133–302.
- Hart, S.C., Perry, D.A., 1999. Transferring soils from high- to low-elevation forests increases nitrogen cycling rates: climate change implications. *Global Change Biol.* 5, 23–32.
- Hashimoto, S. et al. (2015). Global spatiotemporal distribution of soil respiration modeled using a global database. *Biogeosciences* 12, 4121–4132.
- Hawk, G. & Schulze, M. (2010). Plant community typing (2009 update), Andrews Experimental Forest. Long-Term Ecological Research. Forest Science Data Bank, Corvallis, OR. [Database]. Available: <http://andlter.forestry.oregonstate.edu/data/abstract.aspx?dbcode=TV062>. <https://doi.org/10.6073/pasta/1b9d9a1bf44d3df7431c9703c9be602f>. Accessed 2023-05-14.
- Heckman, K., Hicks Pries, C. E., Lawrence, C. R., Rasmussen, C., Crow, S. E., Hoyt, A. M., ... & Wagai, R. (2022). Beyond bulk: Density fractions explain heterogeneity in global soil carbon abundance and persistence. *Global Change Biology*, 28(3), 1178-1196.
- Heckman, K. A., Possinger, A. R., Badgley, B. D., Bowman, M. M., Gallo, A. C., Hatten, J. A., ... & Strahm, B. D. (2023). Moisture-driven divergence in mineral-associated soil carbon persistence. *Proceedings of the National Academy of Sciences*, 120(7), e2210044120.
- Hijmans, R.J. (2020). raster: Geographic Data Analysis and Modeling. R package version 3.4-5. <https://CRAN.R-project.org/package=raster>.

- Högberg, P., Nordgren, A., Högberg, M. N., Ottosson-Löfvenius, M., Singh, B., Olsson, P., & Linder, S. (2004). Fractional contributions by autotrophic and heterotrophic respiration to soil-surface CO₂ efflux in Boreal forests. The carbon balance of forest biomes, 251-267.
- Högberg, P., & Read, D. J. (2006). Towards a more plant physiological perspective on soil ecology. *Trends in ecology & evolution*, 21(10), 548-554.
- Homann, P. S., Harmon, M., Remillard, S., & Smithwick, E. A. (2005). What the soil reveals: Potential total ecosystem C stores of the Pacific Northwest region, USA. *Forest Ecology and Management*, 220(1-3), 270-283.
- Horwath WR, Pretzinger KS, Paul EA (1994). ¹⁴C allocation in tree-soil systems. *Tree Physiol* 14:1163–1176.
- Jackson, R. B., Lajtha, K., Crow, S. E., Hugelius, G., Kramer, M. G., & Piñeiro, G. (2017). The ecology of soil carbon: pools, vulnerabilities, and biotic and abiotic controls. *Annual review of ecology, evolution, and systematics*, 48, 419-445.
- Janzen, H. H. (2015). Beyond carbon sequestration: soil as conduit of solar energy. *European Journal of Soil Science*, 66(1), 19-32.
- Jasiewicz, J. & Stepinski, T. (2013). Geomorphons - a pattern recognition approach to classification and mapping of landforms, *Geomorphology*, vol. 182, 147-156. DOI: 10.1016/j.geomorph.2012.11.005.
- Jenny, H. (1961). E. W. Hilgard and the Birth of Modern Soil Science, *Collana Della Rivista Agrochimica*, Pisa.
- Jenny, H. (2012). *The soil resource: origin and behavior* (Vol. 37). Springer Science & Business Media.
- Jobbágy, E. G., and R. B. Jackson (2000), The vertical distribution of soil organic carbon and its relation to climate and vegetation, *Ecol. Appl.*, 10, 423–436.
- Johnson, D. W., Cole, D. W., Bledsoe, C. S., Cromack, K., Edmonds, R. L., Gessel, S. P., ... & Vogt, K. A. (1982). Nutrient cycling in forests of the Pacific Northwest.
- Johnson, D., Leake, J. R., Ostle, N., Ineson, P., & Read, D. J. (2002). In situ ¹³CO₂ pulse-labelling of upland grassland demonstrates a rapid pathway of carbon flux from arbuscular mycorrhizal mycelia to the soil. *New Phytologist*, 153(2), 327-334.
- Johnson, D. M., Woodruff, D. R., McCulloh, K., & Meinzer, F. C. (2009). Leaf hydraulic conductance, measured in situ, declines and recovers daily: leaf hydraulics, water potential and stomatal conductance in four temperate and three tropical tree species. *Tree Physiology*, 29(7), 879-887.

- Klopatek, J. M. (2008). Litter decomposition contrasts in second-and old-growth Douglas-fir forests of the Pacific Northwest, USA. *Plant Ecology*, 196, 123-133.
- Kuzyakov, Y. (2010). Priming effects: Interactions between living and dead organic matter. *Soil Biology and Biochemistry*, 42, 1363–1371.
- Kuzyakov, Y., Horwath, W. R., Dorodnikov, M., & Blagodatskaya, E. (2019). Review and synthesis of the effects of elevated atmospheric CO₂ on soil processes: No changes in pools, but increased fluxes and accelerated cycles. *Soil Biology and Biochemistry*, 128, 66–78.
- Lajtha, K., Crow, S. E., Yano, Y., Kaushal, S. S., Sulzman, E., Sollins, P., & Spears, J. D. H. (2005). Detrital controls on soil solution N and dissolved organic matter in soils: a field experiment. *Biogeochemistry*, 76(2), 261-281.
- Lajtha, K., Bowden, R. D., Crow, S., Fekete, I., Kotrocó, Z., Plante, A., ... & Nadelhoffer, K. J. (2018). The detrital input and removal treatment (DIRT) network: Insights into soil carbon stabilization. *Science of The Total Environment*, 640, 1112-1120.
- Lal, R. (2004). Soil carbon sequestration to mitigate climate change. *Geoderma*, 123(1-2), 1-22.
- Lavallee, J. M., Soong, J. L., & Cotrufo, M. F. (2020). Conceptualizing soil organic matter into particulate and mineral-associated forms to address global change in the 21st century. *Global change biology*, 26(1), 261-273.
- Liaw, A. & Wiener, M. (2002). Classification and Regression by randomForest. *R News* 2(3), 18--22.
- Lienkaemper, G. & Johnson, S. (2016). Stream network from 1997 survey and 2008 LiDAR flight, Andrews Experimental Forest. Long-Term Ecological Research. Forest Science Data Bank, Corvallis, OR. [Database]. Available: <http://andlter.forestry.oregonstate.edu/data/abstract.aspx?dbcode=HF013>. <https://doi.org/10.6073/pasta/66d98881d4eb6bb5dedcbdb60dbebafa>. Accessed 2023-05-15.
- Lienkaemper, G. & Schulze, M. (2014). Transportation network system including trails, road construction history, and gates for the Andrews Experimental Forest, 1952-2011. Long-Term Ecological Research. Forest Science Data Bank, Corvallis, OR. [Database]. Available: <http://andlter.forestry.oregonstate.edu/data/abstract.aspx?dbcode=GI007>. <https://doi.org/10.6073/pasta/c093067b268705ba0ec2a0d9c85c7fb9>. Accessed 2023-05-15.
- Lienkaemper, G.; Valentine, T. 2005. 10 meter digital elevation model (DEM) clipped to the Andrews Experimental Forest, 1998. Long-Term Ecological Research. Forest Science Data Bank, Corvallis, OR. [Database]. Available: <http://andlter.forestry.oregonstate.edu/data/abstract.aspx?dbcode=GI003>.

- <https://doi.org/10.6073/pasta/f97da4ea1c40917132f6cb15df7c6591>. Accessed 2023-05-15.
- Liu, X., Liang, J., & Gu, L. (2020). Photosynthetic and environmental regulations of the dynamics of soil respiration in a forest ecosystem revealed by analyses of decadal time series. *Agricultural and Forest Meteorology*, 282, 107863.
- Lloyd, J., & Taylor, J. A. (1994). On the temperature dependence of soil respiration. *Functional ecology*, 315-323.
- Mäki, M., Ryhti, K., Fer, I., Ľupek, B., Vestin, P., Roland, M., ... & Kulmala, L. (2022). Heterotrophic and rhizospheric respiration in coniferous forest soils along a latitudinal gradient. *Agricultural and Forest Meteorology*, 317, 108876.
- Makita, N., Kosugi, Y., Sakabe, A., Kanazawa, A., Ohkubo, S., & Tani, M. (2018). Seasonal and diurnal patterns of soil respiration in an evergreen coniferous forest: Evidence from six years of observation with automatic chambers. *PLOS ONE*, 13(2), e0192622. <https://doi.org/10.1371/journal.pone.0192622>.
- Mikan, C.J., Zak, D.R., Kubiske, M.E., Pregitzer, K.S. (2000). Combined effects of atmospheric CO₂ and N availability on the belowground carbon and nitrogen dynamics of aspen mesocosms. *Oecologia* 124:432–445.
- Miller, E. A., & Halpern, C. B. (1998). Effects of environment and grazing disturbance on tree establishment in meadows of the central Cascade Range, Oregon, USA. *Journal of Vegetation Science*, 9(2), 265-282.
- Nadelhoffer, K.J., Aber, J.D., Melillo, J.M., 1985. Fine root production in relation to net primary production along a nitrogen availability gradient in temperate forests: a new hypothesis. *Ecology* 66, 1377–1390.
- Nadelhoffer, K.J., Boone, R.D., Bowden, R.D., Canary, J.D., Kaye, J., Micks, P., Ricca, A., Aitkenhead, J.A., Lajtha, K., McDowell, W.H., 2004. In: Foster, D., Aber, J. (Eds.), *Forests in Time: The Environmental Consequences of 1000 Years of Change in New England*. Yale University Press, pp. 300–315.
- Nolin, A. W., & Daly, C. (2006). Mapping “at risk” snow in the Pacific Northwest. *Journal of Hydrometeorology*, 7(5), 1164-1171.
- Olsson, P., Linder, S., Giesler, R., & Högberg, P. (2005). Fertilization of boreal forest reduces both autotrophic and heterotrophic soil respiration. *Global change biology*, 11(10), 1745-1753.
- Osterloh, K. R. (2018). *Merging Field Work with Machine Learning: Exploring Andic Soil Development in the Cascade Range* [Doctoral Dissertation, Oregon State University].

- Paul, G., Huwaldt, J.A., & Steinhorst, S. (2020). Plot Digitizer. *Sourceforge*.
<https://sourceforge.net/projects/plotdigitizer/files/>.
- Pebesma, E., 2018. Simple Features for R: Standardized Support for Spatial Vector Data. *The R Journal* 10 (1), 439-446, <https://doi.org/10.32614/RJ-2018-009>.
- Phillips, C. L., Kluber, L. A., Martin, J. P., Caldwell, B. A., & Bond, B. J. (2012). Contributions of ectomycorrhizal fungal mats to forest soil respiration. *Biogeosciences*, 9(6), 2099–2110. <https://doi.org/10.5194/bg-9-2099-2012>.
- Pierson, D., Evans, L., Kayhani, K., Bowden, R. D., Nadelhoffer, K., Simpson, M., & Lajtha, K. (2021a). Mineral stabilization of soil carbon is suppressed by live roots, outweighing influences from litter quality or quantity. *Biogeochemistry*, 154(3), 433-449.
- Pierson, D., Peter-Contesse, H., Bowden, R. D., Nadelhoffer, K., Kayhani, K., Evans, L., & Lajtha, K. (2021b). Competing processes drive the resistance of soil carbon to alterations in organic inputs. *Frontiers in Environmental Science*, 9, 527803.
- Popenoe, J. H., Bevis, K. A., Gordon, B. R., Sturhan, N. K., & Hauxwell, D. L. (1992). Soil-vegetation relationships in Franciscan terrain of northwestern California. *Soil Science Society of America Journal*, 56(6), 1951-1959.
- Post, W. M., Emanuel, W. R., Zinke, P. J., & Stangenberger, A. G. (1982). Soil carbon pools and world life zones. *Nature*, 298(5870), 156-159.
- Post, W.M., Pastor, J., Zinke, P.J., Stangenberger, A.G., 1985. Global patterns of soil nitrogen storage. *Nature* 317, 613–616.
- Pribyl, D. W. (2010). A critical review of the conventional SOC to SOM conversion factor. *Geoderma*, 156(3-4), 75-83.
- QGIS Development Team (2009). QGIS Geographic Information System. Open Source Geospatial Foundation Project. <http://qgis.osgeo.org>.
- R Core Team (2021). R: A language and environment for statistical computing. R Foundation for Statistical Computing, Vienna, Austria. URL <https://www.R-project.org/>.
- Rahbek, C., Borregaard, M. K., Antonelli, A., Colwell, R. K., Holt, B. G., Nogues-Bravo, D., ... & Fjeldså, J. (2019). Building mountain biodiversity: Geological and evolutionary processes. *Science*, 365(6458), 1114-1119.
- Ross, N. (2022). fasterize: Fast Polygon to Raster Conversion. R package version 1.0.4. <https://CRAN.R-project.org/package=fasterize>.

- Savage, K., Davidson, E. A., & Tang, J. (2013). Diel patterns of autotrophic and heterotrophic respiration among phenological stages. *Global Change Biology*, 19(4), 1151-1159.
- Scharlemann, J. P., Tanner, E. V., Hiederer, R., & Kapos, V. (2014). Global soil carbon: understanding and managing the largest terrestrial carbon pool. *Carbon Management*, 5(1), 81-91.
- Schindlbacher, A., Zechmeister-Boltenstern, S., & Jandl, R. (2009). Carbon losses due to soil warming: do autotrophic and heterotrophic soil respiration respond equally?. *Global Change Biology*, 15(4), 901-913.
- Soil Survey Staff, Natural Resources Conservation Service, United States Department of Agriculture. Soil Survey Geographic (SSURGO) Database for Oregon. Available online.
- Soil Survey Staff (1999). *Soil Taxonomy: A Basic System of Soil Classification for Making and Interpreting Soil Surveys*, 2nd Edn. Washington, DC: Natural Resources Conservation Service. U.S. Department of Agriculture Handbook 436 (PDF). United States Department of Agriculture; Natural Resources Conservation Service.
- Sollins, P., Swanston, C., Kleber, M., Filley, T., Kramer, M., Crow, S., ... & Bowden, R. (2006). Organic C and N stabilization in a forest soil: evidence from sequential density fractionation. *Soil Biology and Biochemistry*, 38(11), 3313-3324.
- Spies, T. (2015). Aboveground Live Biomass (2008), Andrews Experimental Forest. Long-Term Ecological Research. Forest Science Data Bank, Corvallis, OR. [Database]. Available: <http://andlter.forestry.oregonstate.edu/data/abstract.aspx?dbcode=TV080>.
<https://doi.org/10.6073/pasta/3f91854669d9cccd12b29235f4d7f892>.
- Spies, T. (2016). LiDAR data (August 2008) for the Andrews Experimental Forest and Willamette National Forest study areas. Long-Term Ecological Research. Forest Science Data Bank, Corvallis, OR. [Database]. Available: <http://andlter.forestry.oregonstate.edu/data/abstract.aspx?dbcode=GI010>.
<https://doi.org/10.6073/pasta/c47128d6c63dff39ee48604ecc6fabfc>.
- Subke, J. A., Inghima, I., & Francesca Cotrufo, M. (2006). Trends and methodological impacts in soil CO₂ efflux partitioning: a metaanalytical review. *Global Change Biology*, 12(6), 921-943.
- Sulzman, E. W., Brant, J. B., Bowden, R. D., & Lajtha, K. (2005). Contribution of aboveground litter, belowground litter, and rhizosphere respiration to total soil CO₂ efflux in an old growth coniferous forest. *Biogeochemistry*, 73(1), 231-256.
- Torn, M. S., Trumbore, S. E., Chadwick, O. A., Vitousek, P. M., & Hendricks, D. M. (1997). Mineral control of soil organic carbon storage and turnover. *Nature*, 389(6647), 170-173.

- Wagai, R., Kajiura, M., & Asano, M. (2020). Iron and aluminum association with microbially processed organic matter via meso-density aggregate formation across soils: organo-metallic glue hypothesis. *Soil*, 6(2), 597-627.
- Wang, M., Guo, X., Zhang, S., Xiao, L., Mishra, U., Yang, Y., ... & Luo, Z. (2022). Global soil profiles indicate depth-dependent soil carbon losses under a warmer climate. *Nature Communications*, 13(1), 5514.
- Waring, R. H., & Franklin, J. F. (1979). Evergreen Coniferous Forests of the Pacific Northwest: Massive long-lived conifers dominating these forests are adapted to a winter-wet, summer-dry environment. *Science*, 204(4400), 1380-1386.
- Wickham, H., Chang, W., Henry, L., Pedersen, T. L., Takahashi, K., Wilke, C., Woo, K., Yutani, H. (2021). *ggplot2: Create Elegant Data Visualisations Using the Grammar of Graphics* [Computer software]. R Foundation for Statistical Computing. Available from <https://CRAN.R-project.org/package=ggplot2>.
- Wickham, H., François, R., Henry, L., Müller, K. (2021). *dplyr: A Grammar of Data Manipulation*. R package version 1.0.4. <https://CRAN.R-project.org/package=dplyr>.
- Yano, Y., Lajtha, K., Sollins, P., & Caldwell, B. A. (2004). Chemical and seasonal controls on the dynamics of dissolved organic matter in a coniferous old-growth stand in the Pacific Northwest, USA. *Biogeochemistry*, 71(2), 197-223.
- Zald, H. S., Spies, T. A., Seidl, R., Pabst, R. J., Olsen, K. A., & Steel, E. A. (2016). Complex mountain terrain and disturbance history drive variation in forest aboveground live carbon density in the western Oregon Cascades, USA. *Forest Ecology and Management*, 366, 193-207.